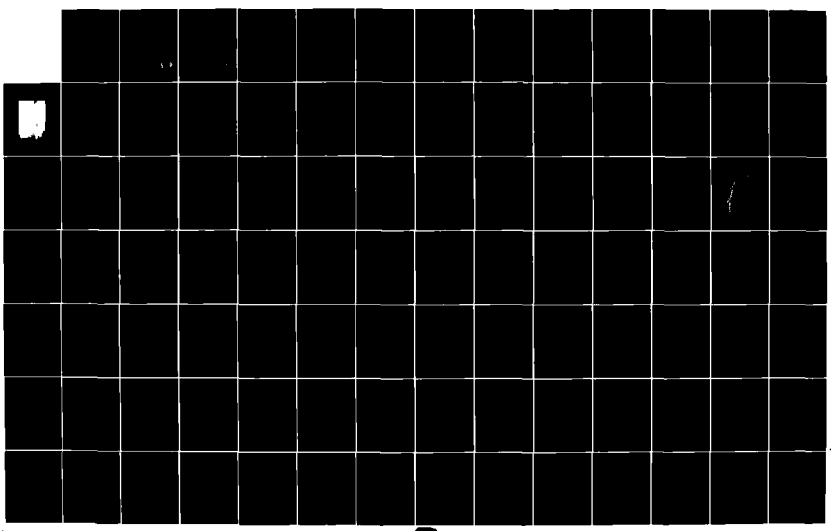
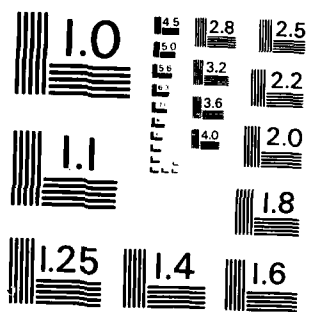


AD A436 919

STOCHASTIC ESTIMATION APPLIED TO THE LAND SPEED OF  
SOUND RECORD ATTEMPT B...UI AIR FORCE INST OF TECH  
WRIGHT PATTERSON AFB OH SCHOOL OF ENGI... D A REINHOLZ  
DECLASSIFIED DEC 83 AFIT/GAE/AA/83D-19 F/G 13/6 NI

1/2





MICROCOPY RESOLUTION TEST CHART  
NATIONAL BUREAU OF STANDARDS - 1963 - A

①

AD A136919



STOCHASTIC ESTIMATION APPLIED TO THE  
 LAND SPEED OF SOUND RECORD ATTEMPT  
 BY A ROCKET CAR

THESIS

David A. Reinholz  
 Captain, USAF

AFIT/GAE/AA/83D/20 19

DTIC FILE COPY

**S** DTIC  
 ELECTE  
 JAN 18 1984  
**D**  
 E

DEPARTMENT OF THE AIR FORCE  
 AIR UNIVERSITY  
**AIR FORCE INSTITUTE OF TECHNOLOGY**

Wright-Patterson Air Force Base, Ohio

This document has been approved  
 for public release and sales in  
 distribution 1 4

84 01 17 068

①

AFIT/GAE/AA/83D-2019

STOCHASTIC ESTIMATION APPLIED TO THE  
LAND SPEED OF SOUND RECORD ATTEMPT  
BY A ROCKET CAR

THESIS

David A. Reinholz  
Captain, USAF

AFIT/GAE/AA/83D/2019

DTIC  
SELECTED  
JAN 18 1984  
S E D

Approved for public release; distribution unlimited

AFIT/GAE/AA/83D-28 17

STOCHASTIC ESTIMATION APPLIED TO THE  
LAND SPEED OF SOUND RECORD ATTEMPT  
BY A ROCKET CAR

THESIS

Presented to the Faculty of the School of Engineering  
of the Air Force Institute of Technology  
Air University  
In Partial Fulfillment of the  
Requirements for the Degree of  
Master of Science in Aeronautical Engineering



David A. Reinholz, B.S.  
Captain, USAF

December 1983

Accession For	
NTIS GRA&I	<input checked="" type="checkbox"/>
DTIC TAB	<input type="checkbox"/>
Unannounced	<input type="checkbox"/>
Justification	
By _____	
Distribution/	
Availability Codes	
Dist	Avail and/or Special
A-1	

Approved for public release; distribution unlimited

### Acknowledgments

I wish to thank several individuals who were instrumental in helping me complete this project. Dr. Peter S. Maybeck provided the motivation to use filtering theory in a practical application. His sequence of courses and textbooks on Stochastic Estimation and Control gave me a solid foundation in the subject. Captain James K. Hodge and Major David R. Audley were the first to interest me in the Budweiser Rocket Car and helped provide guidance throughout my work. The person with the most "corporate knowledge" about the rocket car tests at Edwards AFB is Captain David E. Hamilton, without whose help this report would not have been possible. Mr. Stan Musick of the Air Force Avionics Laboratory at Wright-Patterson AFB provided unlimited support and encouragement. Stan provided much practical guidance on developing a proper filter algorithm and implementation of available software. Thanks are due to Mrs. Sharon Maruna for her patience and excellence in typing the final copy of this report. Finally, I wish to thank my loving wife and family, without whose support and patience I could not have completed this work.

David A.Reinholz

Table of Contents

	<u>Page</u>
Acknowledgments . . . . .	ii
List of Figures . . . . .	v
List of Tables . . . . .	ix
Abstract . . . . .	x
I. Introduction . . . . .	1
Filtering Theory . . . . .	1
Application of Theory . . . . .	3
Description of Rocket Car Test . . . . .	3
Method of Analysis . . . . .	10
II. Background Theory . . . . .	11
Linear Kalman Filter . . . . .	11
Extended Kalman Filter . . . . .	14
Fixed-Interval Smoother . . . . .	19
III. Modeling Techniques . . . . .	22
System Model . . . . .	22
Measurement Model . . . . .	35
IV. Development and Performance Analysis of the Extended Kalman Filter . . . . .	41
Accelerometer Calibration . . . . .	43
Calculation of Measurement Noise Variance . . . . .	53
Check of Filter Implementation . . . . .	64
Extended Kalman Filter Performance Analysis . . . . .	75
Results of One Iteration of the Extended Kalman Filter . . . . .	79
V. Optimal Smoother Results . . . . .	92
One Iteration of Smoother . . . . .	93
Second Iteration of Smoother . . . . .	107

	Page
VI. Hypothesis Testing. . . . .	121
Development of Scalar Speed Standard Deviation. . . . .	121
Calculation of Peak Scalar Speed and Standard Deviation. . . . .	126
Hypothesis Test of Peak Speed and Confidence Level. . . . .	131
VII. Conclusions and Recommendations . . . . .	133
Conclusions . . . . .	133
Recommendations . . . . .	139
Appendix A: Plots from Second Iteration of Extended Kalman Filter . . . . .	142
Appendix B: Optimal Smoother Computer Program. . . .	154
Bibliography. . . . .	170
Vita. . . . .	171



List of Figures

Figure	Page
i. Rocket Car. . . . .	xi
1.1 Rodgers Dry Lake Test Area. . . . .	5
3.1 Coordinate Frames of Reference. . . . .	23
3.2 Accelerometer Time History. . . . .	26
4.1 Extended Kalman filter estimate of x-position and standard deviation with accelerometer model for x velocity (no measurements). . . . .	45
4.2 Extended Kalman filter estimate of y-position and standard deviation with accelerometer model for x velocity (no measurements). . . . .	46
4.3 Extended Kalman filter estimate of x-velocity and standard deviation with accelerometer model for x velocity (no measurements). . . . .	47
4.4 Extended Kalman filter estimate of y-velocity and standard deviation with accelerometer model for x velocity (no measurements). . . . .	48
4.5 Extended Kalman filter estimate of accelerometer error and standard deviation with accelerometer model for x velocity (no measurements). . . . .	49
4.6 Extended Kalman filter estimate of range bias error and standard deviation with accelerometer model for x velocity (no measurements). . . . .	50
4.7 Extended Kalman filter estimate of azimuth bias error and standard deviation with accelerometer model for x velocity (no measurements). . . . .	51
4.8 Extended Kalman filter estimate of scalar speed converted to Mach (no measurements) . . . . .	52
4.9 Residual range measurement based on a track heading of $180^\circ$ true. . . . .	56
4.10 Residual azimuth measurement based on track heading of $180^\circ$ true. . . . .	57

Figure	Page
4.10(a) Corrected coordinate frames of reference. . . .	61
4.11 Residual range measurement based on a track heading of 179° true. . . . .	62
4.12 Residual azimuth measurement based on a track heading of 179° true. . . . .	63
4.13 Extended Kalman filter estimate of x-position with random walk model for x-velocity . . . . .	67
4.14 Extended Kalman filter estimate of y-position with random walk model for x-velocity . . . . .	69
4.15 Extended Kalman filter estimate of x-velocity with random walk model for x-velocity . . . . .	71
4.16 Extended Kalman filter estimate of y-velocity with random walk model for x-velocity . . . . .	73
4.17 Extended Kalman filter estimate of x-position and standard deviation incorporating range and azimuth measurements (first iteration). . . . .	80
4.18 Extended Kalman filter estimate of y-position and standard deviation incorporating range and azimuth measurements (first iteration). . . . .	81
4.19 Extended Kalman filter estimate of x-velocity and standard deviation incorporating range and azimuth measurements (first iteration). . . . .	82
4.20 Extended Kalman filter estimate of y-velocity and standard deviation incorporating range and azimuth measurements (first iteration). . . . .	83
4.21 Extended Kalman filter estimate of accelerometer error and standard deviation incorporating range and azimuth measurements (first iteration). . . . .	84
4.22 Extended Kalman filter estimate of range bias error and standard deviation incorporating range and azimuth measurements (first iteration). . . . .	85
4.23 Extended Kalman filter estimate of azimuth bias error and standard deviation incorporating range and azimuth measurements (first iteration). . . . .	86

Figure	Page
4.24 Residual measurements and residual standard deviations for first iteration of extended Kalman filter. . . . .	87
4.25 Extended Kalman filter estimate of scalar speed converted to Mach (first iteration). . . .	88
5.1 Smoother estimate and variance of x-position after one iteration. . . . .	94
5.2 Smoother estimate and variance of y-position after one iteration. . . . .	95
5.3 Smoother estimate and variance of x-velocity after one iteration. . . . .	96
5.4 Smoother estimate and variance of y-velocity after one iteration. . . . .	97
5.5 Smoother estimate and variance of accelerometer error after one iteration. . . . .	98
5.6 Smoother estimate and variance of range bias error after one iteration. . . . .	99
5.7 Smoother estimate and variance of azimuth bias error after one iteration. . . . .	100
5.8 Smoother estimate and variance of x-position after two iterations . . . . .	108
5.9 Smoother estimate and variance of y-position after two iterations . . . . .	109
5.10 Smoother estimate and variance of x-velocity after two iterations . . . . .	110
5.11 Smoother estimate and variance of y-velocity after two iterations . . . . .	111
5.12 Smoother estimate and variance of accelerometer error after two iterations . . . . .	112
5.13 Smoother estimate and variance of range bias error after two iterations . . . . .	113
5.14 Smoother estimate and variance of azimuth bias error after two iterations . . . . .	114

Figure	Page
5.15 Vehicle trajectory in earth-fixed coordinate frame of reference after two iterations of the smoother. . . . .	115
6.1 Velocity vector and one sigma ellipse of constant likelihood . . . . .	122
A.1 Residual range measurement based on track heading of 179.209° true. . . . .	144
A.2 Extended Kalman filter state estimate and standard deviation of x-position after two iterations. . . . .	145
A.3 Extended Kalman filter state estimate and standard deviation of y-position after two iterations. . . . .	146
A.4 Extended Kalman filter state estimate and standard deviation of x-velocity after two iterations. . . . .	147
A.5 Extended Kalman filter state estimate and standard deviation of y-velocity after two iterations. . . . .	148
A.6 Extended Kalman filter state estimate and standard deviation of accelerometer error after two iterations. . . . .	149
A.7 Extended Kalman filter state estimate and standard deviation of range bias error after two iterations. . . . .	150
A.8 Extended Kalman filter state estimate and standard deviation of azimuth bias error after two iterations. . . . .	151
A.9 Residual measurements and standard deviations after two iterations of extended Kalman filter.	152
A.10 Scalar speed estimate converted to Mach number after two iterations of the extended Kalman filter. . . . .	153

List of Tables

Table	Page
I. Filter Performance Analysis. . . . .	78
II. Comparison of First and Second Smoother Iterations . . . . .	116
III. Speed Estimate at FIM Trap (18.65 seconds) . . . .	135
IV. Peak Scalar Speed Estimates. . . . .	135

Abstract

Optimal linear smoothing theory is applied to the data from the Speed of Sound record attempt of a three-wheeled rocket car on 17 December 1979. A forward-backward estimation method is used which employs a seven state forward-running extended Kalman filter and a Meditch-form backward recursive "fixed-interval" smoothing algorithm. Data for this analysis is supplied by a longitudinal accelerometer mounted on the vehicle and tracking radar measurements of range, azimuth, and elevation. States of interest include two components of vehicle position and velocity, accelerometer time-correlated error, and radar range and azimuth bias errors.

Two iterations of the forward-backward smoothing algorithm provide excellent convergence of state estimates and error variance. Based on this analysis a peak speed estimate of 1082.028 ft/sec or 1.008 Mach is obtained at 16.85 seconds from the start of the high speed run. After two iterations of the smoother the standard deviation of the peak speed estimate is reduced to 1.055 ft/sec. We conclude with a confidence level of nearly one, based on the assumptions and modeling techniques employed in this analysis, that the rocket car did, in fact, exceed the reference speed of sound on 17 December 1979.

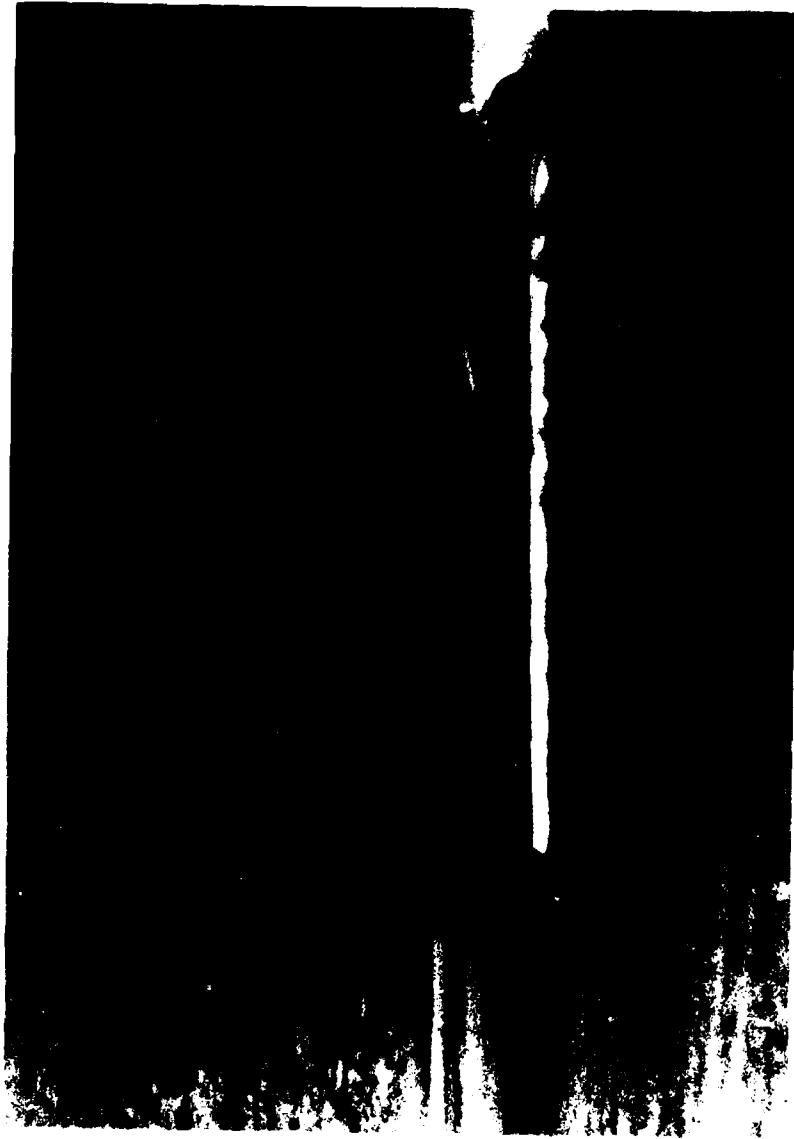


Fig. i - Rocket Car (Courtesy Mr. Ray VanAken)

STOCHASTIC ESTIMATION APPLIED TO THE  
LAND SPEED OF SOUND RECORD ATTEMPT  
BY A ROCKET CAR

I. Introduction

Filtering Theory

Any engineering problem inherently involves the use of measured or calculated information. The engineer bases his decisions on a variety of issues by using mathematical models of the "real world" to predict results obtained by experimentation. The mathematical models seldom describe every factor impacting a particular issue, but are simplifications in order to describe the most important characteristics of the problem and maintain tractability. Likewise, no measurement device can be considered "perfect", no matter what accuracy is claimed. How, then, does the engineer meet the ever-increasing demand for accuracy when he must rely on imperfect models and measurement devices?

One method for obtaining better answers is to model the important characteristics of a system and include the effects of model simplifications and measurement imperfections. This is the basic idea behind filtering theory, developed by several individuals, most notably Kalman. Filtering theory is concerned with estimating the "state" or status of a system of interest at any time,  $t_i$ , by incorporating the time



history of measurements up through time  $t_i$ . Another method of estimation, called the predictor algorithm, computes a state estimate at any time,  $t_i$ , based on the time history of measurements received before time,  $t_i$ . The "Kalman filter" algorithm combines both prediction of the state estimate before time  $t_i$  and correction of this predicted value based on the measurements received up through time  $t_i$ . With the advent of high-speed digital computers, the "Kalman filter" has proven to be very suitable in a number of applications most frequently in guidance and control problems. In this implementation, state estimates are generated in an "on-line" manner utilizing the measurement time history up through the time at which an estimate of state values is required. When the entire time history of measurements over a particular time interval of interest has been recorded, "off-line" estimation methods can be implemented. In this case, a "smoother" algorithm can be employed to generate state estimates based on all of the measurements, before and after any time  $t_i$ . Since the smoother algorithm has more information available for state estimation, it is the preferred method for post-run data analysis.

The Kalman filter algorithm requires a linear model to describe the dynamics of a particular system and a linear relationship between available measurements and the states of interest. More often than not, the system model or observation relationships are non-linear. This requires linearization about some reference values for the states as in the

"linearized Kalman filter", or re-linearization about the current state estimate provided by the "extended Kalman filter". The extended Kalman filter is most appropriate when the nominal (reference) state trajectory is unknown or when deviations from the nominal trajectory may become severe.

### Application of Theory

The purpose of this report is to apply estimation theory in post-run data analysis of the "Budweiser Rocket Car" speed of sound attempt. The method used is to develop an extended Kalman filter to describe the vehicle dynamics and available measurements of vehicle position provided by a tracking radar. The events leading up to this unique event have been well documented in many publications, most notably Road and Track Magazine, April 1980. It is not my purpose here to provide a historical account of the "Budweiser Rocket Car" or to analyze Air Force involvement in this project. However, some brief background information may be helpful.

### Description of Rocket Car Test

In the summer of 1979 a company known as Speed of Sound, Inc. (SOS) requested and received permission from the Air Force to use Rodgers Dry Lake at Edwards Air Force Base. Their purpose was to drive a rocket-powered land vehicle at the reference speed of sound. If successful, their rocket car would be the first to attain such a speed on land. The "Budweiser Rocket Car" was not designed for high sustained speeds due to very limited fuel storage capability and short

duration thrust augmentation (Sidewinder motor). The SOS plan was to reach peak speed very quickly and then slow to a stop. For these reasons, an official "land speed record" attempt would not be made. The Air Force Flight Test Center (AFFTC) provided a safe test area for conducting high speed runs. The speed runs were not allowed to impact in any way with normal operations at the base, and the government was reimbursed. At the request of SOS, the AFFTC provided computer analysis of the final high speed run.

The test track used for all the high speed runs at Edwards AFB began at the northwest corner of Rodgers Dry Lake (Fig. 1.1). The starting position varied but was located approximately 200 feet from the lake shore. The course followed a straight line on a heading of nearly true south from remote camera site A8 to the intersection of lakebed runways 17/35 and 15/33. From here it made a 12 degree turn to the right and followed runway 17 to the end. This turn began at about the seven mile point and had a radius of five miles. Use of the curve was required to take full advantage of the length of the lake and would only be used if the normal deceleration systems on the vehicle (parachute and brakes) failed. Every quarter mile along the course there were a pair of yellow flags mounted 30 feet either side of centerline to help guide the driver. Special red flags were used to signal the driver when to fire the thrust augmentation system. Approximately two miles from the starting position was a photoelectric "speed trap" system erected by the Federation Internationale

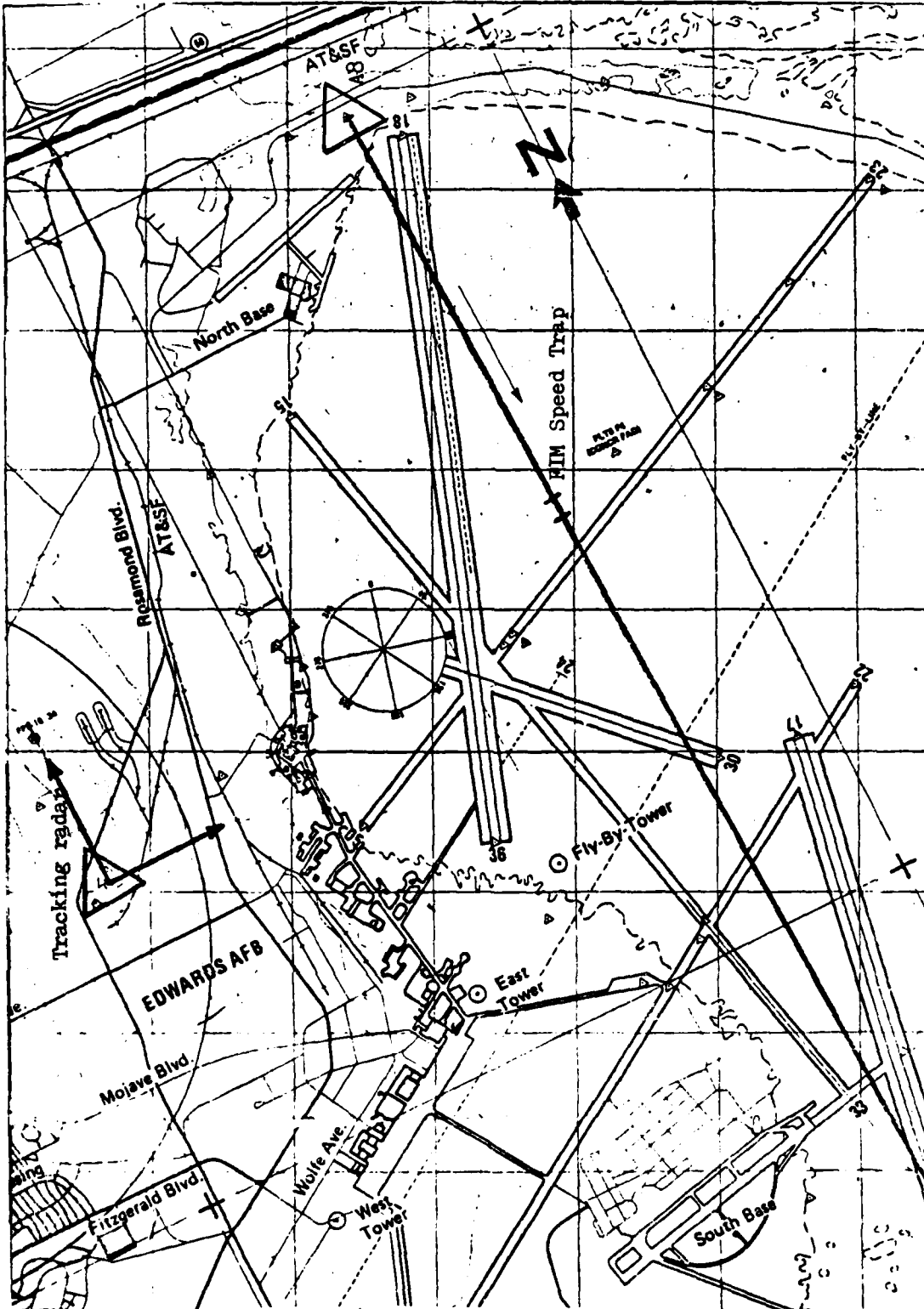


Fig. 1.1 Rodgers Dry Lake Test Area

des Motorcyclistes (FIM), official speed recorder for the event. The "trap" was actually a series of four precisely measured gates lined with lights that would flash at very precise time intervals to measure average speed through the gate. The traps were installed and not moved during the runs, which posed a difficult problem for the SOS engineers.

The idea was to hit the FIM speed trap at peak velocity which would presumably be just as the main engine or augmented system ran out of fuel. The speed was gradually raised on each successive run by increasing the amount of main engine fuel and adjusting the timing for Sidewinder ignition. The point at which the vehicle would reach peak speed for a given fuel load/configuration was estimated using a simulation of vehicle performance. Based on the data from this simulation, the starting position was adjusted to reach peak speed at the traps. In most cases the peak speed was seldom achieved at the traps but slightly before due to underestimated vehicle drag (3). The speed trap system proved to be a very unreliable measurement of peak velocity due to the problems stated above.

In addition to the FIM speed trap system several other instruments were used to record speed. A magnetic pickup on a rear wheel was used to convert wheel rotations into velocity. This device proved to be useless above 500 miles per hour due to inadequate frequency response of the device and a severe buildup of dirt over the run. A pitot tube installed on the nose of the vehicle measured air speed. Due to

compressibility errors near Mach one and the unknown influence of ground effect this device was not considered reliable (3). Longitudinal and lateral accelerations were measured by a set of accelerometers installed on the vehicle. Accelerometer data was not used to find velocity by the SOS engineers, only as a check on the number of acceleration units (g's) the driver was exposed to. Data from these devices were recorded via frequency modulated (FM) telemetry. An Air Force tracking radar was used to track the car and provide a backup of vehicle performance. This radar coverage was considered training for the operators and in no way impacted on any mission requirements at Edwards.

On the final day of the high speed runs, the fuel load on the vehicle was increased to maximum capacity and a Side-winder motor was installed. The run was set for early morning to take advantage of light winds and lower temperatures. Radar coverage was provided by a tracking radar located approximately 4.5 miles from the starting position on a hill overlooking Rodgers Dry Lake (Fig. 1.1). Temperature at the speed trap was recorded by an FIM official as 20 degrees Fahrenheit. Using the familiar relationship for the calculation of the reference speed of sound, a,

$$a = \sqrt{\gamma RT} \quad (1-1)$$

where

$\gamma$  ratio of specific heats for air = 1.4

R gas constant = 1715 ft<sup>2</sup>/sec<sup>2</sup>-R

T temperature in degrees Rankine = 479.66 R

we find

$$a = 1073.536213 \text{ ft/sec} = 931.956 \text{ mph}$$

The speed of sound depends primarily on the temperature of the air. The value at a given temperature can also vary due to changes in relative humidity. For this analysis, we have no information on the accuracy of the FIM temperature recording system, or relative humidity. Since the run was made in desert conditions we assume any changes to the calculated speed of sound due to relative humidity can be ignored. We also assume that the recorded temperature of 20 degrees is exact. The calculated speed of sound is used as a reference velocity to compare rocket car performance. A peak speed of 931.956 mph, therefore, was the goal of SOS people.

At 0726 Pacific Standard time the main rocket engine ignited, followed 12 seconds later by ignition of the Side-winder. The vehicle ran out of fuel about a fifth of a mile prior to the speed traps and thus was already decelerating as it passed through them. The four traps showed the vehicle speed to be 666.234 mph, 646.725 mph, 640.112 mph, and 632.522 mph, respectively (3). Since the speed trap measurements were made after the vehicle had reached peak speed they could not be used. The radar measurements would have to provide the estimate of top speed. Unfortunately, the radar range broke lock at the critical point during the run and followed a larger vehicle running parallel to the test track and approximately 1500 feet beyond the rocket car. After two seconds the radar again picked up the car. The Air Force

radar became the only check of actual vehicle performance with the FIM speed trap system unavailable and unreliable wheel speed and air speed indicators. The radar azimuth and elevation data were considered valid for the following reasons (3). The Air Force radar operator used a television monitor aligned with the axis of the radar dish and manually adjusted azimuth and elevation tracking rates. Using a set of "cross-hairs" on the monitor, the operator kept the car centered on the television screen. To attempt to correct the erroneous range data, another vehicle was driven over the tracks of the rocket car. The same tracking radar followed this vehicle and measured range and azimuth. Azimuth data from the rocket car and this second vehicle were aligned and a corrected range measurement for the rocket car was found. Based on this corrected range data, Air Force computer analysis showed three data points above the reference speed of sound, 731.96 mph. Speed of Sound, Inc. averaged these three points and claimed a maximum speed of 739.66 mph or 1.0106 Mach.

Speed of Sound, Inc. elected not to make any more high speed runs as the engineers felt they could get no more performance from the vehicle and the driver had complained of stability problems. Thus, the speed of 739.66 mph became the "official" figure that was claimed as the top speed of the "Budweiser Rocket Car".



### Method of Analysis

The data available for this analysis includes raw radar range, azimuth, and elevation sampled at 20 points per second. Also we have the data from the longitudinal accelerometer which measured specific force continuously. The telemetry data for the accelerometer is digitized at 250 samples per second. Using these data sources, a model for the dynamics of the vehicle is developed and put in proper form for use in an extended Kalman filter algorithm. A measurement model for the radar measurements is used to relate the states of interest to the available measurements. To find the best estimate of vehicle performance with the lowest achievable error, a "fixed-interval" smoother algorithm is used. The filtering theory used in this analysis and specific modeling methods are developed in the next two chapters. Chapter IV will present the results of the extended Kalman filter, while Chapter V details two iterations of the extended Kalman filter-fixed interval smoother estimation scheme. Finally, Chapter VI will present a hypothesis test of the peak velocity estimate and give a confidence level for this estimate.

## II. Background Theory

The problem as defined in Chapter I is to obtain better estimates of vehicle position and velocity by proper modeling of vehicle dynamics and measurement devices. By combining data from all measurement sources and including the effects of identifiable errors and noise through the use of a Kalman filter, one hopes to get improved state estimates. The standard form for the model to describe the dynamics of a problem for which a Kalman filter is to be developed is a first order vector differential equation. Generally, a discrete-time (sampled data) measurement model is used to relate observations to the states of interest. The basic Kalman filter equations will be presented here with little explanation. It is assumed that the reader is generally familiar with Kalman filtering. An excellent text on this subject is available by Maybeck (4).

### Linear Kalman Filter

The basic equation to describe system dynamics has the following continuous-time form:

$$\dot{\underline{x}}(t) = \underline{f}[\underline{x}(t), \underline{u}(t), t] + \underline{G}(t)\underline{w}(t) \quad (2-1)$$

where

$\underline{x}(t)$  - n-state vector

$\underline{u}(t)$  - r-input vector (controls)

$\underline{f}$  - dynamics vector (possibly non-linear)

$\underline{Q}(t)$  - time dependent coefficient matrix (n-by-s)

$\underline{w}(t)$  - zero-mean, white Gaussian noise s-vector of strength  $\underline{Q}(t)$  such that

$$E[\underline{w}(t)\underline{w}(t+\tau)^T] = \underline{Q}(t)\delta(\tau) \quad (s\text{-by-}s) \quad (2-2)$$

where  $\delta(\tau)$  is the Dirac delta function. Available discrete-time measurements are modeled by the following relation

$$\underline{z}(t_i) = \underline{h}[\underline{x}(t_i), t_i] + \underline{v}(t_i) \quad (2-3)$$

where

$t_i$  - discrete measurement time

$\underline{z}(t_i)$  - m-vector of discrete measurements

$\underline{h}$  - measurement model vector function (possibly non-linear)

$\underline{x}(t_i)$  - n-state vector

$\underline{v}(t_i)$  - zero mean, white, Gaussian discrete-time m-vector noise process, independent of system noise and of covariance  $\underline{R}(t_i)$ , i.e. such that

$$E[\underline{v}(t_i)\underline{v}(t_j)^T] = \underline{R}(t_i)\delta_{ij} \quad (m\text{-by-}m) \quad (2-4)$$

The initial condition on the state is only known with some uncertainty, and is modeled as a Gaussian random n-vector, assumed independent of  $\underline{w}(t)$  and  $\underline{v}(t_i)$ , with mean and covariance:

$$E[\underline{x}(t_0)] = \hat{\underline{x}}_0 \quad (2-5)$$

$$E[(\underline{x}(t_0) - \hat{\underline{x}}_0)(\underline{x}(t_0) - \hat{\underline{x}}_0)^T] = \underline{P}_0 \quad (2-6)$$

The Kalman filter algorithm is most easily generated when the dynamics and measurement models are linear relationships. If the vectors  $\underline{f}$  and  $\underline{h}$  are linear combinations of the states, the dynamics model and measurement relation become linear relationships:

$$\dot{\underline{x}}(t) = \underline{F}(t)\underline{x}(t) + \underline{B}(t)\underline{u}(t) + \underline{G}(t)\underline{w}(t) \quad (2-7)$$

$$\underline{z}(t_i) = \underline{H}(t_i)\underline{x}(t_i) + \underline{v}(t_i) \quad (2-8)$$

where  $\underline{F}(t)$  and  $\underline{H}(t_i)$  become time-dependent (or possibly time invariant) coefficient matrices of dimensions n-by-n and m-by-n, respectively, and  $\underline{B}(t)$  is an n-by-r matrix relating control inputs to the dynamics model.

The Kalman filter incorporates measurement updates using the following relations:

$$\underline{K}(t_i) = \underline{P}(t_i^-)\underline{H}^T(t_i)[\underline{H}(t_i)\underline{P}(t_i^-)\underline{H}^T(t_i) + \underline{R}(t_i)]^{-1} \quad (2-9)$$

$$\hat{\underline{x}}(t_i^+) = \hat{\underline{x}}(t_i^-) + \underline{K}(t_i)[\underline{z}_i - \underline{H}(t_i)\hat{\underline{x}}(t_i^-)] \quad (2-10)$$

$$\underline{P}(t_i^+) = \underline{P}(t_i^-) - \underline{K}(t_i)\underline{H}(t_i)\underline{P}(t_i^-) \quad (2-11)$$

where

$t_i^-$  - before measurement update at time  $t_i$

$t_i^+$  - after measurement update at time  $t_i$

$\underline{K}(t_i)$  - Kalman filter gain matrix (m-by-n)

$\hat{\underline{x}}(t_i)$  - n-state estimate vector

$\underline{z}_i$  - m vector of measurements

$\underline{P}(t_i)$  - error covariance matrix (n-by-n)

The state estimate and covariance are propagated forward to the next sample time from the initial condition,  $\hat{\underline{x}}(t_{i-1}^+)$  and  $\underline{P}(t_{i-1}^+)$  at time  $t_{i-1}$ , by integrating

$$\dot{\hat{\underline{x}}}(t/t_{i-1}) = \underline{F}(t)\hat{\underline{x}}(t/t_{i-1}) + \underline{B}(t)\underline{u}(t) \quad (2-12)$$

$$\begin{aligned} \dot{\underline{P}}(t/t_{i-1}) = & \underline{F}(t)\underline{P}(t/t_{i-1}) + \underline{P}(t/t_{i-1})\underline{F}^T(t) \\ & + \underline{G}(t)\underline{Q}(t)\underline{G}(t)^T \end{aligned} \quad (2-13)$$

where  $t/t_{i-1}$ , indicates integration forward from the previous measurement update time,  $t_{i-1}$ .

#### Extended Kalman Filter

The case where either the vector of dynamics relations,  $\underline{f}$ , or the measurement equation vector,  $\underline{h}$ , is non-linear in the states requires special consideration. The method most commonly used when system dynamics or measurement non-linearities exist is the "extended Kalman filter". The approach used in this method is to relinearize the dynamics and/or measurement equations about the most recent estimate of the state,  $\hat{\underline{x}}(t_i^-)$ , at update time, or  $\hat{\underline{x}}(t/t_{i-1})$  in the ensuing sample period. Thus, the matrices  $\underline{F}$ ,  $\underline{H}$ ,  $\underline{K}$ , and  $\underline{P}$  are evaluated by knowing the most recent estimate of the nominal (reference) state trajectory.

The system matrix,  $\underline{F}(t)$ , in (2-13) and observation matrix,  $\underline{H}(t_i)$  in (2-9) and (2-11) become partial derivative matrices in the extended Kalman filter:

$$\underline{F}[t; \hat{\underline{x}}(t/t_{i-1})] = \left. \frac{\partial \underline{f}[\underline{x}(t), \underline{u}(t), t]}{\partial \underline{x}} \right|_{\underline{x} = \hat{\underline{x}}(t/t_{i-1})} \quad (2-14)$$

$$\underline{H}[t_i; \hat{\underline{x}}(t_i^-)] = \left. \frac{\partial \underline{h}[\underline{x}(t_i), t_i]}{\partial \underline{x}} \right|_{\underline{x} = \hat{\underline{x}}(t_i^-)} \quad (2-15)$$

In equations (2-14) and (2-15) the differentiation is done so that the derivative of a scalar with respect to a column vector is a row vector. The matrices resulting from this differentiation have dimensions n-by-n and m-by-n, respectively. These matrices relate small perturbations in the state vector,  $\underline{x}(t)$ , to changes in the equations for  $\dot{\underline{x}}(t)$  and  $\underline{z}(t_i)$ . The  $\underline{F}$  matrix is called the "filter dynamics partial matrix" and the  $\underline{H}$  matrix the "measurement sensitivity matrix". Defining the perturbation of the state,  $\underline{x}(t)$ , from its current estimate,  $\hat{\underline{x}}(t_i^-)$  as

$$\delta \underline{x}(t) \triangleq \underline{x}(t) - \hat{\underline{x}}(t_i^-) \quad (2-16)$$

the perturbation  $\delta \underline{x}(t)$  is called the error state while  $\underline{x}(t)$  is the full state.

We expand equations (2-1) for  $\dot{\underline{x}}(t)$  and (2-3) for  $\underline{z}(t_i)$  in a Taylor series about the current state estimate in powers of  $\delta \underline{x}(t)$ . Since  $\delta \underline{x}(t)$  is assumed small, powers of  $\delta \underline{x}(t)$  higher than one are ignored. We arrive at the following linearized perturbation equations in  $\delta \underline{x}(t)$ :

$$\dot{\delta \underline{x}}(t) = \underline{F}[t; \hat{\underline{x}}(t/t_{i-1})] \delta \underline{x}(t) + \underline{G}(t) \underline{w}(t) \quad (2-17)$$

$$\underline{\delta z}(t_i) = \underline{H}[t_i; \hat{\underline{x}}(t_i^-)] \underline{\delta x}(t_i) + \underline{v}(t_i) \quad (2-18)$$

where  $\underline{F}$  and  $\underline{H}$  are defined as in (2-14) and (2-15), respectively.

Equations (2-17) and (2-18) are in the proper form for use in a conventional filter. Thus, an estimate  $\hat{\underline{\delta x}}(t_i^+)$  of the error state  $\underline{\delta x}(t)$  can be made from perturbation measurements,  $\underline{\delta z}(t_i)$ , using equations (2-9) through (2-11). The measurement difference  $\underline{\delta z}(t_i)$  is called the residual. It is formed by subtracting the predicted measurements  $\hat{\underline{z}}(t_i)$  from the actual measurements  $\underline{z}(t_i)$  :

$$\underline{\delta z}(t_i) = \underline{z}_i - \underline{h}[\hat{\underline{x}}(t_i^-), t_i] \quad (2-19)$$

Equation (2-10) provides an updated estimate of the error state,  $\hat{\underline{\delta x}}(t_i^+)$ . By using equation (2-16) we can obtain an updated estimate of the whole value state,  $\hat{\underline{x}}(t_i^+)$  :

$$\hat{\underline{x}}(t_i^+) = \hat{\underline{x}}(t_i^-) + \hat{\underline{\delta x}}(t_i^+) \quad (2-20)$$

This equation places all of the available information into the whole-value state estimate. This allows  $\underline{\delta x}(t_i^+)$  to be reset to zero for propagation of the state estimate to the next update time. At any time,  $t_i$ ,  $\underline{\delta x}(t)$  has a conditional mean,  $\hat{\underline{\delta x}}(t_i)$ , and conditional covariance  $\underline{P}_\delta(t_i)$  such that:

$$E[\underline{\delta x}(t_i) | \underline{Z}(t_i)] = \hat{\underline{\delta x}}(t_i) \quad (2-21)$$

and

$$E[[\underline{\delta x}(t_i) - \hat{\underline{\delta x}}(t_i)][\underline{\delta x}(t_i) - \hat{\underline{\delta x}}(t_i)]^T | \underline{z}(t_i)] = \underline{P}_\delta(t_i) \quad (2-22)$$

where  $\underline{z}(t_i)$  is defined as the entire measurement history up through time  $t_i$ . If we assume a zero mean initial condition on the error state,

$$\hat{\underline{\delta x}}(t_0) = \underline{0} \quad (2-23)$$

then  $\hat{\underline{\delta x}}(t)$  will be zero over the entire interval between updates such that:

$$\hat{\underline{\delta x}}(t) = 0 \quad \text{for} \quad t_{i-1} \leq t \leq t_i \quad (2-24)$$

With  $\hat{\underline{\delta x}}(t_{i-1}^-)$  zero, the error state update equation from (2-10)

$$\hat{\underline{\delta x}}(t_i^+) = \hat{\underline{\delta x}}(t_i^-) + \underline{K}(t_i) \underline{\delta z}(t_i) \quad (2-25)$$

simplifies to

$$\hat{\underline{\delta x}}(t_i^+) = \underline{K}(t_i) \underline{\delta z}(t_i) \quad (2-26)$$

which upon substitution into the full state update equation (2-20) produces

$$\hat{\underline{x}}(t_i^+) = \hat{\underline{x}}(t_i^-) + \underline{K}(t_i) \underline{\delta z}(t_i) \quad (2-27)$$

where  $\underline{\delta z}(t_i)$  is given by (2-19).

Consider the conditional covariance,  $\underline{P}_\delta(t_i)$  of the error state,  $\underline{\delta x}(t)$ , given by (2-21). We wish to relate this conditional covariance to the conditional covariance,  $\underline{P}(t_i)$  of the whole state,  $\underline{x}(t)$ . From (2-21)

$$\begin{aligned} \underline{P}_\delta(t_i) &= E[[\underline{\delta x} - \hat{\underline{\delta x}}][\underline{\delta x} - \hat{\underline{\delta x}}]^T | \underline{z}(t_i)] \\ &= E[[\underline{\delta x}][\underline{\delta x}]^T | \underline{z}(t_i)] \quad \text{from (2-24)} \end{aligned}$$



$$\begin{aligned}
&= E[[\underline{x}-\hat{\underline{x}}][\underline{x}-\hat{\underline{x}}]^T | \underline{z}(t_i)] \quad \text{from (2-16)} \\
&= \underline{P}(t_i)
\end{aligned}$$

Thus, the error covariance of  $\underline{x}(t)$  is identical to that of  $\delta\underline{x}(t)$ . Equations (2-13) and (2-11) describe the propagation and update of the error state covariance,  $\underline{P}(t)$ , with  $\underline{F}(t)$  and  $\underline{H}(t)$  in these equations replaced by equations (2-14) and (2-15), respectively.

The extended Kalman filter algorithm is summarized here. The measurement vector at time  $t_i$ ,  $\underline{z}(t_i)$ , is incorporated using

$$\begin{aligned}
\underline{K}(t_i) &= \underline{P}(t_i^-) \underline{H}^T[t_i; \hat{\underline{x}}(t_i^-)] \times \\
&\quad [ \underline{H}[t_i; \hat{\underline{x}}(t_i^-)] \underline{P}(t_i^-) \underline{H}^T[t_i; \hat{\underline{x}}(t_i^-)] + \underline{R}(t_i) ]^{-1} \quad (2-28)
\end{aligned}$$

$$\hat{\underline{x}}(t_i^+) = \hat{\underline{x}}(t_i^-) + \underline{K}(t_i) [ \underline{z}_i - \underline{h}[\hat{\underline{x}}(t_i^-), t_i] ] \quad (2-29)$$

$$\underline{P}(t_i^+) = \underline{P}(t_i^-) - \underline{K}(t_i) \underline{H}[t_i; \hat{\underline{x}}(t_i^-)] \underline{P}(t_i^-) \quad (2-30)$$

The estimate is propagated forward to the update time,  $t_i$ , from the previous update time,  $t_{i-1}$ , by integrating

$$\dot{\hat{\underline{x}}}(t/t_{i-1}) = \underline{f}[\hat{\underline{x}}(t/t_{i-1}), \underline{u}(t), t] \quad (2-31)$$

and

$$\begin{aligned}
\dot{\underline{P}}(t/t_{i-1}) &= \underline{F}[t; \hat{\underline{x}}(t/t_{i-1})] \underline{P}(t/t_{i-1}) + \underline{P}(t/t_{i-1}) \underline{F}^T[t; \hat{\underline{x}}(t/t_{i-1})] \\
&\quad + \underline{G}(t) \underline{Q}(t) \underline{G}(t)^T \quad (2-32)
\end{aligned}$$

from time  $t_{i-1}$  to  $t_i$ , using the initial conditions provided by:

$$\hat{\underline{x}}(t_{i-1}/t_{i-1}) = \hat{\underline{x}}(t_{i-1}^+) \quad (2-33)$$

$$\underline{P}(t_{i-1}/t_{i-1}) = \underline{P}(t_{i-1}^+) \quad (2-34)$$

Upon integrating (2-31) and (2-32) to the next update time,  $t_i$ ,  $\hat{\underline{x}}(t_i^-)$  and  $\underline{P}(t_i^-)$  are defined as

$$\hat{\underline{x}}(t_i^-) = \hat{\underline{x}}(t_i/t_{i-1}) \quad (2-35)$$

$$\underline{P}(t_i^-) = \underline{P}(t_i/t_{i-1}) \quad (2-36)$$

where the time notation  $t_i/t_{i-1}$  indicates that  $\hat{\underline{x}}(t_i/t_{i-1})$  has been integrated to time  $t_i$  but is conditioned on measurements through  $t_{i-1}$  only. Thus, the initial condition for propagation of the state estimate and covariance from one sample time to the next is constantly being redeclared based on the most recent state estimate,  $\hat{\underline{x}}(t_{i-1}^+)$  and covariance,  $\underline{P}(t_{i-1}^+)$ .

#### Fixed-Interval Smoother

The standard Kalman filter algorithm can be called "forward-running" in the way current state estimates are computed. Several authors, including Meditch (5) have shown that the state estimate and covariance can be calculated more accurately by allowing access to "future" measurements. The values for the state and covariance at time  $t_i$  from a forward-running Kalman filter are optimally combined with estimates of these quantities from a "backward-running" Kalman filter. This type of algorithm was developed by Fraser (1,2) and is called an "optimal smoother".

The Fraser form of the optimal "fixed interval" smoother incorporates a "backward filter" that propagates the state estimate and covariance backward in time from the respective boundary conditions at the final time of interest,  $\hat{\underline{x}}(t_f^+)$  and  $\underline{P}(t_f^+)$ . At each time of interest,  $t_i$ , the state estimates and covariances from the independent forward and backward filters are optimally combined to yield a "smoothed" state estimate and updated covariance. Such an algorithm is described in detail by Maybeck (4). The optimal smoother has the advantage of being able to "see" the entire measurement history through the final time,  $\underline{Z}(t_f)$ . Calculations of the state mean and the covariance conditioned on all of  $\underline{Z}(t_f)$ , and not just the "current"  $\underline{Z}(t_i)$ , by this method can significantly improve state estimation primarily by using the future data.

Meditch (5) has shown that a mathematically equivalent algorithm to the combined forward/backward filter scheme can be used. The Meditch form of the "fixed-interval smoother" algorithm uses the output of a forward-running Kalman filter where the state estimates and covariances before and after measurement update  $\hat{\underline{x}}(t_i^-)$ ,  $\hat{\underline{x}}(t_i^+)$ ,  $\underline{P}(t_i^-)$ , and  $\underline{P}(t_i^+)$ , respectively, from the initial to final time have been stored. Starting from the boundary conditions at the final time,  $t_f$ ,

$$\hat{\underline{x}}(t_f/t_f) = \hat{\underline{x}}(t_f^+) \quad (2-37)$$

$$\underline{P}(t_f/t_f) = \underline{P}(t_f^+) \quad (2-38)$$

the smoothed estimate is generated backward in time using

$$\hat{\underline{x}}(t_i/t_f) = \hat{\underline{x}}(t_i^-) + \underline{A}(t_i) [\hat{\underline{x}}(t_{i+1}/t_f) - \hat{\underline{x}}(t_{i+1}^-)] \quad (2-39)$$

where the "smoothing estimator gain matrix"  $\underline{A}(t_i)$  is given by

$$\underline{A}(t_i) = \underline{P}(t_i^+) \underline{\Phi}^T(t_{i+1}, t_i) \underline{P}^{-1}(t_{i+1}^-) \quad (2-40)$$

and  $\underline{\Phi}(t_{i+1}, t_i)$  is the state transition matrix for propagating adjoint system quantities backward in time (4).

The covariance of the zero mean Gaussian estimation error  $[\underline{x}(t_i) - \hat{\underline{x}}(t_i/t_f)]$  can be generated backward from the boundary condition by

$$\underline{P}(t_i/t_f) = \underline{P}(t_i^+) + \underline{A}(t_i) [\underline{P}(t_{i+1}/t_f) - \underline{P}(t_{i+1}^-)] \underline{A}^T(t_i) \quad (2-41)$$

The method of analysis chosen to analyze available data from the rocket car is to develop such a "fixed-interval smoother" algorithm based on the state trajectory (time history) generated from an extended Kalman filter. The extended Kalman filter will be shown as the appropriate choice due to non-linear measurement relations. The amount of pseudo-noise is adjusted to achieve optimum filter performance in a "tuning" process described more fully in Chapter IV. The next chapter describes the methods used to model vehicle dynamics, errors to be estimated, and available measurements for implementation in an extended Kalman filter.

### III. Modeling Techniques

#### System Model

The test track described in Chapter I has no surveyed positions from which to reference vehicle position. The best information on the starting position is provided by the radar which was set on the vehicle for several minutes before the start of the high speed run. It is this position provided by the radar to which changes in vehicle position are referenced.

The coordinate system for the dynamics of the rocket car is chosen as a Cartesian system fixed at the starting point of the run. This system is shown in Fig. 3.1 and has the x-axis aligned with the straight portion of the test track (true south) and the y-axis aligned with true east. The time interval of interest is the first 24 seconds of the run, as the vehicle achieved its maximum velocity at approximately 17 seconds into the run. Thus, the velocity and position along the x and y axis is taken with respect to a fixed position on the earth corresponding to an inexact starting position. The elevation of the car is ignored due to minimal change in vertical displacement ( $\pm 20$  feet). Therefore, the coordinate frame we are concerned with becomes planar or two-dimensional. Post-run inspection of the test track indicated that the vehicle deviated very little from track centerline (3). Therefore, y components of position and velocity are minimal with the motion restricted to the x-axis almost entirely.

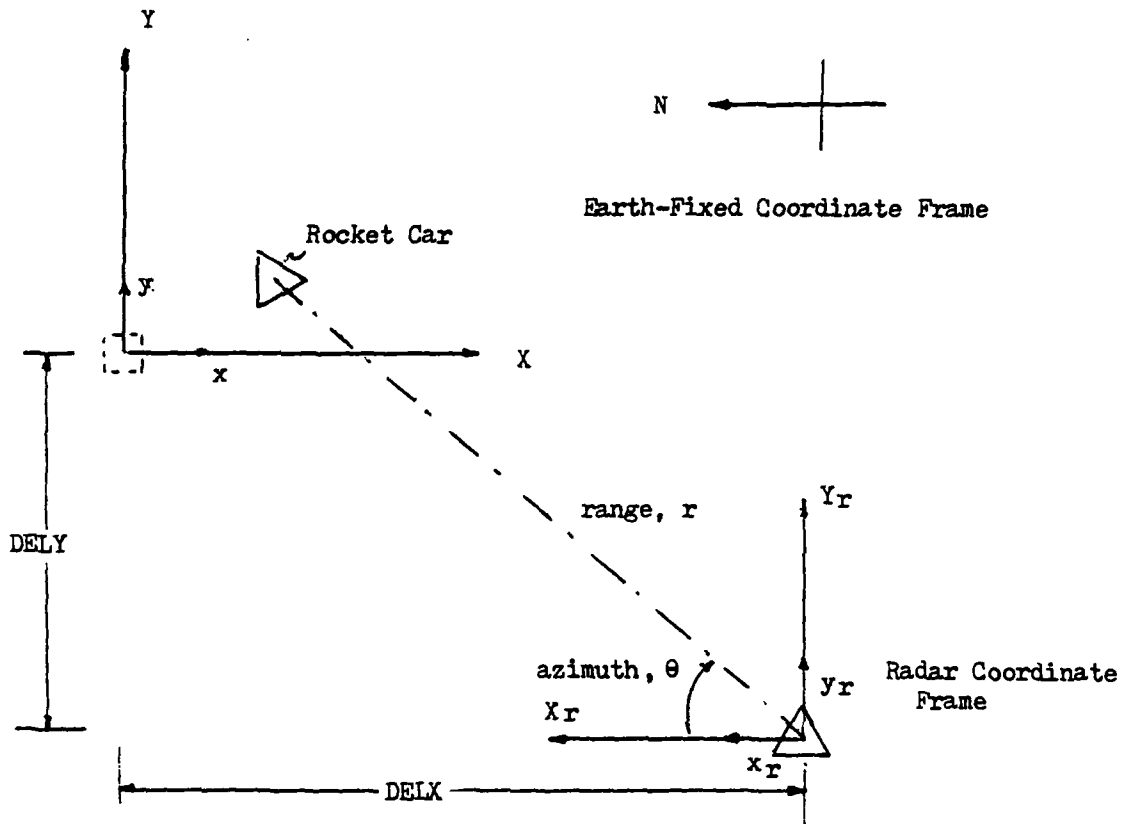


Fig. 3-1(a). Top View of Coordinate Systems

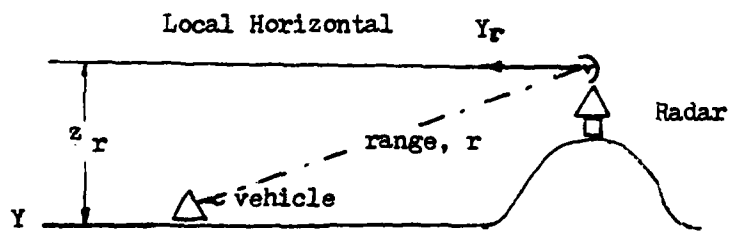


Fig. 3-1(b). Side View of Coordinate Systems

No information is available on engine thrust or vehicle drag for use in a model of these forces as they relate to the acceleration and time-dependent mass of the vehicle. We have only the specific force measurements from the longitudinal accelerometer. Thus, the model chosen to represent vehicle dynamics is a straight-forward two-dimensional kinematic model. In such a model, the components of acceleration are the time derivatives of the velocity components. The velocity components, in turn, are the time derivatives of the position components. In addition to the components of position and velocity, we desire to model inherent errors in the accelerometer and radar. These error states are "augmented" to the states of position and velocity in order to estimate their value and compensate for their effect.

No data from the lateral accelerometer is available, so we cannot estimate accelerometer misalignment error. The tremendous vibration of the vehicle at high speed can conceivably cause a time-correlated error in the longitudinal accelerometer. Scale factor (due to digitizing accelerometer data) and bias error are neglected due to lack of information and observability problems associated with trying to estimate more than one error term in a single accelerometer configuration.

The radar range and azimuth measurements are assumed to be corrupted by some unknown bias (constant) errors. Very little information is available on the accuracy of the radar or types of inherent errors, so that these bias terms are

the only assumed inaccuracies in these measurements. Thus, the additional states to be estimated include one error state for the accelerometer, and two error states for the radar. Lack of additional measurements and resulting observability problems precluded the identification of any other errors. It will be shown in the next chapter that even these states are only weakly observable.

The states to be estimated become:

$x_1$  - position component along x-axis

$x_2$  - position component along y-axis

$x_3$  - velocity along x-axis

$x_4$  - velocity along y-axis

$x_5$  - longitudinal accelerometer time-correlated error

$x_6$  - radar range bias error

$x_7$  - radar azimuth bias error

The first four states are related by deterministic means (i.e., velocity is the first derivative of position, etc.). The error states are modeled as stochastic processes in the following manner.

The time-correlated error of the accelerometer is modeled as a first order Gauss-Markov process, the output of a first order lag, which is driven by white, Gaussian noise. Figure 3.2 shows the output of the longitudinal accelerometer indicating the extreme fluctuations in specific force sensed by this device. Such rapid fluctuations are due to extreme vibrations caused by rough ground and engine "pulsing" (3). Conceivably, the accelerometer error state can also vary



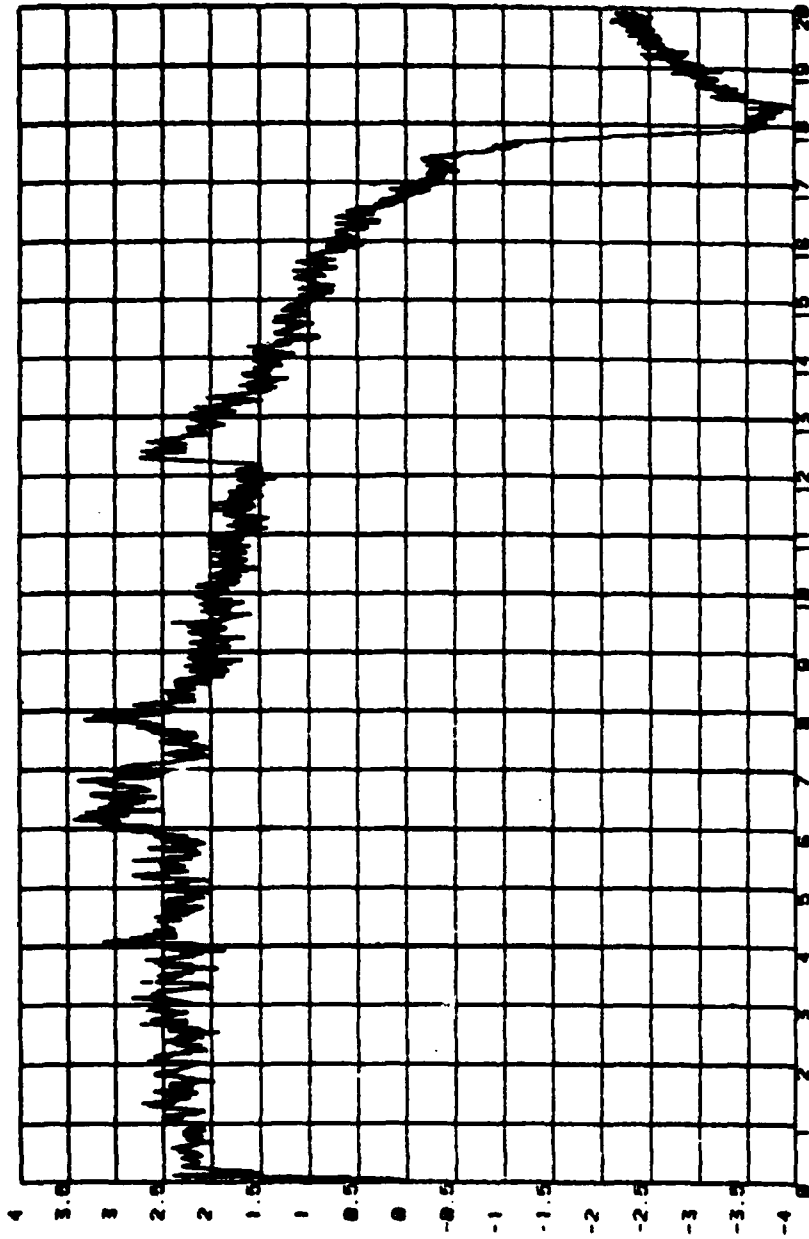


Fig 3-2. Accelerometer Time History (G's vs. time)

due to such vibration. We desire the filter to continually "expect" changes in this error and estimate them. With no better information on the types of inherent errors in this accelerometer, the first-order lag model is chosen. The initial choice for correlation time,  $T$ , is one second. This is a subjective "guess" of how much this error will vary over time.

The error states on the radar are not expected to vary significantly, if at all, during the 24 second time interval of interest. Consequently, these states are modeled as random walk.

Random walk is defined as the output of an integrator driven by white noise, while a random constant is the output of an undriven integrator. A random walk model for an error state indicates to the filter that we are not "absolutely" sure the value of this state never changes. The values for radar bias errors are allowed to vary (slowly) over the time interval of interest. By using such a model for the radar bias error states, the filter gains in these channels remain non-zero and so the filter is able to detect changes in these states. If a random constant model were used, the filter would assume that once it calculates a value for these states, they will not vary. Thus, random walk is preferable to the random constant model without detailed information on the radar error characteristics.

The first order differential vector dynamics model for the propagation of the seven states of interest plus additive "driving" noise becomes:

$$\begin{aligned}\dot{x}_1(t) &= x_3 \\ \dot{x}_2(t) &= x_4 \\ \dot{x}_3(t) &= a_x + x_5(t) \\ \dot{x}_4(t) &= w_4(t) \\ \dot{x}_5(t) &= -1/Tx_5(t) + w_5(t) \\ \dot{x}_6(t) &= w_6(t) \\ \dot{x}_7(t) &= w_7(t)\end{aligned}$$

Here  $\underline{w}(t)$  is a white Gaussian vector noise process of strength  $\underline{Q}(t)$  over the time interval  $[t_o, t_f]$ . Off-line "tuning" of the system noise matrix,  $\underline{Q}(t)$ , can be used to match the available data as closely as desired. This was not done in this analysis. Instead, the noise matrix,  $\underline{Q}(t)$  is adjusted "on-line" in a performance analysis in order to achieve lowest possible variance in the state estimates. The results of this tuning process are detailed in the next chapter.

In the system model presented above the longitudinal accelerometer output  $a_x$  is used to "drive" the propagation of the x component of velocity. The output of the accelerometer is corrupted by a time correlated error which is expected to vary frequently during the run. With no lateral accelerometer data available, we assume the y velocity component,  $x_4$ , is well modeled as a constant with zero value. A

small amount of "pseudo-noise" is added to this state to allow the filter to estimate deviations in the y velocity from zero. Small amounts of pseudo-noise are added to the radar error states,  $x_6$  and  $x_7$ , for the same reason. The amount of pseudo-noise is adjusted to achieve optimum filter performance in a "tuning" process described more fully in Chapter IV.

The model for the accelerometer time-correlated error deserves some further explanation. We have chosen a Gauss-Markov process, which is the output of a first order lag of the form:

$$\dot{x}_5(t) = -1/Tx_5(t) + w_5(t) \quad (3-1)$$

where T is the correlation time.

The concept of a time-correlated random process,  $\underline{x}$ , can be generalized from the "second central moment" or covariance matrix,  $\underline{P}_{xx}(t)$ , defined as

$$\underline{P}_{xx}(t) \triangleq E[[\underline{x}(t) - \underline{m}_x(t)][\underline{x}(t) - \underline{m}_x(t)]^T] \quad (3-2)$$

where  $\underline{m}_x(t)$  is the mean. This covariance is an indication of the spread of values about the mean at time t. Generalizing (3-2) we can obtain additional information about how fast  $\underline{x}(t)$  sample values can change in time. The covariance "kernel",  $\underline{P}_{xx}(t_1, t_2)$ , is defined for all  $t_1, t_2$  in some time interval T as:

$$\underline{P}_{xx}(t_1, t_2) \triangleq E[[\underline{x}(t_1) - \underline{m}_x(t_1)][\underline{x}(t_2) - \underline{m}_x(t_2)]^T] \quad (3-3)$$

For zero mean processes (3-3) becomes the "second non-central moment" which generalizes to the "correlation kernel" (4) defined for all  $t_1, t_2 \in T$  as

$$\underline{\psi}_{xx}(t_1, t_2) \stackrel{\Delta}{=} E[\underline{x}(t_1)\underline{x}(t_2)^T] \quad (3-4)$$

From (3-3) and (3-4), it can be seen that

$$\underline{\psi}_{xx}(t_1, t_2) = \underline{P}_{xx}(t_1, t_2) + \underline{m}_x(t_1)\underline{m}_x(t_2)^T \quad (3-5)$$

and thus, if  $\underline{x}(t)$  is a zero-mean process,  $\underline{\psi}_{xx}(t_1, t_2) = \underline{P}_{xx}(t_1, t_2)$ . A scalar time-correlated random process  $x(t)$  of zero-mean has a correlation kernel function (4) of the form:

$$\psi_{xx}(t_1, t_2) = P_{xx}(t_1, t_2) = \sigma^2 e^{-[t_1 - t_2]/T} \quad (3-6)$$

where  $T$  is the correlation time. If we compare this random process  $x(t)$  to another zero mean process  $y(t)$  with correlation time ten times that of  $x(t)$  such that

$$\psi_{yy}(t_1, t_2) = P_{yy}(t_1, t_2) = \sigma^2 e^{-[t_1 - t_2]/10T} \quad (3-7)$$

we can say that there is higher correlation between the values of  $y(t_1)$  and  $y(t_2)$  than between  $x(t_1)$  and  $x(t_2)$ . One would expect a typical sample of  $x(t)$  to exhibit more rapid variations in magnitude than  $y(t)$ .

If a random process,  $x(t)$ , is wide-sense stationary (4) then we can define the "power spectral density", PSD, of such a process as the Fourier transform of the correlation function  $\underline{\psi}_{xx}(\tau)$  where  $\tau$  is the time difference between

two sample times. An inverse Fourier transform of the PSD, in turn, yields the "autocorrelation function". The power spectral density of a device to be modeled can be plotted versus frequency. The resulting PSD function can be integrated over the range of frequencies to obtain the mean squared value of the process. This method of obtaining PSD and the related autocorrelation helps describe the errors inherent in a device to enable proper modeling of these errors.

If we had such PSD information for the rocket car accelerometer we could make more realistic modeling decisions. Without such information we must make some subjective modeling decisions. The correlation time for the accelerometer error model specifies how much we expect the mean squared value of this zero mean process to vary over time. Choosing T as one second indicates that the mean squared value for this process can vary by approximately 63 percent in one second. A correlation time of one second will be shown to be adequate for our purposes.

The amount of driving noise on the accelerometer error state,  $q_5$ , can be obtained from specifying the desired steady-state variance,  $P_5(\infty)$ . This will be explained in detail below. Given a continuous-time system that can be described by the linear vector differential equation

$$\dot{\underline{x}}(t) = \underline{F}(t)\underline{x}(t) + \underline{G}(t)\underline{w}(t) \quad (3-8)$$

where

$$E[\underline{w}(t)] = \underline{0}$$

$$E[\underline{w}(t)\underline{w}(t+\tau)^T] = \underline{Q}(t)\delta(\tau) \quad (3-9)$$

the propagation of the covariance of the state estimate is described by:

$$\dot{\underline{P}}(t) = \underline{F}(t)\underline{P}(t) + \underline{P}(t)\underline{F}^T(t) + \underline{G}(t)\underline{Q}(t)\underline{G}^T(t) \quad (3-10)$$

The strength of the driving noise on the accelerometer error state,  $x_5$ , is found in the following manner. Referring to equation (3-1) we can solve for the steady state value of the covariance. In this case,  $\underline{F} = -1/T$ ,  $\underline{Q} = q$ , and  $\underline{G} = 1$  so that (3-10) becomes:

$$\dot{P}_5(t) = -2/TP_5(t) + q_5 \quad (3-11)$$

and

$$P_5(t) = P_{05} e^{-2(t-t_0)/T} + q_5 T/2 [1 - e^{-2(t-t_0)/T}]; \quad t \geq t_0 \quad (3-12)$$

For  $t_0 = 0$  we find

$$P_5(t_0) = P_{05} \quad (3-13a)$$

and the steady state variance,  $P_5(\infty)$ , becomes:

$$P_5(\infty) = q_5 T/2 \quad (3-13b)$$

By specifying the steady state variance we can solve for the amount of driving noise to be added to the propagation of the accelerometer error state,  $x_5$ .

The only information available on the longitudinal accelerometer is calibration data taken before and after the high speed run of the rocket car. This data indicates that the accelerometer calibration varied by an average of .003 g's between the two calibration checks. With no more information on the inherent errors in the accelerometer, we are forced to refer to information on comparable models. We desire a comparable accelerometer which has a specified bias error on the order of .003 g's. The model chosen in this case is a Honeywell solid-state low-cost accelerometer. The specified RMS error for this model is listed at .005g. Thus, we use this specified error as the steady-state deviation in error of the accelerometer actually used in this test run. Obviously, we need to vary this value in order to check filter performance, but .005g will serve as a "first-guess". We now can solve for the driving noise,  $q_5$

$$P_5(\infty) = (.005g)^2 = q_5T/2 \quad (3-13c)$$

and

$$q_5(t) = 2(.005g)^2 = .0518 \text{ (ft/sec}^2\text{)}^2/\text{sec} \quad (3-13d)$$

Choosing the initial variance,  $P_5(0)$ , to be equal to the steady-state variance,  $P_5(\infty)$ , results in a "stationary" process (4) for the accelerometer error state,  $x_5$ . This stationary characteristic is, in fact, implemented in the system model for the rocket car.

The initial condition of the state vector at the start of the run is known only with some uncertainty and is



modeled as a Gaussian random variable of zero-mean and covariance,  $\underline{P}_0$ , such that:

$$E[\underline{x}(t_0)] = \hat{\underline{x}}_0 = \underline{0} \quad (3-14)$$

$$E[[\underline{x}(t_0) - \hat{\underline{x}}_0][\underline{x}(t_0) - \hat{\underline{x}}_0]^T] = \underline{P}_0 \quad (3-15)$$

Initially, our uncertainty in the state values is very high. We choose the following values for  $\underline{P}_0$ :

$$\underline{P}_0 = \begin{bmatrix} 10000 & & & & & & & & \\ & 10000 & & & & & & & \\ & & 100 & & \underline{0} & & & & \\ & & & 100 & & & & & \\ \underline{0} & & & & .0259 & & & & \\ & & & & & 225 & & & \\ & & & & & & .25E-6 & & \end{bmatrix} \quad (3-16)$$

The initial guess on the last three diagonal elements is obtained by using specified Root Mean Squared (RMS) errors for the accelerometer, range, and azimuth respectively:

$$P_{05} = (.005g)^2 = .0259 \text{ [ft/sec}^2\text{]}^2$$

$$P_{06} = (15 \text{ ft})^2 = 225 \text{ ft}^2$$

$$P_{07} = (.0005 \text{ rad})^2 = .25E - 6 \text{ rad}^2$$

The initial variances of the first four states are subjective values based on relatively high uncertainty in state values. Having developed the dynamics model for propagating the states of interest, it is now necessary to relate these

states to the available measurements of radar range, azimuth, and elevation.

#### Measurement Model

The radar measured quantities are taken with respect to the coordinate system of the radar, shown in Fig. 3.1. These measured values must be related to the vehicle as it moves in an earth-fixed coordinate frame, both translated and rotated from that of the radar. The radar range measurement can be related to the radar coordinate system by the following model:

$$\text{Range} = \Delta (x_r^2 + y_r^2 + z_r^2)^{\frac{1}{2}} \quad (3-17)$$

where  $x_r$ ,  $y_r$ , and  $z_r$  are distance components along the three axes of the radar coordinate system. The radar azimuth measurement is related to radar coordinate components by:

$$\text{Azimuth} = \Delta \arctan (y_r/x_r) \quad (3-18)$$

The radar measurement of elevation,  $z_r$ , is used only to adjust the value of range as the car proceeds along the track. It is now necessary to relate radar measured components,  $x_r$ ,  $y_r$ , and  $z_r$  to components in the earth-fixed system,  $x_1$  and  $x_2$ .

The origin for the earth-fixed coordinate system is taken to be the starting point of the run. The radar is set on the car prior to the start of the run, and computed values of distance  $x_r = 16104$  feet, and  $y_r = 18374$  feet are taken from the initial range measurement. These initial

values are held constant as the car travels down the track in order to relate differing range and azimuth measurements to changes in position in the earth-fixed coordinate system. Labeling the initial distance along  $x_r$  and  $y_r$  as DELX and DELY respectively, one can relate the distance traveled in the earth-fixed frame to radar measurements by the following translation:

$$\begin{aligned}x_r &= \text{DELX} - x_1 \\y_r &= \text{DELY} + x_2\end{aligned}\quad (3-19)$$

As the car moves along the track, radar distance  $x_r$  will decrease to a point where  $x_r = 0$ . At this point  $x_1 = \text{DELX}$  and the azimuth angle,  $\theta$ , equals 90 degrees. Substituting these translations into the range and azimuth equations we find:

$$\text{Range} = [(\text{DELX}-x_1)^2 + (\text{DELY}+x_2)^2 + z_r^2]^{\frac{1}{2}} \quad (3-20)$$

and

$$\text{Azimuth} = \arctan [( \text{DELY}+x_2 ) / ( \text{DELX}-x_1 )] \quad (3-21)$$

Thus, we have related the radar measurements to the states we desire to estimate. Note that the 180 degree rotation of the radar coordinate system to align with the earth frame simplifies the relations. The measurement model is summarized here:

$$\begin{aligned}z_i(t_i) &= [(\text{DELX}-x_1(t_i))^2 + (\text{DELY}+x_2(t_i))^2 + z_r(t_i)^2]^{\frac{1}{2}} \\&\quad + x_6(t_i) + v_1(t_i)\end{aligned}\quad (3-22)$$

$$z_2(t_i) = \arctan [(DELY+x_2(t_i))/(DELX-x_1(t_i))] + x_7(t_i)+v_2(t_i) \quad (3-23)$$

In these equations each measurement is corrupted by an inherent bias error state, and some scalar, zero-mean white noise to account for measurement and model inaccuracies. This white noise vector  $\underline{v}(t_i)$  has a strength  $\underline{R}(t_i)$  during the 24 second interval of interest.

It is apparent from (3-22) and (3-23) that the measurement relations are non-linear in the states. Since we have no reference values for the behavior of the states, especially the error states, we cannot use a perturbation model based on such a trajectory. Thus, we choose the extended Kalman filter algorithm. Applying equations (2-28) through (2-30), we arrive at the proper implementation of the extended Kalman filter for the rocket car analysis. The observation sensitivity matrix,  $\underline{H}[t_i; \hat{\underline{x}}(t_i^-)]$  in equations (2-29) and (2-30) is developed from (2-15). For convenience, only the non-zero elements of this m-by-n matrix are presented here. For notational ease,  $\underline{H}[t_i; \hat{\underline{x}}(t_i^-)]$  is given as  $\underline{H}$  and  $\hat{\underline{x}}(t_i^-)$  is given as  $\hat{\underline{x}}^-$ .

$$\begin{aligned} H(1,1) &= -(\text{DELX}-\hat{x}_1^-) / [(\text{DELX}-\hat{x}_1^-)^2 + (\text{DELY}+\hat{x}_2^-)^2 + z_r(t_i)^2]^{1/2} \\ H(1,2) &= (\text{DELY}+\hat{x}_2^-) / [(\text{DELX}-\hat{x}_1^-)^2 + (\text{DELY}+\hat{x}_2^-)^2 + z_r(t_i)^2]^{1/2} \\ H(1,6) &= 1.0 \\ H(2,1) &= (\text{DELY}+\hat{x}_2^-) / [(\text{DELX}-\hat{x}_1^-)^2 + (\text{DELY}+\hat{x}_2^-)^2] \\ H(2,2) &= (\text{DELX}-\hat{x}_1^-) / [(\text{DELX}-\hat{x}_1^-)^2 + (\text{DELY}+\hat{x}_2^-)^2] \\ H(2,7) &= 1.0 \end{aligned} \quad (3-24)$$

Thus, the extended Kalman filter incorporates the measurements at time,  $t_i$  by using:

$$\underline{K}(t_i) = \underline{P}(t_i^-) \underline{H}^T [ \underline{H} \underline{P}(t_i^-) \underline{H}^T + \underline{R}(t_i) ]^{-1} \quad (3-25)$$

$$\hat{\underline{x}}(t_i^+) = \hat{\underline{x}}(t_i^-) + \underline{K}(t_i) \underline{\delta z}(t_i) \quad (3-26)$$

$$\underline{P}(t_i^+) = \underline{P}(t_i^-) - \underline{K}(t_i) \underline{H} \underline{P}(t_i^-) \quad (3-27)$$

where  $\underline{\delta z}(t_i)$  is given by:

$$\underline{\delta z}(t_i) = \begin{bmatrix} \delta z_1(t_i) \\ \delta z_2(t_i) \end{bmatrix} = \begin{bmatrix} z_1 - [ [ (\text{DELX} - \hat{x}_1^-)^2 + (\text{DELY} + \hat{x}_2^-)^2 + z_r^2 ] + \hat{x}_6^- ] \\ z_2 - [ \arctan [ (\text{DELY} + \hat{x}_2^-) / (\text{DELX} - \hat{x}_1^-) ] + \hat{x}_7^- ] \end{bmatrix} \quad (3-28)$$

The state estimate at time  $t_{i-1}$  is propagated forward to the next sample time  $t_i$  by integrating:

$$\dot{\hat{\underline{x}}}(t/t_{i-1}) = \begin{bmatrix} \hat{x}_3(t/t_{i-1}) \\ \hat{x}_4(t/t_{i-1}) \\ \hat{x}_5(t/t_{i-1}) + a_x \\ 0 \\ -1/T \hat{x}_5(t/t_{i-1}) \\ 0 \\ 0 \end{bmatrix} \quad (3-29)$$

The error covariance  $\underline{P}(t/t_{i-1})$  is propagated forward by integrating equation (2-32) in which

$$\underline{F}[t; \hat{\underline{x}}(t/t_{i-1})] = \begin{bmatrix} 0 & 0 & 1 & 0 & 0 & 0 & 0 \\ 0 & 0 & 0 & 1 & 0 & 0 & 0 \\ 0 & 0 & 0 & 0 & 1 & 0 & 0 \\ 0 & 0 & 0 & 0 & 0 & 0 & 0 \\ 0 & 0 & 0 & 0 & -1/T & 0 & 0 \\ 0 & 0 & 0 & 0 & 0 & 0 & 0 \\ 0 & 0 & 0 & 0 & 0 & 0 & 0 \end{bmatrix} \quad \text{by} \quad (2-14)$$

The initial value for the system noise matrix in (2-32) is chosen as:

$$\underline{Q}(t) = \begin{bmatrix} 0 & & & & & & \\ & 0 & & & & & \underline{0} \\ & & 0 & & & & \\ & & & .01 & & & \\ & \underline{0} & & & .0518 & & \\ & & & & & 1 & \\ & & & & & & 0.1E-7 \end{bmatrix} \quad (3-30)$$

The initial values for the diagonal elements of  $\underline{Q}(t)$  are chosen to indicate our relative uncertainty of the behavior of the corresponding states over the time interval of interest. The initial value for driving noise on the accelerometer error state,  $x_5$ , has been previously calculated (3-13d). The remaining diagonal elements of  $\underline{Q}(t)$  are chosen by subjectively deciding how much these states will vary from constant values. By comparing  $Q_{44}(t)$ ,  $Q_{66}(t)$  and  $Q_{77}(t)$  one can see that we have little doubt that the azimuth bias error,  $x_7$ , is a constant. We are less certain about the behavior of the y velocity,  $x_4$ , and even more uncertain about the range bias error state,  $x_6$ . The initial value for  $Q_{44}(t)$  is based on our knowledge of the rocket car trajectory -

described as nearly a straight line along the x-axis (3). We do not expect the y velocity to vary significantly from a constant value of zero. Use of the radar in a "look-down" mode increases our uncertainty in how the range bias state,  $x_6$ , will behave over the 24 second interval. The azimuth bias error is not expected to vary significantly from the behavior of a constant. The initial value for  $Q(t)$  presented in (3-30) is adjusted in a "tuning" process to achieve lowest possible variance values for the seven states of interest. This performance analysis is detailed in the next chapter along with the results of the seven state extended Kalman filter developed here.

#### IV. Development and Performance Analysis of the Extended Kalman Filter

The previous chapters have developed an extended Kalman Filter estimation algorithm for post-run data analysis of the Budweiser Rocket Car. This chapter describes the results obtained by using the seven state filter outlined previously. The amount of computer programming required by this analysis is minimal due to existing software available for the development of a Kalman filter.

The computer software used in this analysis is a Monte Carlo Simulation for Optimal Filter Evaluation (SOFE) available at Wright-Patterson AFB (6,7). The program was developed under contract by the Air Force Avionics Laboratory (AFAL) and is well documented by Musick (6). SOFE is invaluable when designing Kalman Filters. The normal method used is a Monte Carlo analysis (4) whereby a suboptimal (reduced order) Kalman filter is evaluated against a "truth model". The suboptimal filter is adjusted to achieve the best possible performance when compared to a much higher order "truth model". The idea is to track the important characteristics of a physical system adequately using a simpler model. Such a reduced order filter could then be implemented in an operational system where computer capability may be limited.

For the purpose of analyzing the rocket car data, SOFE is used to integrate the dynamics equations and update the



states of interest at measurement times. There is no truth model available for tuning purposes, nor do we have the ability to generate sample statistics. SOFE implements the Kalman filter equations for either the linear or extended Kalman filter presented in Chapter II. The user simply specifies the dynamics and measurement relations for his system. SOFE propagates the state and covariance estimates forward from the specified initial time, using a fifth order Kutta-Merson integration algorithm (6). Updates of state and covariance estimates based on available measurements are provided at user-specified intervals. The user can specify any number of measurements to be incorporated at a given update time. Use of SOFE greatly reduces the amount of computer programming necessary in developing a Kalman filter and allows the user to concentrate on the finer details of his particular problem.

The fifth-order Kutta-Merson integrator implemented in SOFE requires a step-size no greater than approximately two milliseconds for the chosen integration tolerances. The integrator uses a variable step size to automatically maintain the integration error below a specified value. The user can specify a fixed step size mode if exterior factors, such as a high measurement rate, cause the step size to remain small regardless of dynamics. If, in order to handle severe dynamics, the integrator reduces its step size to a minimum specified value without satisfying error tolerances, an integration failure occurs and the program stops. The default

parameters for the integrator are variable step size, error tolerance of .0001, maximum step size of  $1.0 \text{ E} + 9$ , minimum step size of .0001, and initial step size of .01. We are unsure of exact vehicle dynamics but expect rapid changes in acceleration over a very short time interval. We desire to allow the integrator to automatically adjust its step size in order to reduce integration error and avoid "stepping-over" any fluctuations in the solution. A variable step size also reduces computer time. For these reasons, we interpolate the accelerometer data to .002 second intervals for integration purposes.

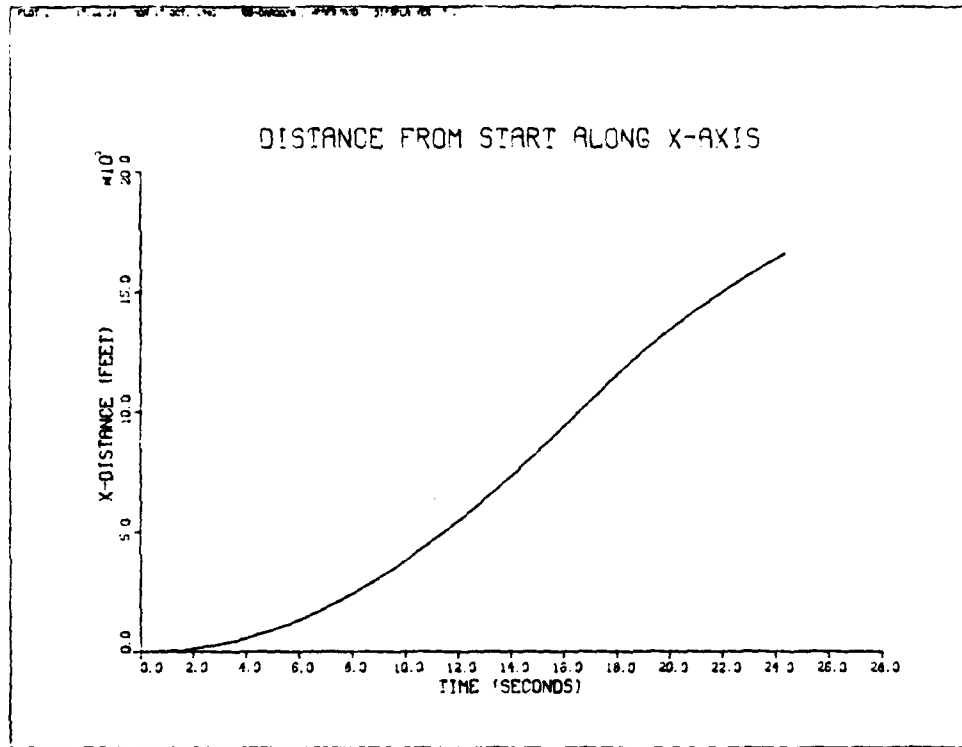
SOFE implements user-supplied data records from one external tape and expects the same number of records every time the tape is read. The external data provided for the rocket car includes accelerometer, range, azimuth, and elevation data. This data is interpolated to .002 second intervals using the cubic spline interpolator implemented in SOFE. Thus, accelerometer data for integration purposes is available every .002 seconds while the specified measurement update interval of .05 seconds insures that actual, not interpolated values for the radar measurements are used.

#### Accelerometer Calibration

The first run through the data using SOFE is made to check the calibration of the accelerometer data. The seven state extended Kalman filter as implemented in SOFE is run without incorporating any radar measurements. Integration

of accelerometer data provides state estimates of  $x$  position and velocity. We desire to compare the estimate of  $x$  velocity from SOFE at FIM trap entry time to the actual value recorded by the FIM system. The FIM officials had used a small radio transmitter to record the time of vehicle entry into the first trap. This constant frequency transmitter was designed to stop transmission while the car was in the first trap, and then begin transmission upon trap exit. Based on frequency data from this transmitter, AFFTC engineers calculated trap entry time as 18.65 seconds from the start of the run (3). The estimate of state  $x_3$ , velocity along the  $x$ -axis, based on integrating the accelerometer data is checked against the trap reading at this time. The vehicle trajectory generated by integrating the accelerometer data is presented in Figs. 4.1 through 4.8. The speed as measured by the FIM speed trap at 18.65 seconds is 666.234 mph or 977.1432 ft/sec. The state estimate of  $x$ -velocity at this time based on integration of accelerometer data is 978.582 ft/sec. The FIM system showed that the vehicle was in the first speed trap for .108 seconds (3). At an average speed of 978.582 ft/sec over the trap distance of 105.6 ft, we confirm a time of .1079 seconds in the trap. The peak speed based on integration of accelerometer data alone is 1080.05 ft/sec or 736.4 mph. This velocity occurs at 16.85 seconds into the run and results in a Mach number of 1.006 when referenced to the speed of sound of 1073.536 ft/sec. The accelerometer data indicates

(a)



(b)

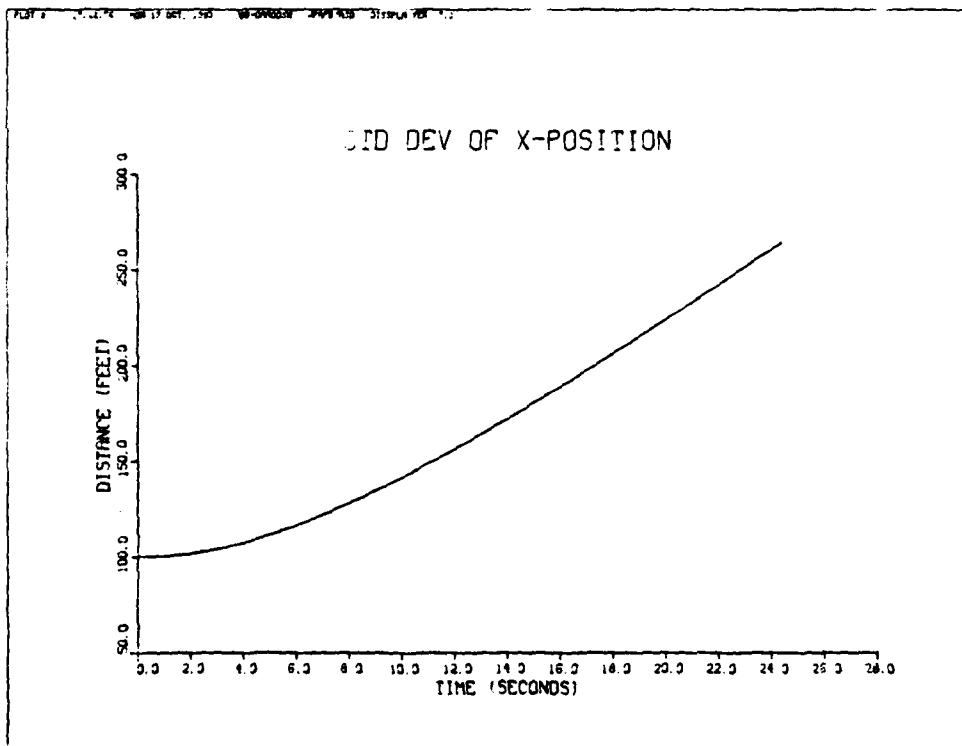
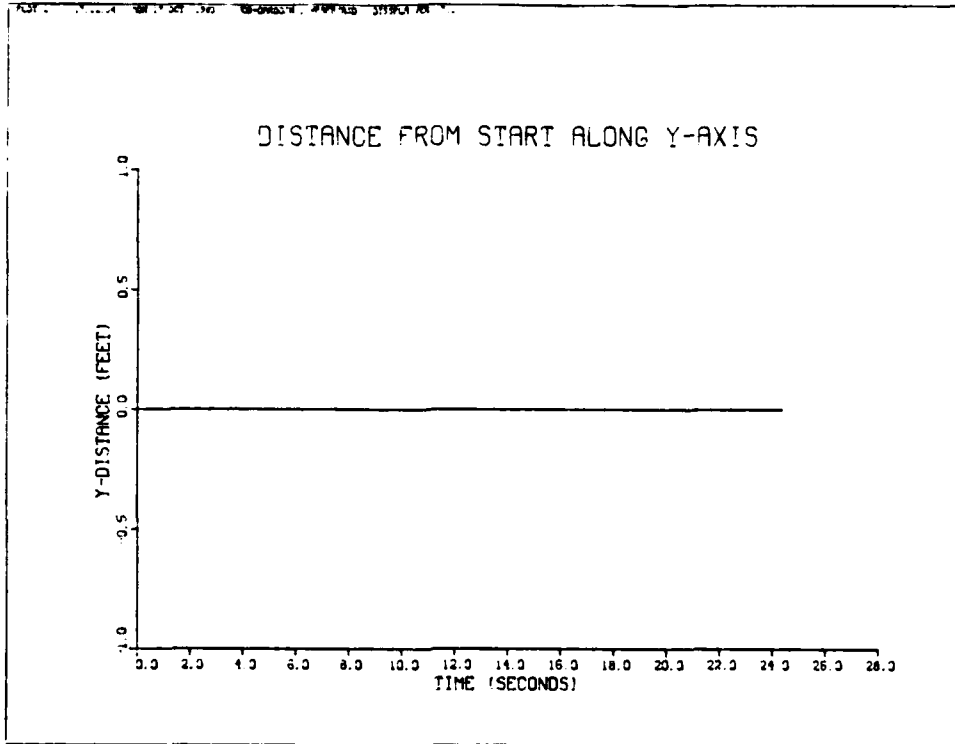


Fig. 4.1(a),(b) Accelerometer model for  $x_3$  - No measurements

(a)



(b)

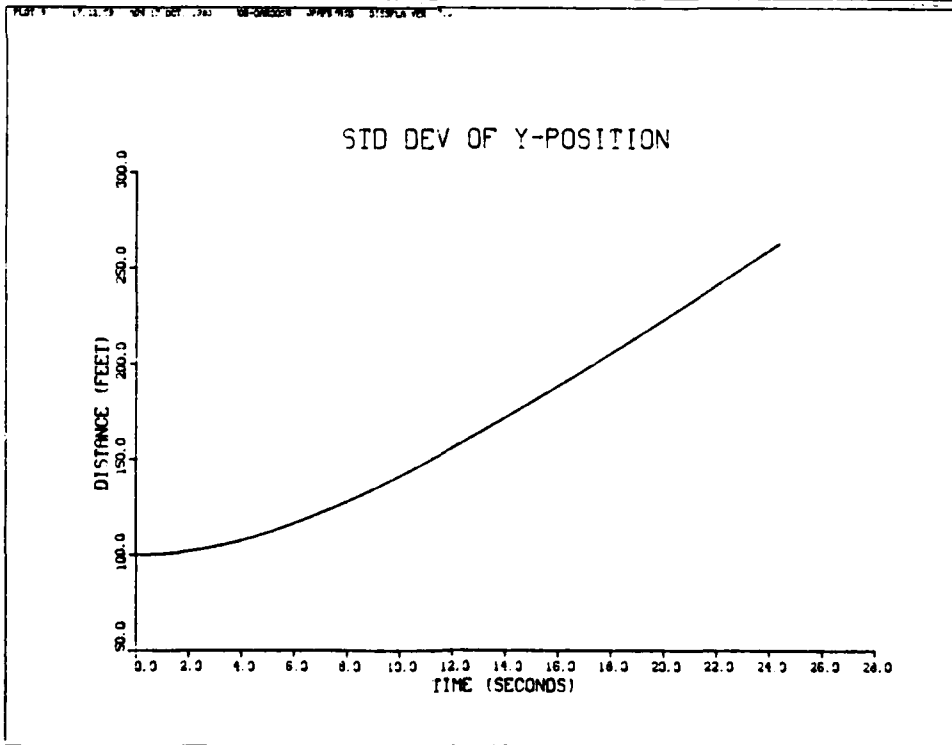
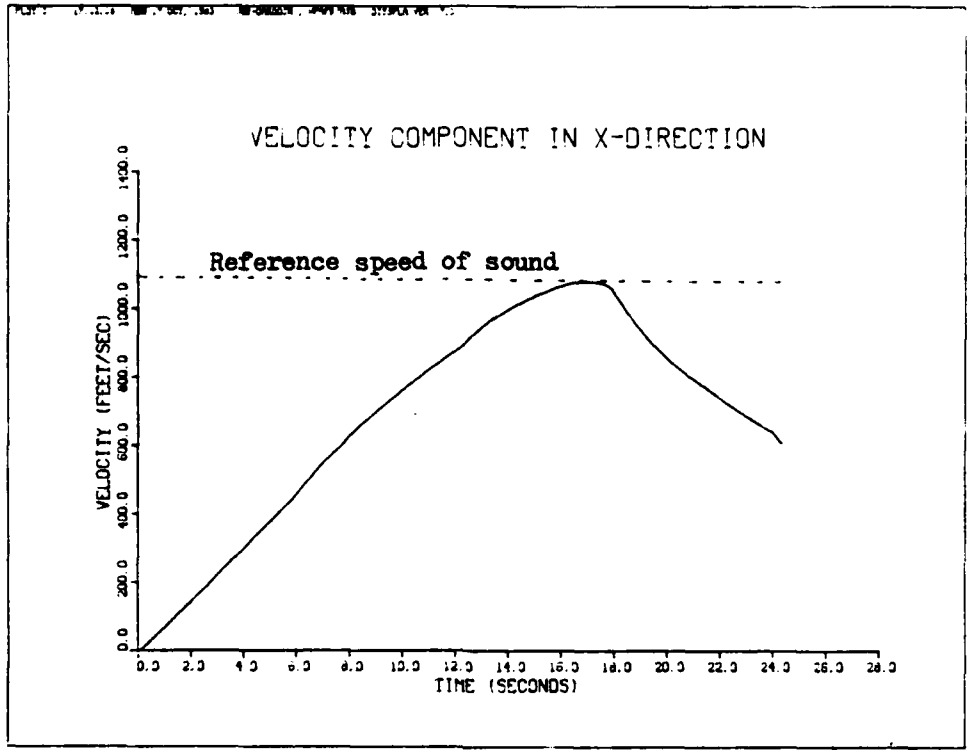


Fig.4.2(a),(b) Accelerometer model for  $x_3$  - No measurements

(a)



(b)

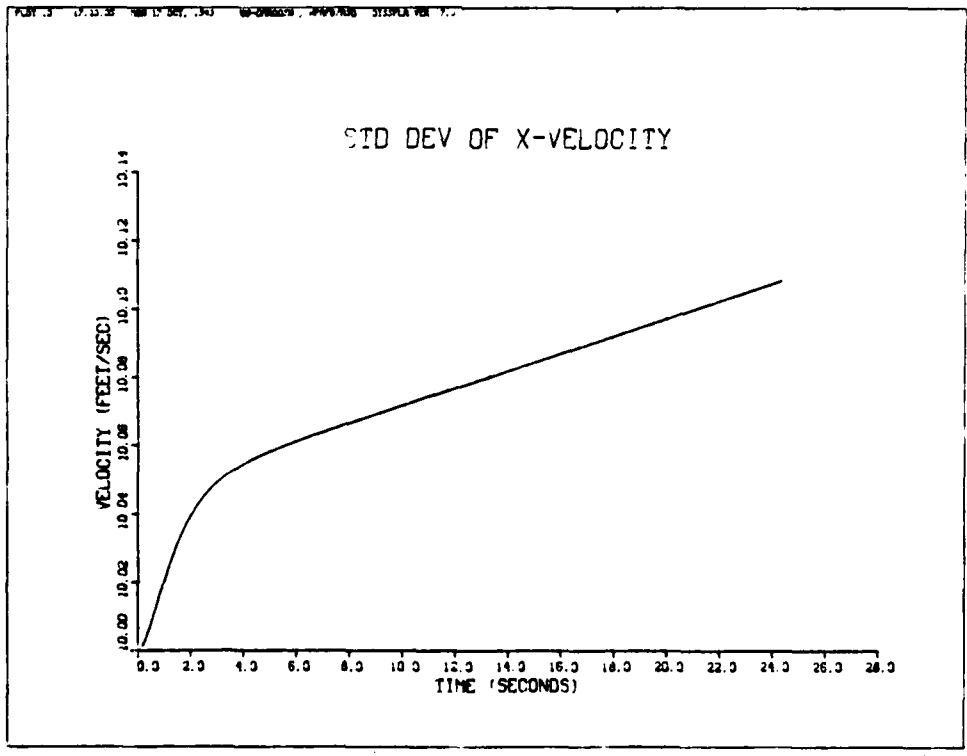
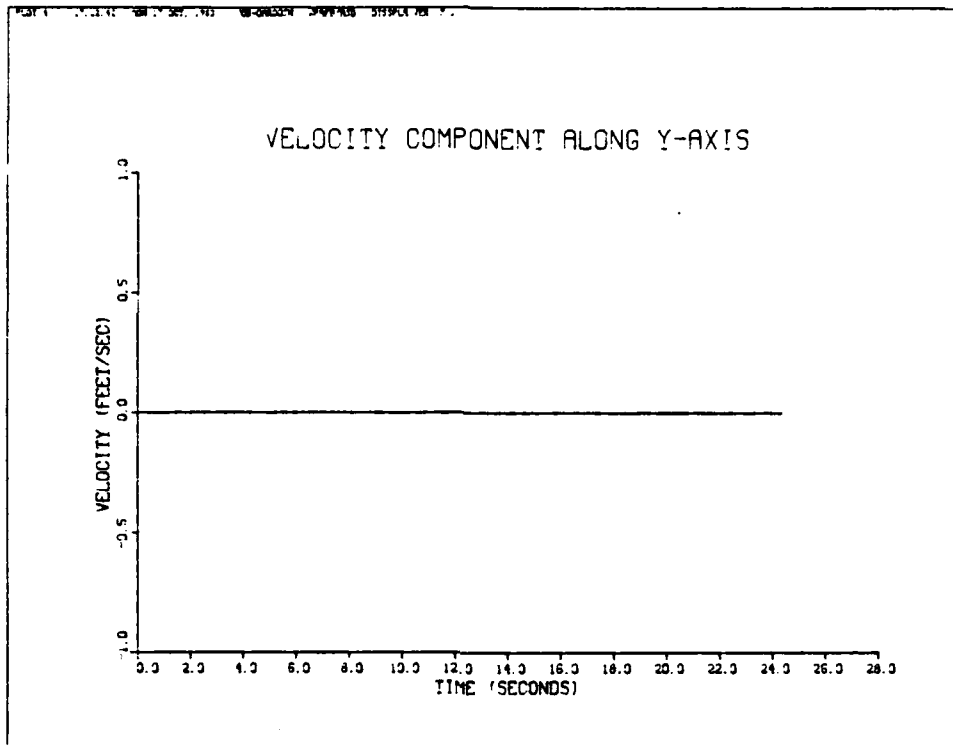


Fig. 4.3(a),(b) Accelerometer model for  $x_3$  - No measurements

(a)



(b)

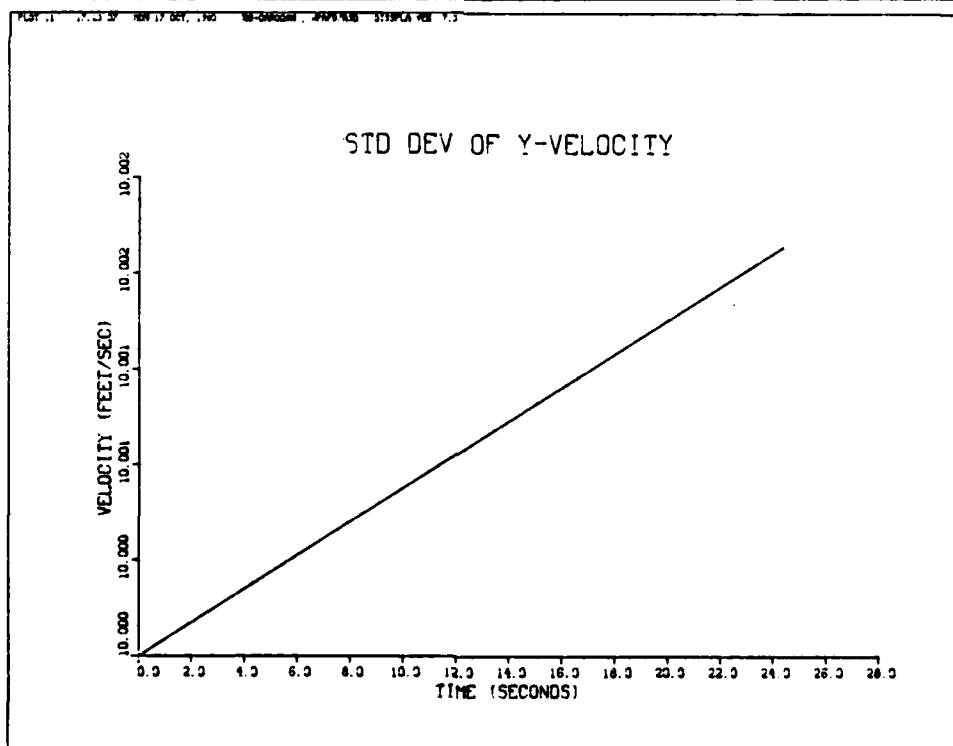
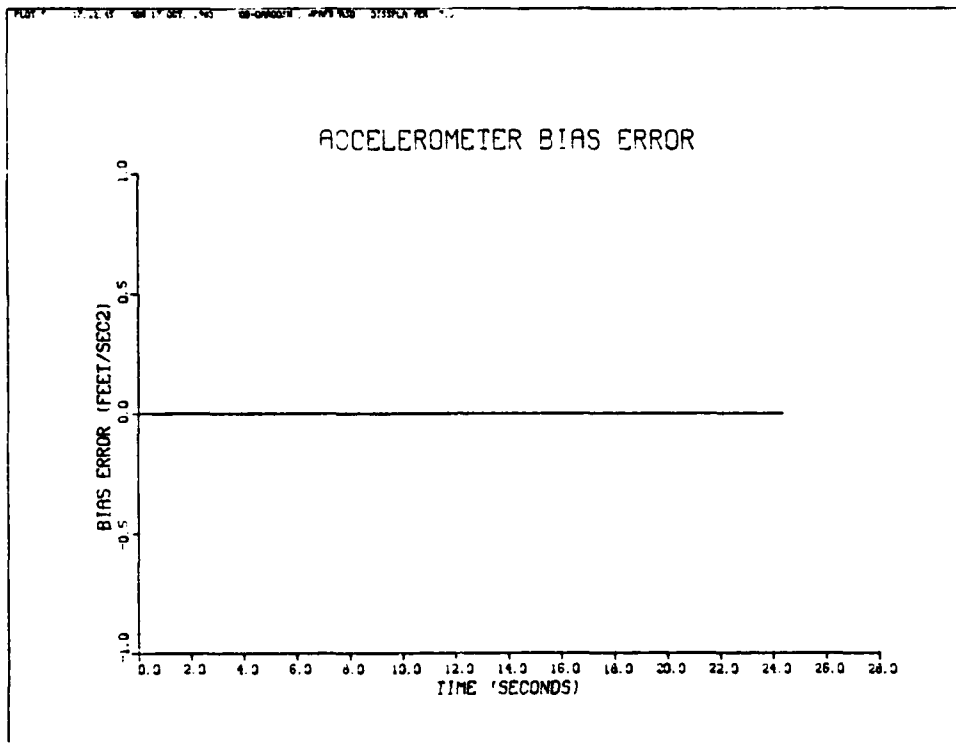


Fig. 4.4(a),(b) Accelerometer model for  $x_3$  - No measurements

(a)



(b)

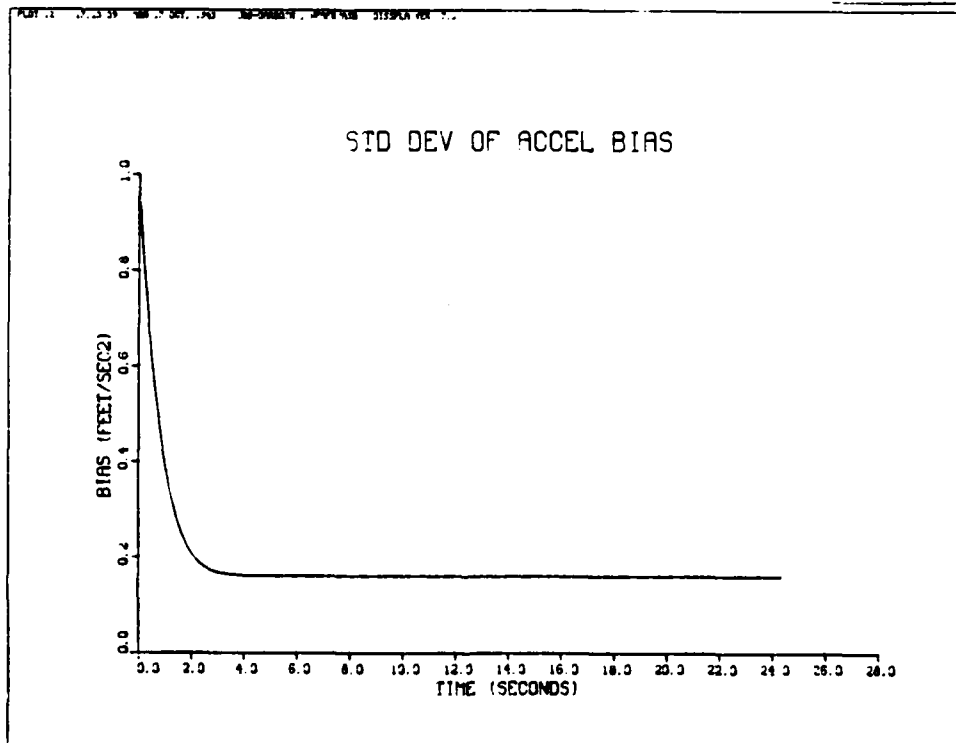
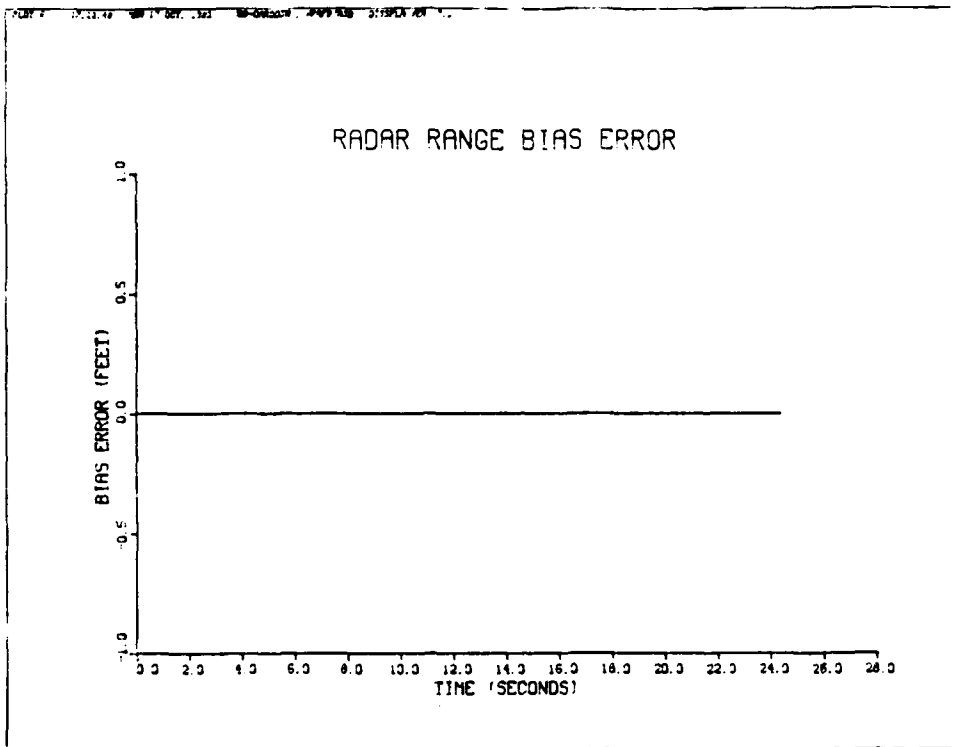


Fig. 4.5(a),(b) Accelerometer model for  $x_3$  - No measurements



(a)



(b)

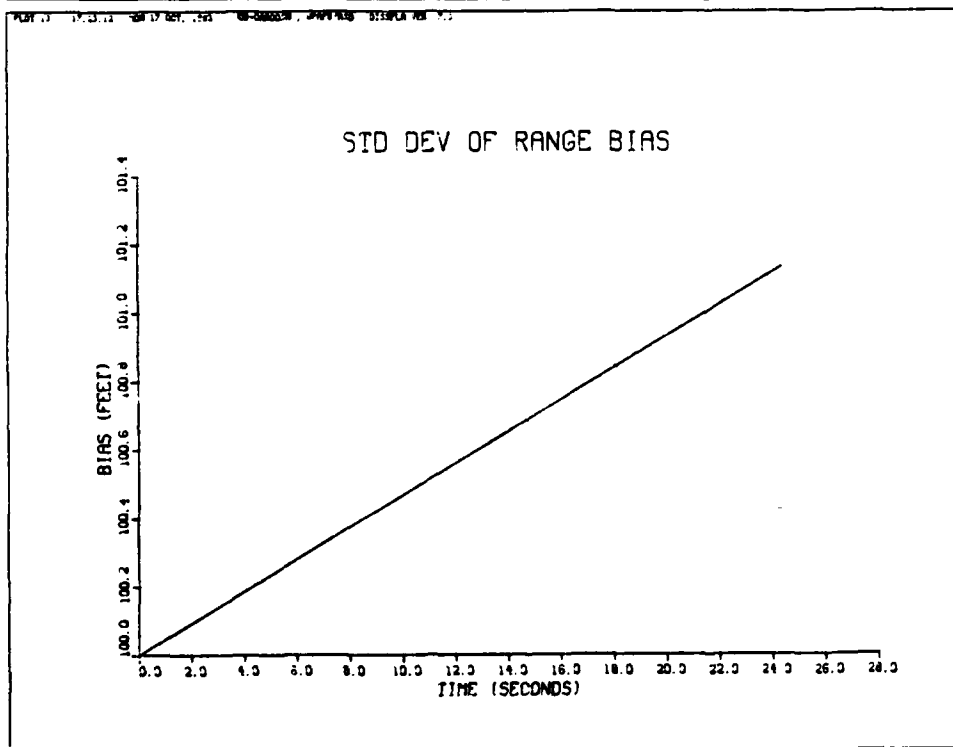
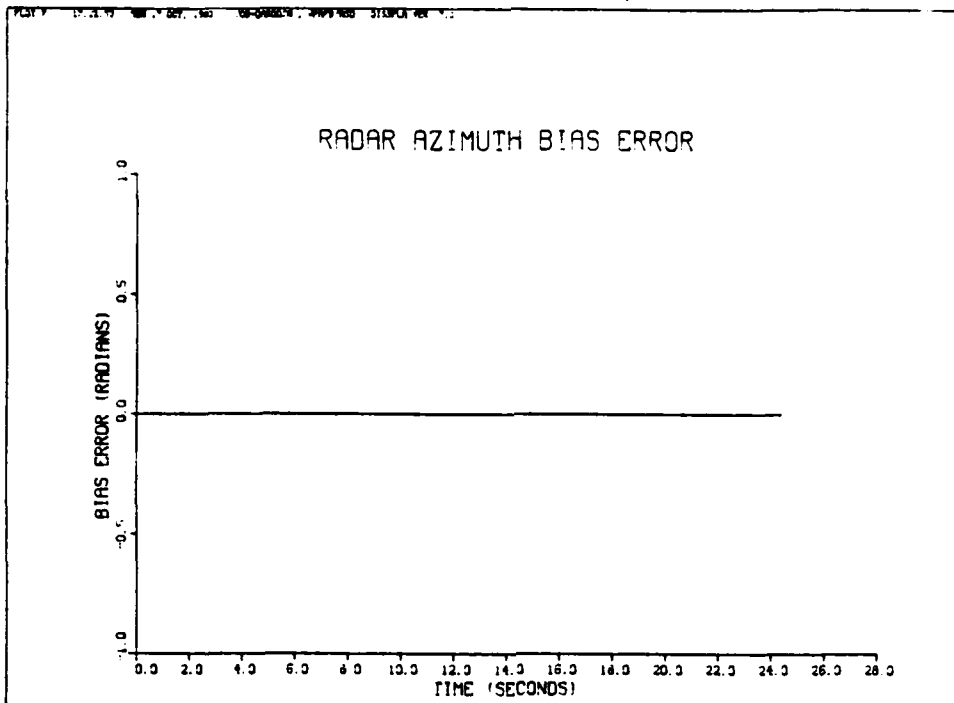


Fig. 4.6(a),(b) Accelerometer model for  $x_3$  - No measurements

(a)



(b)

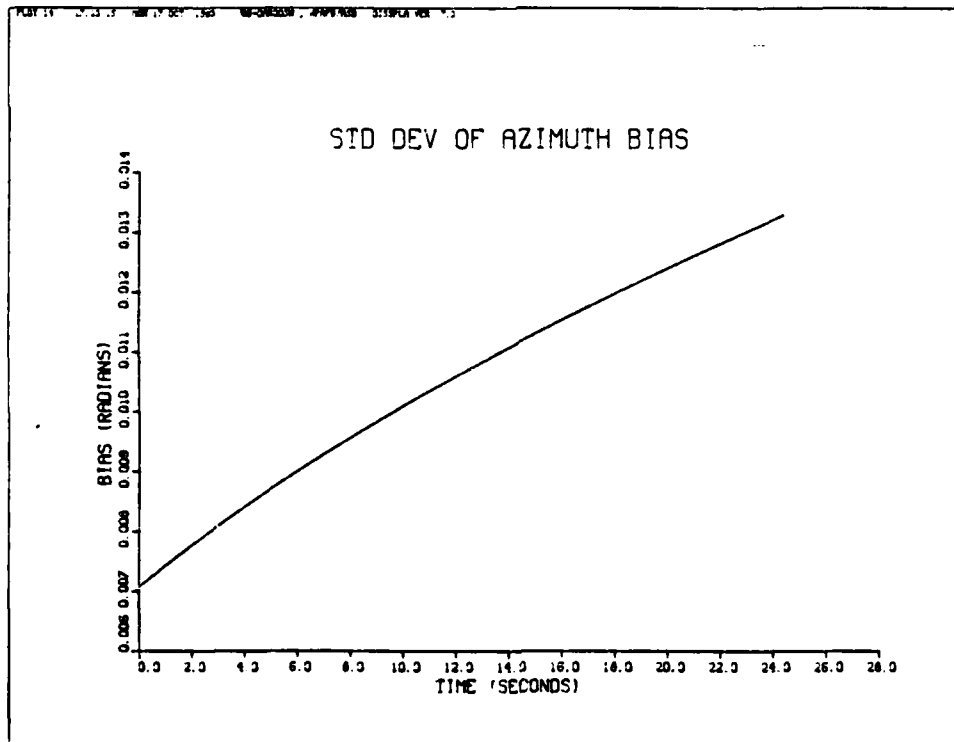
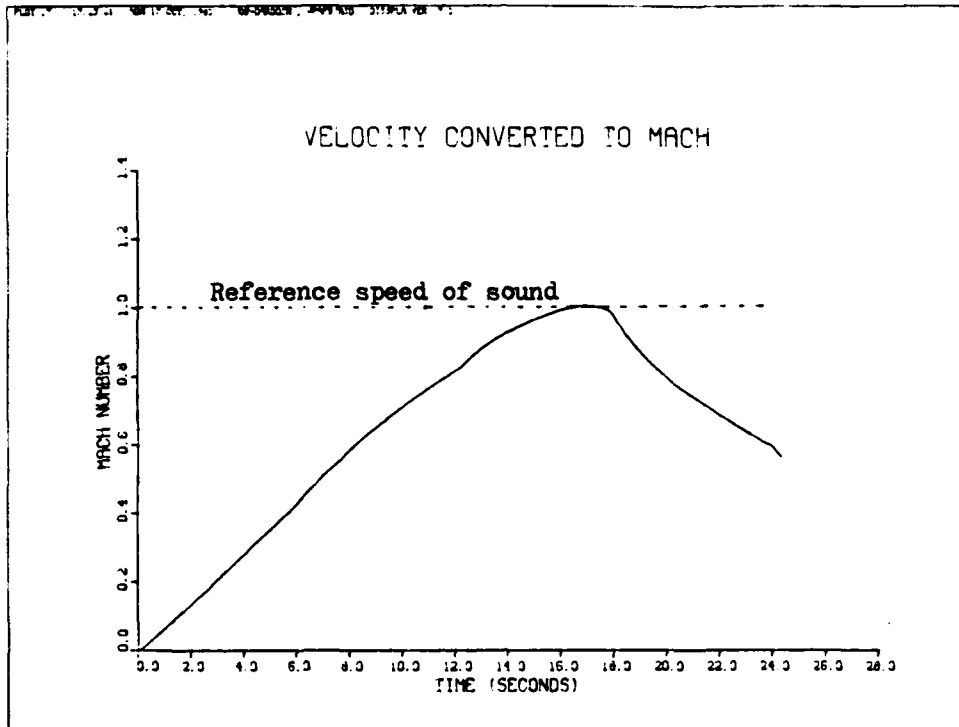


Fig 4.7(a),(b) Accelerometer model for  $x_3$  - No measurements

(a)



(b)

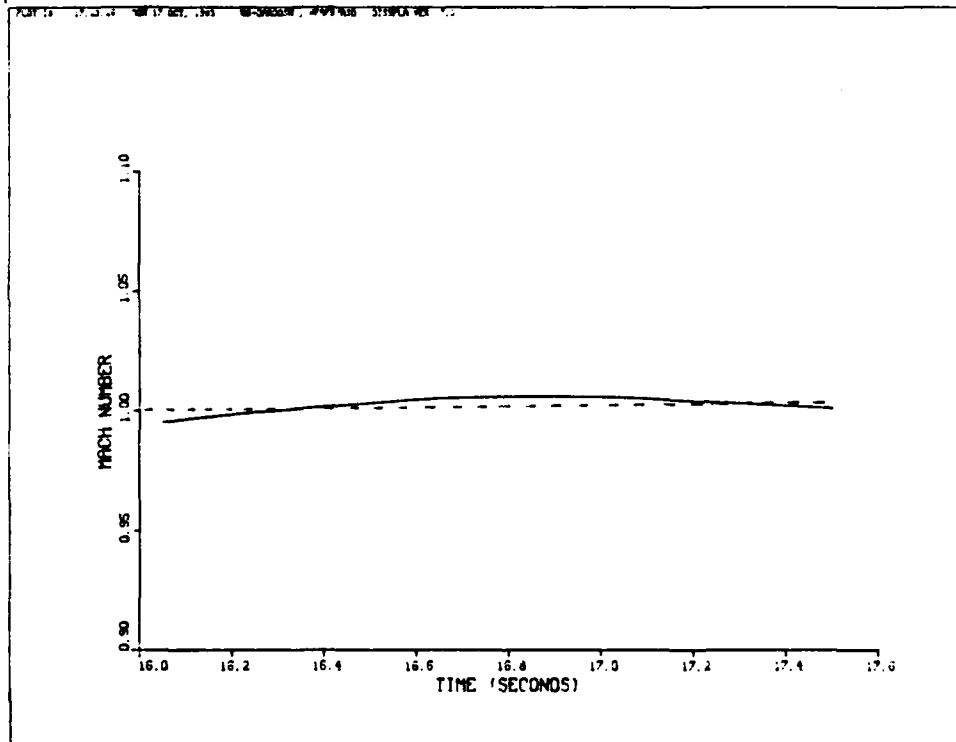


Fig. 4.8(a),(b) Accelerometer model for  $x_3$  - No measurements

the rocket car was above the reference Mach number of one for approximately 1.25 seconds.

Figure 4.2(a) indicates that there is no deviation from center-line due to our model for y velocity. Without any measurements, no estimate of y position or velocity can be made. Note also that the standard deviations of state estimates increase over the time interval. No reduction in our initial values for standard deviation is possible without incorporating measurements.

#### Calculation of Measurement Noise Variance

Before incorporating the available radar measurements of range and azimuth it is necessary to determine the errors inherent in these observations. Although the specifications for the radar are available, one has sufficient reason to doubt the validity of these numbers. The main reason for concern is the way the radar is used to track the vehicle. This particular radar is located up to 4.5 miles from the vehicle on a hill overlooking the lake bed. A tracking radar normally used to track airborne vehicles equipped with transponders is being used in a "look-down" mode into ground clutter at a target not equipped with a transponder. As described in Chapter I, we know the range measurement has a two-second-long interval when the radar picked up a larger vehicle. In addition to the known error in the range measurement this data is highly suspect for the reasons outlined above. Certainly we cannot rely on the specified range RMS error of 15 feet.

Nor is the azimuth measurement expected to maintain the specified RMS error of .005 radian.

The manual tracking adjustment used to align the radar dish with the car is subject to operator errors. An AFFTC review of the video-tape from the television monitor used to adjust azimuth tracking rate shows that the operator was able to keep the cross-hairs on the vehicle for most of the run (3). However, at the beginning of the run when the car is accelerating the most, and immediately after engine burn-out when the car is reaching maximum deceleration, the operator is off the vehicle by up to three car lengths (3). This very subjective estimate of azimuth deviation corresponds to approximately 108 feet. At the minimum range of 18000 feet, this deviation contributes an error in azimuth of up to about .006 radian. This error is therefore the best we could hope for, assuming no inherent azimuth bias error. To estimate the accuracy of range and azimuth measurements, some comparison of actual to expected values is necessary.

Using equations (3-22) and (3-23) for radar range and azimuth based on estimates of x and y position, we desire to compare actual measurements of range and azimuth to filter estimated values without incorporating radar measurements. The dynamics model using accelerometer data is used to derive the estimated range and azimuth trajectories. Based on this model, y position remains at zero while the estimate of x position is provided by twice integrating accelerometer output. By comparing actual to estimated measurements we not

only can find the noise strength of the measurements, but check our equations for range and azimuth used in the filter.

Figures 4.9(a) and 4.9(b) are plots of actual range and estimated range. Figure 4.9(a) includes a plot of the difference between these two values for radar range. It is obvious from these plots that between 16 and 18 seconds the range is tracking a larger vehicle beyond the rocket car. It is also apparent from these plots that the range measurement is indeed extremely "noisy" and has significant errors.

The azimuth measurement, however, appears to be much better. Referring to Fig. 4.10, we can see that the actual and estimated azimuth values are very close. This confirms our assumption that the radar operator did a good job of tracking the car in azimuth.

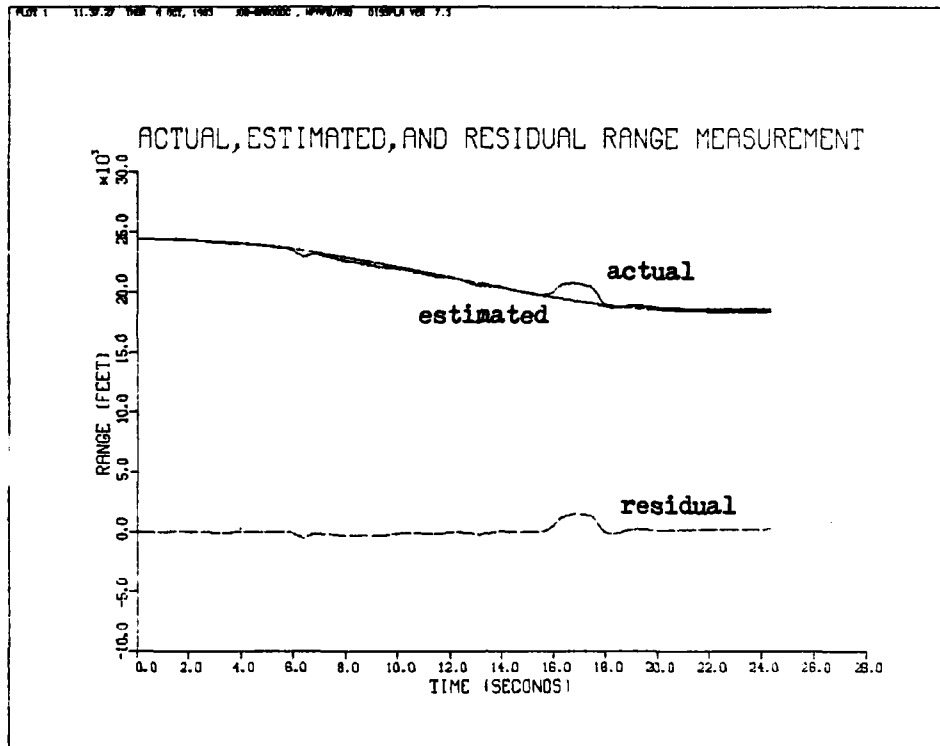
The purpose of comparing actual to estimated measurements is to determine realistic values for the diagonal terms in the measurement noise matrix,  $R(t_i)$ . To accomplish this, we sum the "residuals", or difference between actual and estimated measurements, over the entire time interval. We then calculate a mean and variance for the residual values using the following equations

$$\text{Mean, } \mu_{\text{res}} = 1/N-1 \sum_{i=1}^N r_i \quad (4-1)$$

$$\text{Variance, } \sigma_{\text{res}}^2 = 1/N-1 \sum_{i=1}^N (r_i^2 - \mu^2) \quad (4-2)$$

where  $r_i$  is the residual measurement at a given sample time and  $N$  is the number of sample periods used in the calculations.

(a)



(b)

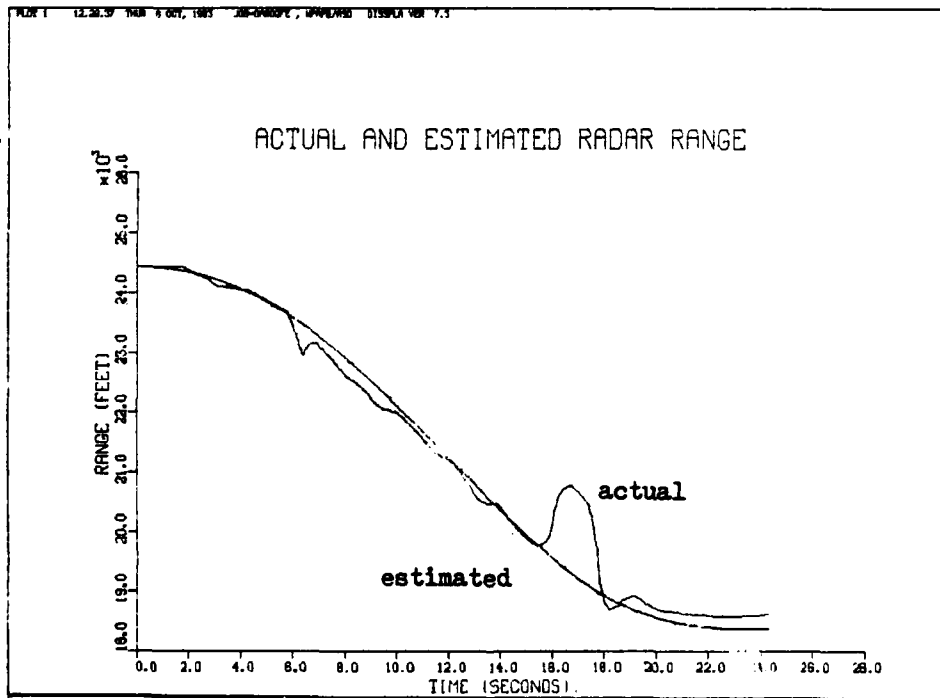


Fig. 4.9(a),(b) Residual range analysis based on an assumed track heading of 180 degrees true.

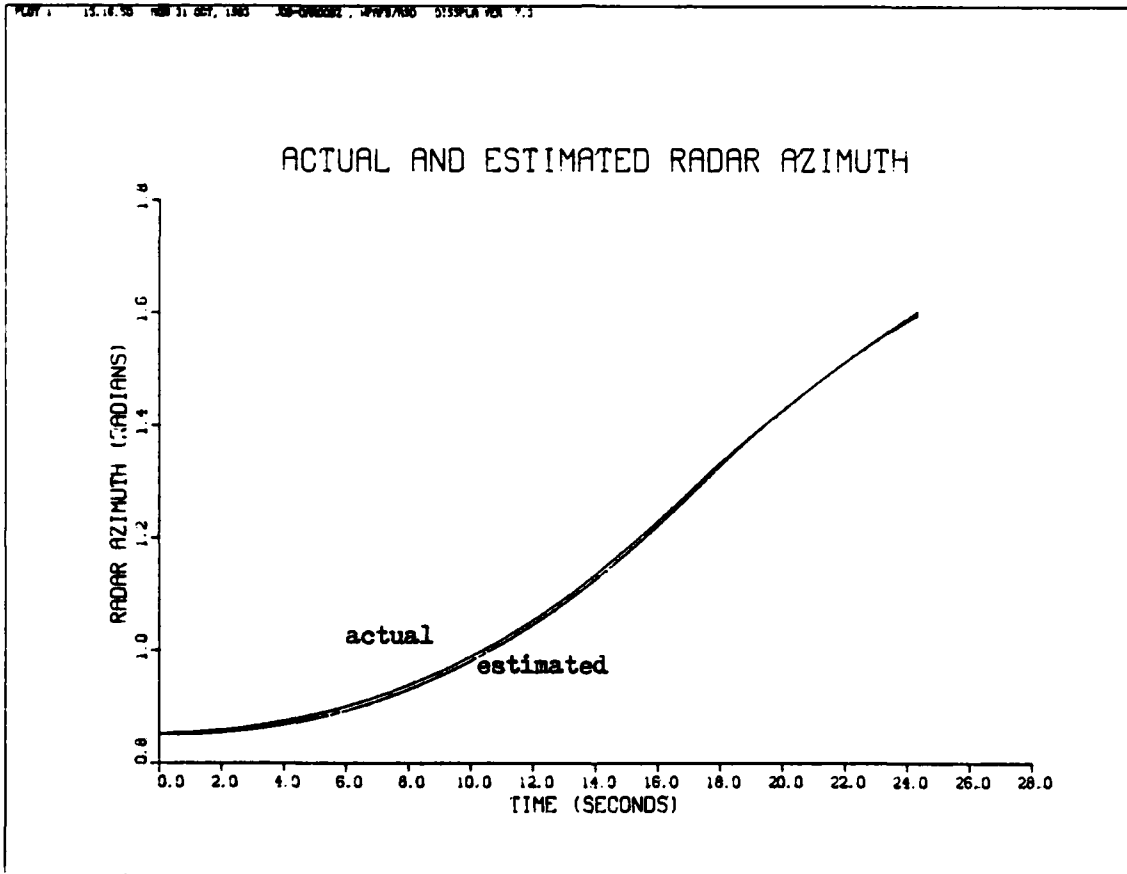


Fig. 4.10 Residual azimuth analysis based on an assumed track heading of 180 degrees true.



An inherent assumption in this residual analysis is that we can employ the principle of "ergodicity" (4). This principle says simply that we can determine the statistics of a random process using only the results of one run through the data rather than a Monte Carlo analysis. We assume that the statistics of the residual measurements can be adequately described using data over the 24 second time interval of interest. The residual sequence can be shown to be a white Gaussian sequence with zero mean and covariance

$$\sigma_{res}^2 = [\underline{H}(t_i)\underline{P}(t_i^-)\underline{H}^T(t_i)+\underline{R}(t_i)] \quad (4-3)$$

Thus we can solve for an estimate of the measurement noise,  $\hat{R}(t_i)$ , for each observation using:

$$\hat{R}(t_i) = \sigma_{res}^2 - \underline{H}(t_i)\underline{P}(t_i^-)\underline{H}^T(t_i) \quad (4-4)$$

Once the filter calculated values for error variance  $\underline{P}(t_i^-)$ , reach "steady state" conditions, the second term in (4-4) becomes negligible when compared to the residual variance  $\sigma_{res}^2$ . Thus, we use the calculated residual variance from (4-2) to yield the initial estimate of measurement noise,  $\hat{R}(t_i)$ .

In calculating the range error variance no residuals in excess of 300 feet are used. This effectively "blocks" the erroneous range measurements between 16-18 seconds, resulting in the use of 450 of 487 total measurements between 0 to 24.3 seconds. All of the azimuth measurements between 0 to

24.3 seconds are used to calculate the mean and variance of the azimuth residual.

The result of this residual analysis indicates an error variance on the range residual of 22455.82 ft<sup>2</sup>. The azimuth residual analysis shows an error variance of  $.5389 \times 10^{-4}$  rad<sup>2</sup>. These variances yield calculated RMS errors of 149.85 ft and  $0.734 \times 10^{-2}$  radian for the range and azimuth measurements, respectively. As expected, the range measurement error is much greater than the specified error due to the way the radar is used to track the vehicle. The azimuth error is very close to the first guess of .006 radian.

The actual and estimated radar range measurements appear to diverge after approximately 20 seconds. Referring to Fig. 4.9(b), the actual radar range looks fairly good between 20 and 24 seconds. This divergence of filter computed and actual range values caused some concern. In fact, the initial extended Kalman filter runs indicated that the state  $x_2$ , y position, grew unrealistically to approximately 300 feet by 24 seconds. This growth in  $x_2$  is caused by the range measurement which appears accurate between 20 to 24 seconds. It would seem that perhaps our initial assumption of the test track heading is incorrect. In fact, if the actual track heading is 179 degrees true, not due south, this one degree deviation would cause an approximate change in y position of 300 feet if the car is 17000 feet down-track. Thus, it is necessary to correct the relations between radar measured components,  $x_r$  and  $y_r$ , to the earth-fixed coordinate system.

Referring to Fig. 4.10(a), the coordinate translation becomes:

$$x_r = DELX + (\cos 179^\circ)x_1 + (\sin 179^\circ)x_2 \quad (4-5)$$

$$y_r = DELY + (\sin 1^\circ)x_1 + (\cos 1^\circ)x_2 \quad (4-6)$$

or

$$x_r = DELX - .99985x_1 + .01745x_2$$

$$y_r = DELY + .01745x_1 + .99985x_2$$

When these corrections are applied to (3-22) and (3-23) and the residual plotting and variance calculations are made, the actual and estimated range measurements are much closer. The corrected plots of range and azimuth are shown in Fig. 4.11(a), (b) and 4.12. With these corrections, calculated residual variance for range becomes  $16807.66 \text{ ft}^2$  and azimuth variance reduces to  $.3573 \times 10^{-4} \text{ rad}^2$ . These lower variances result in RMS errors for range and azimuth of 129.88 feet and .005977 radian, respectively. Note that we have calculated an error for the azimuth which matches our initial guess of .006 radian. It is apparent that the one degree correction is closer to the true track heading and reduces the majority of modeling error. Thus, we have computed the estimated measurement noise strength matrix,  $\hat{R}(t_i)$ :

$$\hat{R}(t_i) = \begin{bmatrix} 16807.66 & 0 \\ 0 & .3573E-4 \end{bmatrix} \quad (4-7)$$

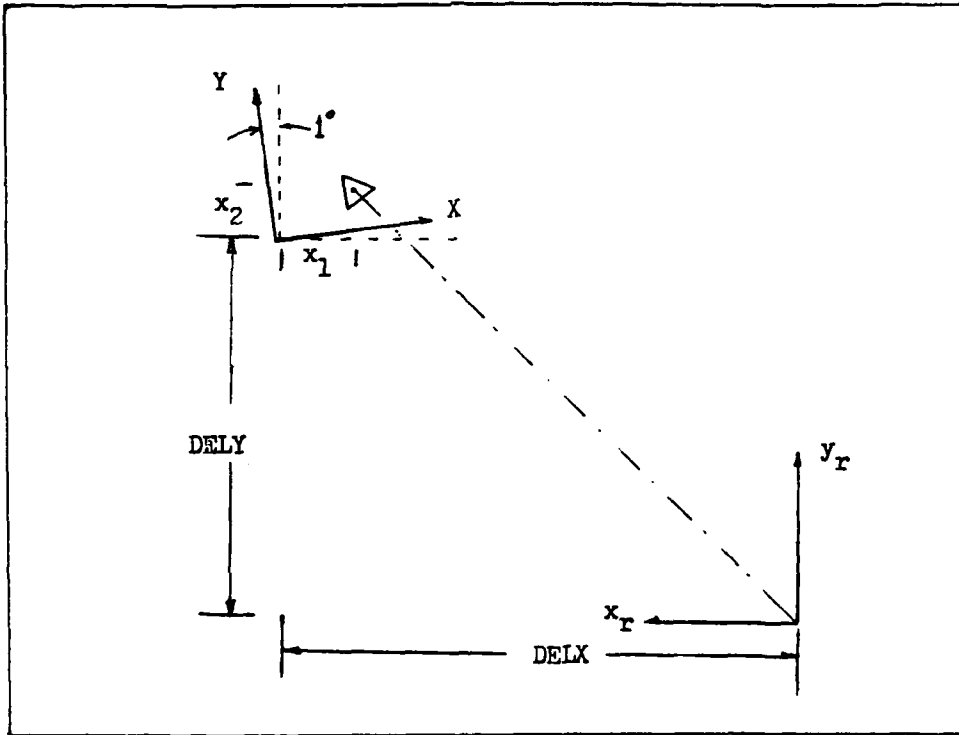
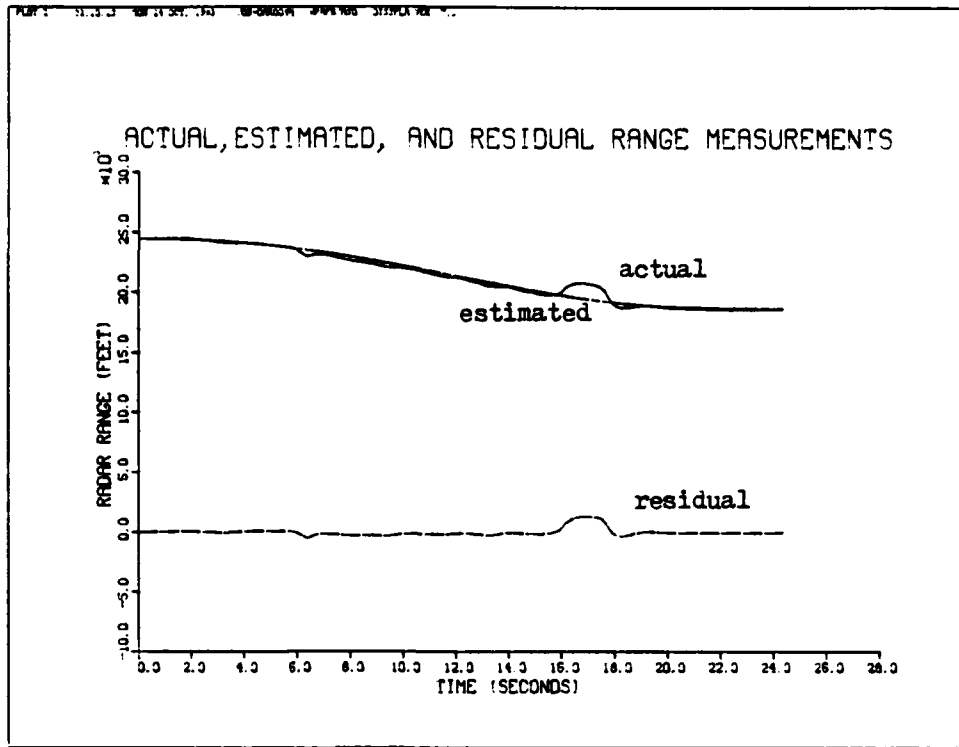


Fig. 4.10 (a) Corrected Coordinate Frame

(a)



(b)

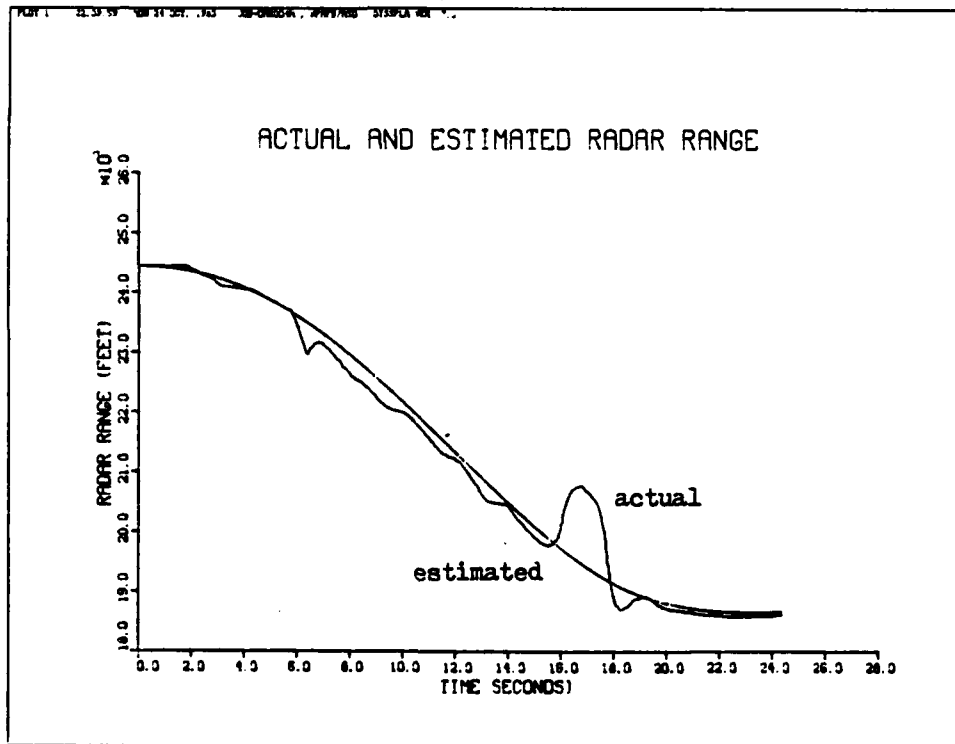


Fig. 4.11(a),(b) Residual range analysis based on assumed track heading of 179 degrees true.

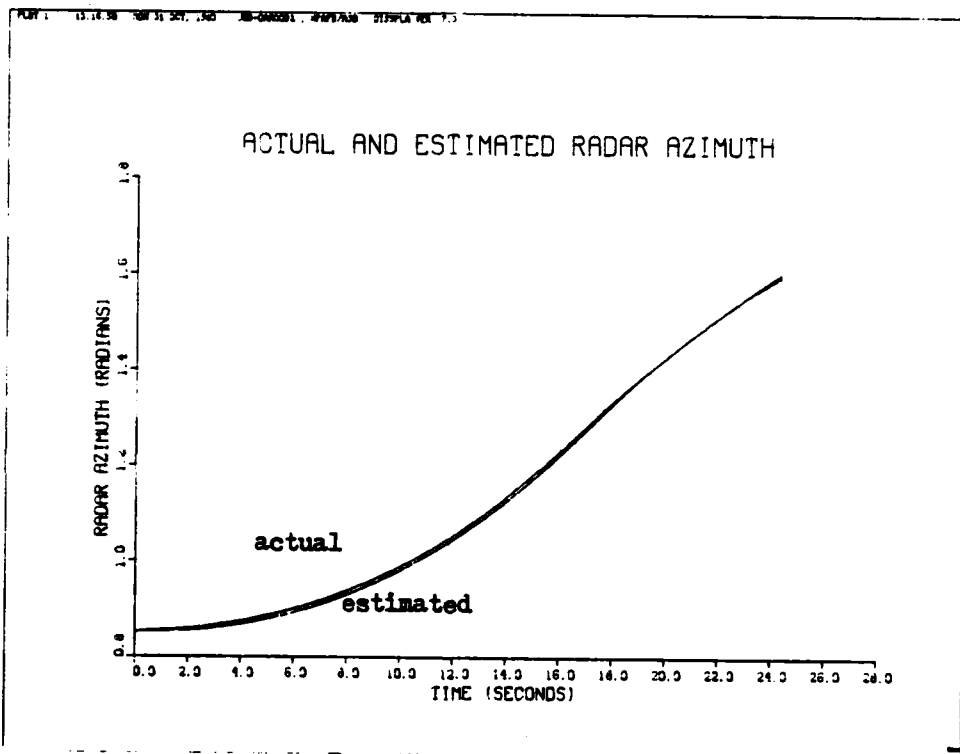


Fig. 4.12 Residual azimuth analysis based on assumed track heading of 179 degrees true.

### Check of Filter Implementation

Based on the vehicle trajectory generated from the accelerometer data, we desire to check the calculation of the observation matrix,  $H[t_i; \hat{x}(t_i^-)]$ . The model we are using to describe the propagation of x velocity,  $x_3$ , relies heavily on the accelerometer measurements of specific force. The filter receives very good information on the behavior of x velocity and position, but relatively poor information on y velocity and position. To check our implementation of range and azimuth measurements in the filter, we desire to remove accelerometer specific force from the model for  $x_3$ . If the range and azimuth measurements independently track the basic trajectory of the vehicle, we can be reasonably sure the observation matrix linearization has been calculated correctly. Note that we are looking for trends and not specific confirmation of state estimates. Thus, we expect the range and azimuth to show a similar trajectory for the car to that generated by the accelerometer, but not a one-for-one comparison. The purpose of such an analysis is simply to insure that we have correctly incorporated the measurements into the extended Kalman filter state and covariance update relations. The model for the radar range and azimuth measurements is repeated here for reference:

$$z_1 = [(\text{DELX} - .99985x_1 + .01745x_2)^2 + (\text{DELY} + .01745x_1 + .99985x_2)^2 + z_r^2]^{1/2} + x_6 + v_1$$

$$z_2 = \arctan[(\text{DELY} + .01745x_1 + .99985x_2) / (\text{DELX} - .99985x_1 + .01745x_2)] + x_7 + v_2$$

Applying (2-15) to these equations we form the observation sensitivity matrix,  $\underline{H}[t_i; \hat{\underline{x}}(t_i^-)]$ . It is the model for measurement incorporation,  $\underline{z}(t_i)$ , and the calculation of  $\underline{H}[t_i; \hat{\underline{x}}(t_i^-)]$  that we desire to check. By comparing state trajectories of position and velocity independently obtained from each measurement, we hope to confirm our calculations and modeling techniques.

The primary reason for deviations between measurement trajectories and the accelerometer profile is due to the rather crude model we substitute for the x-velocity state,  $x_3$ . We now choose this state to be modeled as a random walk of the form

$$\dot{x}_3 = w_3(t)$$

where the driving noise,  $w_3(t)$ , has a relatively high strength to account for our uncertainty in such a model and allow closer tracking of actual data. Modeling this state as we have, the x velocity is considered a constant. Any change to its value based on measurement updates is done in a step-like manner. Therefore, we do not expect to get exact agreement with accelerometer results.

The model for x-velocity is incorporated into a six state extended Kalman filter where accelerometer error,  $x_5$ , has been removed. The filter is run using range measurements



only, azimuth measurements only, and both measurements combined. The results of these three runs of the extended Kalman filter are shown in Fig. 4.13 to 4.16. Plots are made of the estimates of  $x$  and  $y$  position and velocity. Part (a) of each figure is the depicted state estimate generated using range measurements only. Part (b) is the state estimate generated using azimuth measurements only, while part (c) of each figure shows the result of combining both range and azimuth. We see, in fact, that position and velocity along the  $x$ -axis behave as we would expect from the accelerometer trajectory shown in Figs. 4.1 through 4.4. However, the geometry of the radar position to the vehicle is not conducive to accurate estimates of deviations along the earth-fixed  $y$ -axis. The range measurement is the only means by which we can hope to estimate position and velocity along the  $y$ -axis. The state estimates of these values are subject to any errors in the range measurement and indicate only weak observability of these states. The range measurement is ignored between 16-18 seconds to account for the known error in this measurement during this interval. Due to the geometry of the problem, the range measurement is even less likely to track the vehicle along the  $x$ -axis correctly. This can be seen from comparing the plots of  $x$ -position and velocity for range only to the plots of these states with azimuth only and both measurements combined. From these plots, it is apparent that the azimuth does a credible job of tracking changes in position and velocity along the  $x$ -axis. Conversely, the azimuth

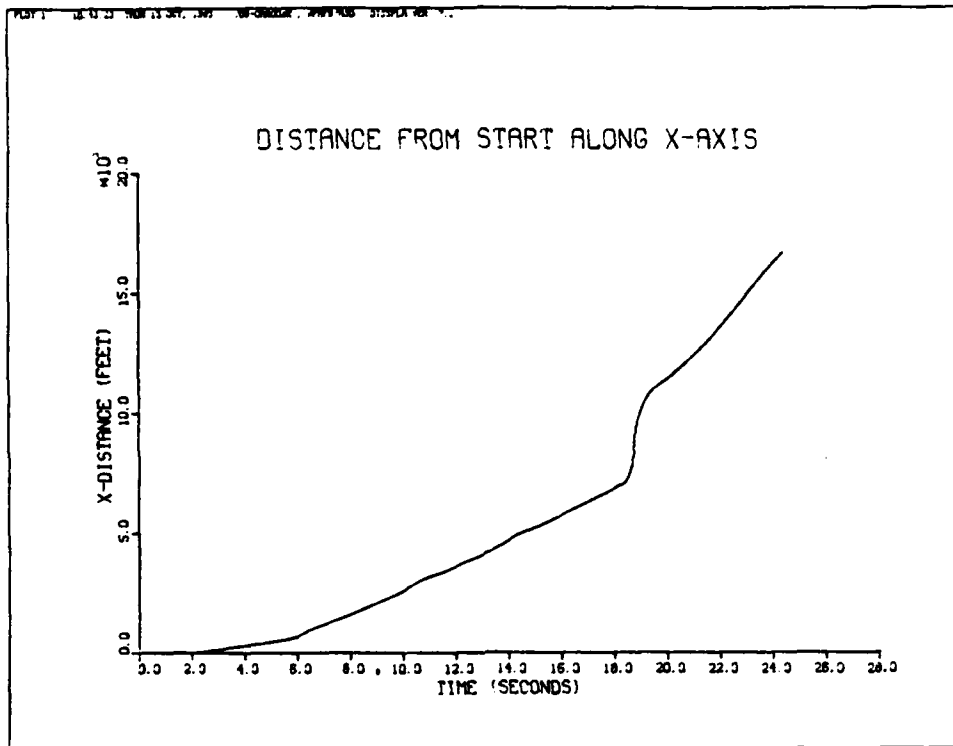


Fig. 4.13(a) Random walk model for  $x_3$  - Range only

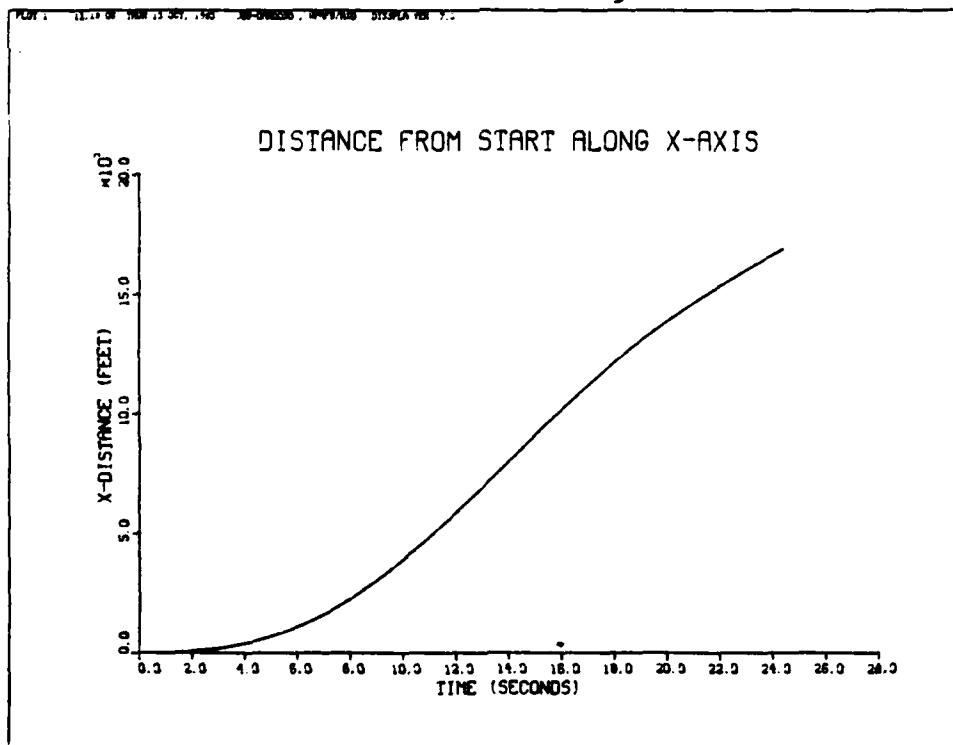


Fig. 4.13(b) Random walk model for  $x_3$  - Azimuth only

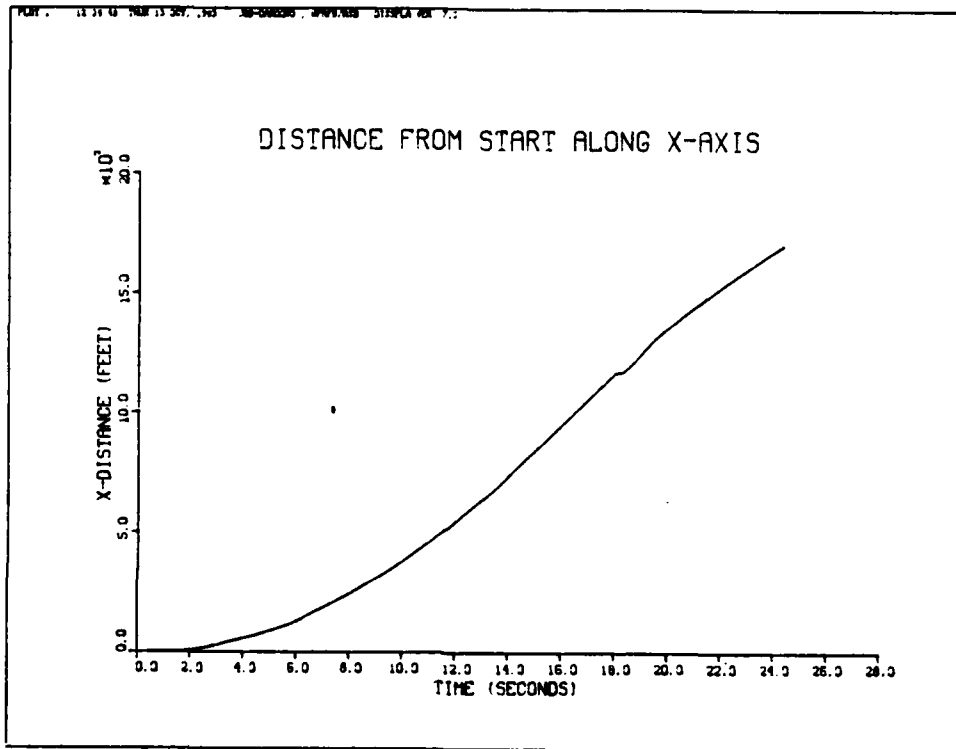


Fig. 4.13(c) Random walk model for  $x_3$  - Range and Azimuth

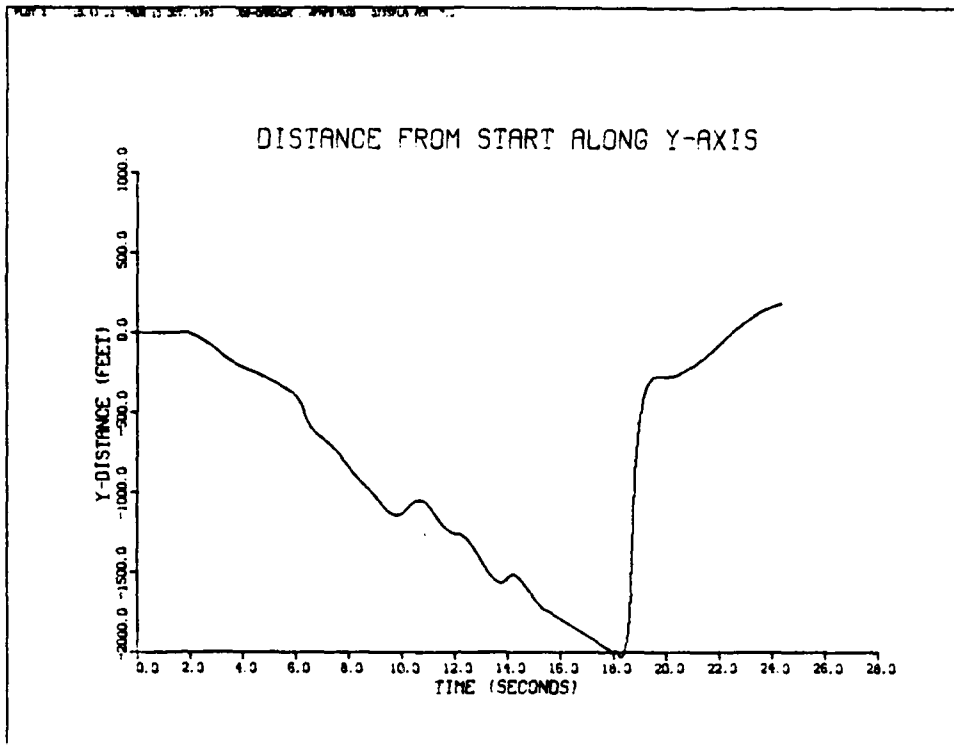


Fig. 4.14(a) Random walk model for  $x_3$  - Range only

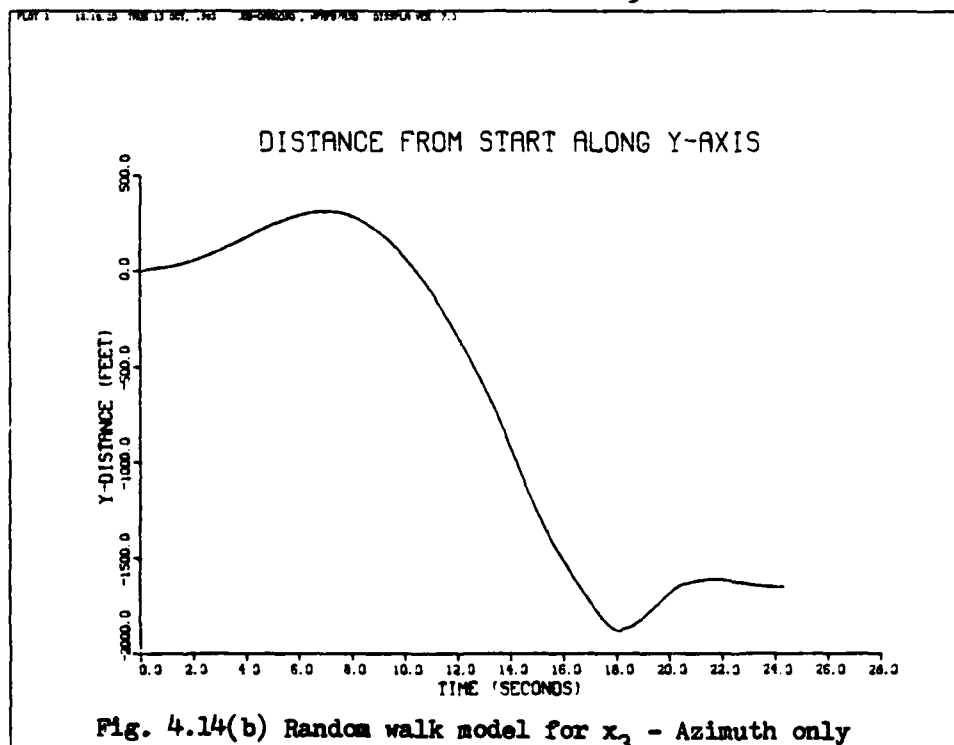


Fig. 4.14(b) Random walk model for  $x_3$  - Azimuth only

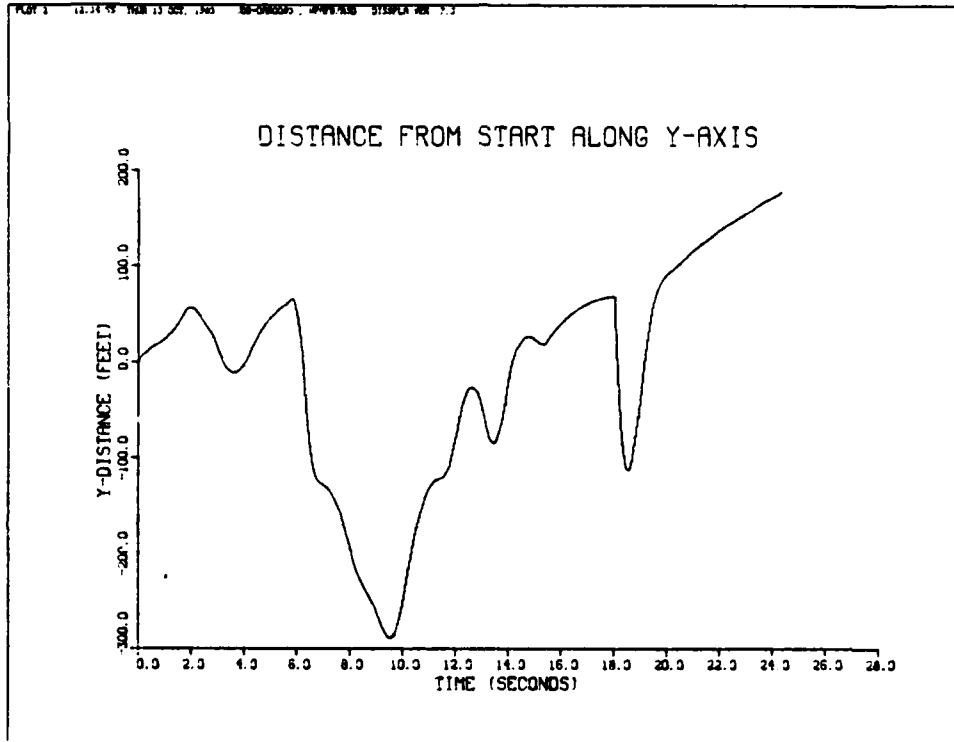


Fig. 4.14(c) Random walk model for  $x_3$  - Range and Azimuth

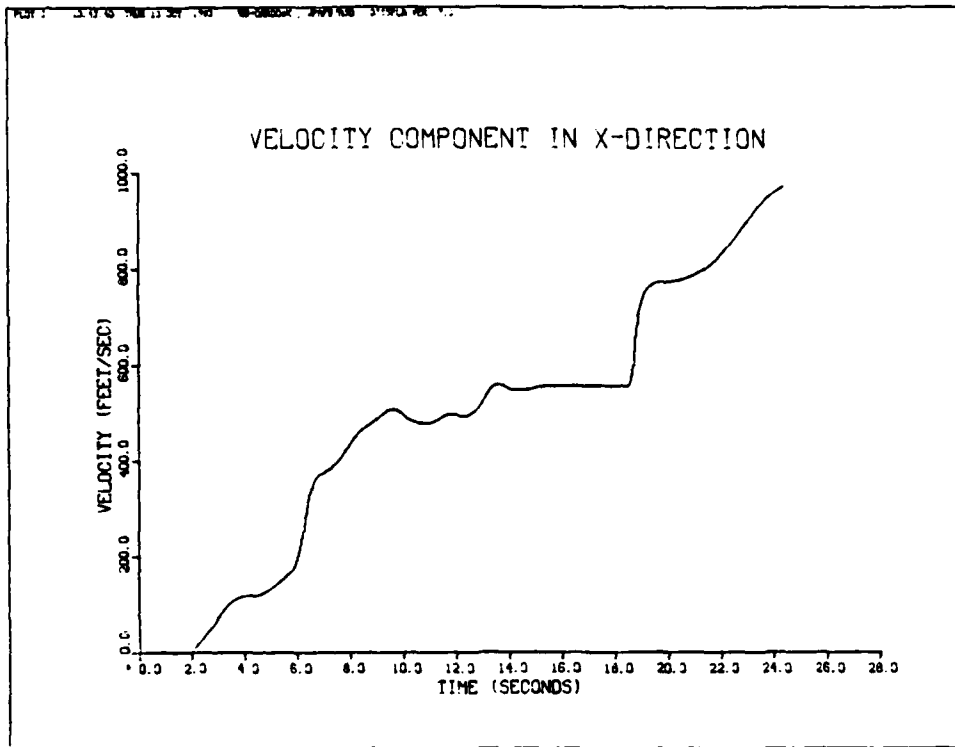


Fig. 4.15(a) Random walk model for  $x_3$  - Range only

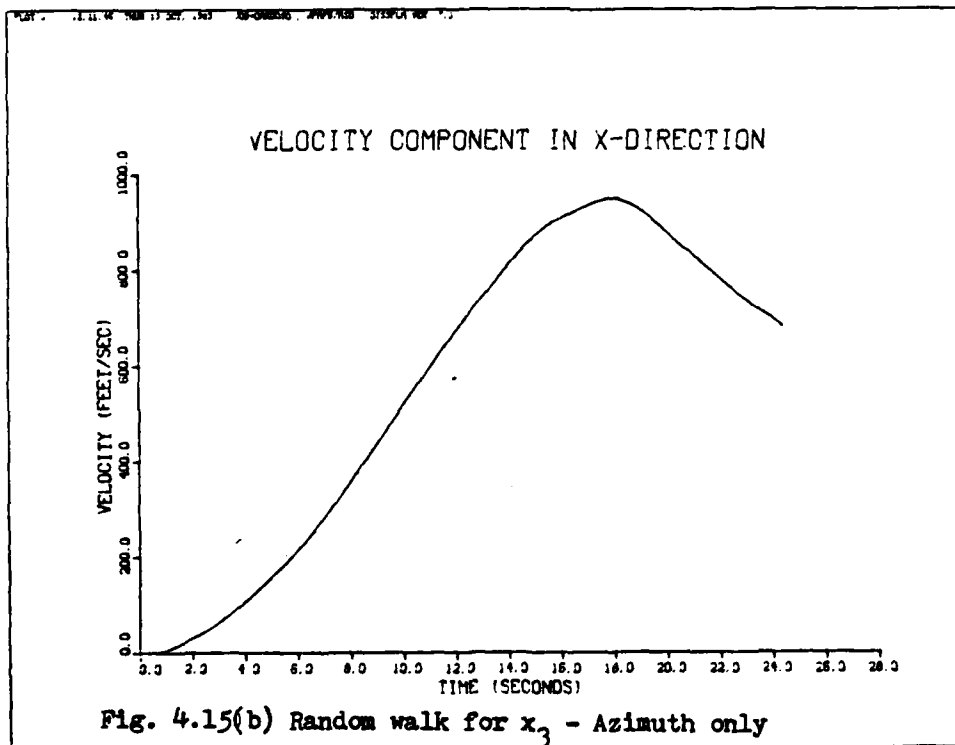


Fig. 4.15(b) Random walk for  $x_3$  - Azimuth only

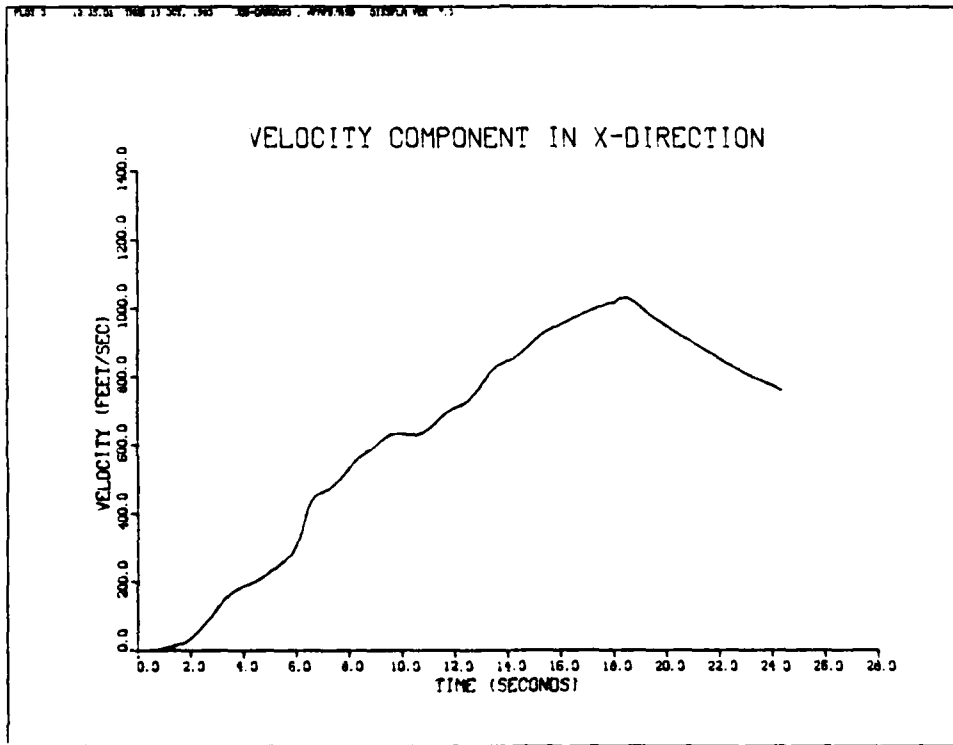


Fig. 4.15(c) Random walk model for  $x_3$  - Range and Azimuth

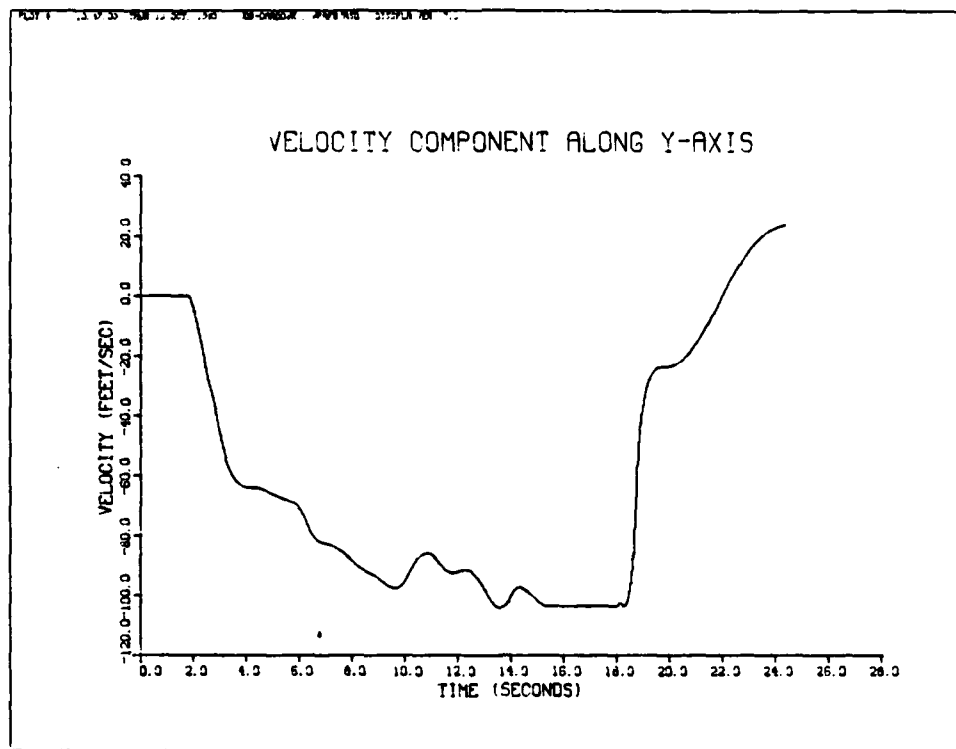


Fig. 4.16(a) Random walk model for  $x_3$  - Range only

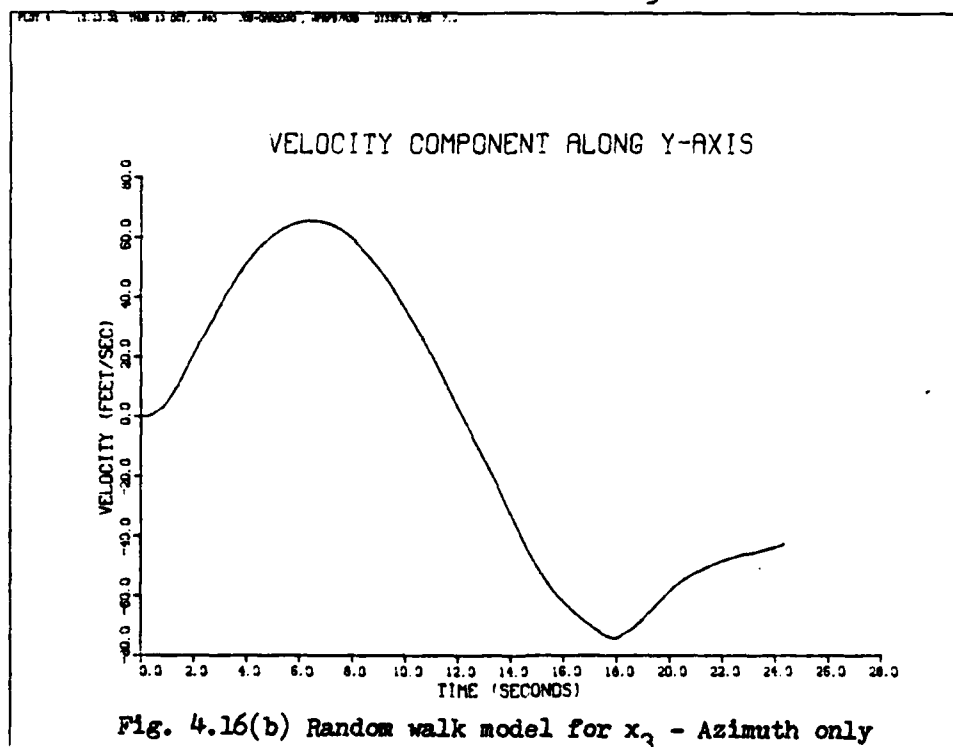


Fig. 4.16(b) Random walk model for  $x_3$  - Azimuth only



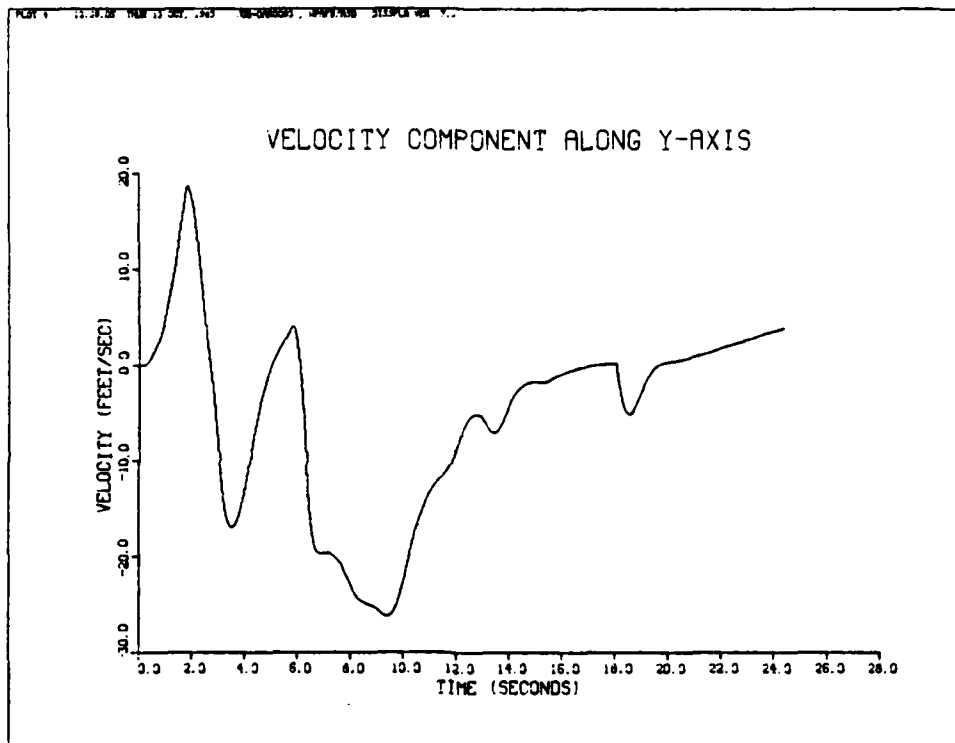


Fig. 4.16(c) Random walk for  $x_3$  - Range and Azimuth

measurement can tell very little about y-axis changes of position and velocity. Again, the geometry of the radar and vehicle track causes this observability problem.

Figures 4.13 (c) through 4.16 (c) are generated by utilizing both azimuth and range measurements. Again, the estimates of x position and velocity are fairly consistent with the estimates of these values generated by using accelerometer data. Deviations from track centerline are less severe but still subject to range measurement errors. It is apparent from this analysis that the basic trajectory of the vehicle generated using accelerometer data is reconfirmed. Thus, we conclude that the extended Kalman filter is correctly calculating the observation matrix,  $H[t_i; \hat{x}(t_i^-)]$ , and that our model for  $z(t_i)$  is correct.

#### Extended Kalman Filter Performance Analysis

Having calculated measurement noise strengths for range and azimuth and also having checked the calculation of the observation matrix, we are now ready to run the extended Kalman filter modeled in Chapter III. The initial condition for the propagation of the state vector is chosen as zero-mean Gaussian random variable with mean

$$E [\underline{x}(t_0)] = \hat{\underline{x}}_0 = \underline{0} \quad (4-8)$$

and covariance

$$E[(\underline{x}(t_0) - \hat{\underline{x}}_0)(\underline{x}(t_0) - \hat{\underline{x}}_0)^T] = \underline{P}_0 \quad (4-9)$$

where the initial covariance matrix from (3-16) is specified as:

$$\underline{P}_0 = \begin{bmatrix} 10000 & & & & & & & & \\ & 10000 & & & & & & & \\ & & 100 & & & & & & \\ & & & 100 & & & & & \\ & & & & .0259 & & & & \\ & & & & & 225 & & & \\ & & & & & & .25E-6 & & \\ & & & & & & & & \end{bmatrix} \quad (4-10)$$

The initial values for the diagonal entries of the system noise matrix,  $\underline{Q}(t)$ , are repeated here for reference:

$$\underline{Q}(t) = \begin{bmatrix} 0 & & & & & & & & \\ & 0 & & & & & & & \\ & & 0 & & & & & & \\ & & & .01 & & & & & \\ & & & & .0518 & & & & \\ & & & & & 1.0 & & & \\ & & & & & & .1E-7 & & \\ & & & & & & & & \end{bmatrix} \quad (4-11)$$

The extended Kalman filter as implemented in SOFE is run with several different combinations of  $\underline{Q}(t)$ ,  $\underline{P}_0$ , and  $\underline{R}(t_i)$ . This analysis is necessary to monitor the behavior of the error variance of each state estimate in order to check filter performance. We desire to obtain the lowest possible error variance on each state after 24 seconds of filter operation, using realistic values of initial covariance,  $\underline{P}_0$ , system noise,  $\underline{Q}(t)$ , and measurement noise,  $\underline{R}(t_i)$ . This performance analysis can be thought of as "tuning" the extended Kalman filter. The results obtained from a large number of noise and initial covariance combinations are summarized here.

The initial value for the error variance matrix,  $\underline{P}_0$ , proved to be adequate for all the states except range and azimuth biases. The initial covariance for range bias and azimuth bias had to be increased to  $1600 \text{ ft}^2$  and  $.5\text{E-}4 \text{ rad}^2$ , respectively, to see some reduction in the error variances of these states. After 24 seconds of filter operation, the filter only reduces the error variance on these states to  $1190 \text{ ft}^2$  and  $.88\text{E-}5 \text{ rad}^2$ , respectively due to limited observability. The filter's ability to estimate accelerometer error is relatively unaffected by changes to driving noise on this state. The error variance on the filter estimate of accelerometer error converges very quickly to its minimum value regardless of changes in driving noise or initial covariance. Likewise, changes to the pseudonoise values on states  $x_6$  and  $x_7$ , range and azimuth bias, do not effect the filter's ability to estimate these states.

The greatest reduction in error variance on all the states of interest results from the recalculation of the measurement noise matrix,  $\underline{R}(t_1)$ , based on analysis of the range and azimuth measurement residuals. This is expected since the filter now "puts more stock" in the measurements of range and azimuth than it did for higher values of  $\underline{R}(t_1)$ . Since we are most concerned with estimates of vehicle velocity,  $x_3$  and  $x_4$ , we present the results of the tuning process on the error variance of these state estimates. The minimum error variances for these states occur after 24 seconds of filter operation. The error variance of x and y velocity

estimates and associated driving noise strengths and measurement noise is presented in Table I. The initial variance on each state is  $100 \text{ (ft/sec)}^2$ , or  $\pm 10 \text{ ft/sec}$ .

TABLE I  
Filter Performance Analysis

Driving Noise $q$	Measurement Noise, $R(t_i)$	$P(t = 24 \text{ sec})$
$q_4 = .2E-2$	22456/.5388E-4	$P_3 = 2.4$
$q_5 = .0518$	" "	$P_4 = 6.36$
$q_6 = 10.0$	" "	
$q_7 = .5E-5$	" "	
$q_4 = .1E-2$	22456/.5388E-4	$P_3 = 3.193$
$q_5 = .0515$	" "	$P_4 = 6.43$
$q_6 = 1.0$	" "	
$q_7 = .1E-7$	" "	
$q_4 = .1E-3$	22456/.5388E-4	$P_3 = 2.57$
$q_5 = .3E-1$	" "	$P_4 = 6.24$
$q_6 = .10$	" "	
$q_7 = .1E-7$	" "	
$q_4 = .1E-7$	16808/.3573E-4	$P_3 = 2.27$
$q_5 = .3E-1$	" "	$P_4 = 5.92$
$q_6 = .01$	" "	
$q_7 = .1E-7$	" "	

The combination of system noise, initial covariance, and measurement noise chosen as a result of this performance analysis is presented here:

$$\underline{P}_0 = \begin{bmatrix} 10000 & & & & & & & & \\ & 10000 & & & & & & & \\ & & 100 & & & & & & \\ & & & 100 & & & & & \\ & & & & .03 & & & & \\ & & & & & 1600 & & & \\ & & & & & & .5E-4 & & \end{bmatrix} \quad \underline{Q}(t) = \begin{bmatrix} 0 & & & & & & & & \\ & 0 & & & & & & & \\ & & 0 & & & & & & \\ & & & .1E-7 & & & & & \\ & & & & .03 & & & & \\ & & & & & .01 & & & \\ & & & & & & .1E-7 & & \end{bmatrix}$$

$$\underline{R}(t_i) = \begin{bmatrix} 16808 & 0 \\ 0 & .3573E-4 \end{bmatrix}$$

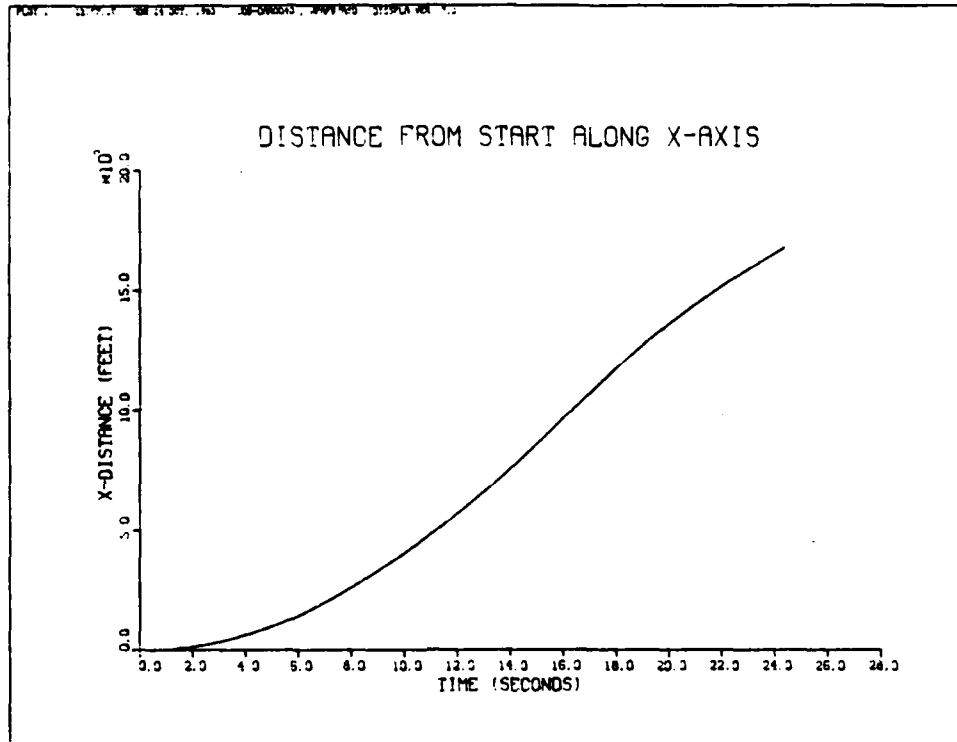
Results of One Iteration of the Extended Kalman Filter

State estimates and error standard deviation in these estimates for the "tuned" extended Kalman filter are presented in Fig. 4.17 through Fig. 4.25. These plots are generated using the values for  $\underline{P}_0$ ,  $\underline{Q}(t)$ , and  $\underline{R}(t_i)$ , specified above. Figure 4.24(a) is a plot of the range measurement residual bracketed by the residual standard deviation. The azimuth measurement residual and associated residual standard deviation is plotted in Fig. 4.24(b). It should be noted that a "residual monitoring" routine has been included in the basic software for SOFE. This routine calculates the residual standard deviation at each sample time from:

$$\sigma_{res} = [\underline{H}(t_i)\underline{P}(t_i^-)\underline{H}^T(t_i)+\underline{R}(t_i)]^{\frac{1}{2}}$$

and compares the residual measurement to this value for  $\sigma_{res}$ . If the residual measurement,  $\underline{\delta z}(t_i)$ , is greater than  $3\sigma_{res}$ , the measurement is ignored. As a result of residual

(a)



(b)

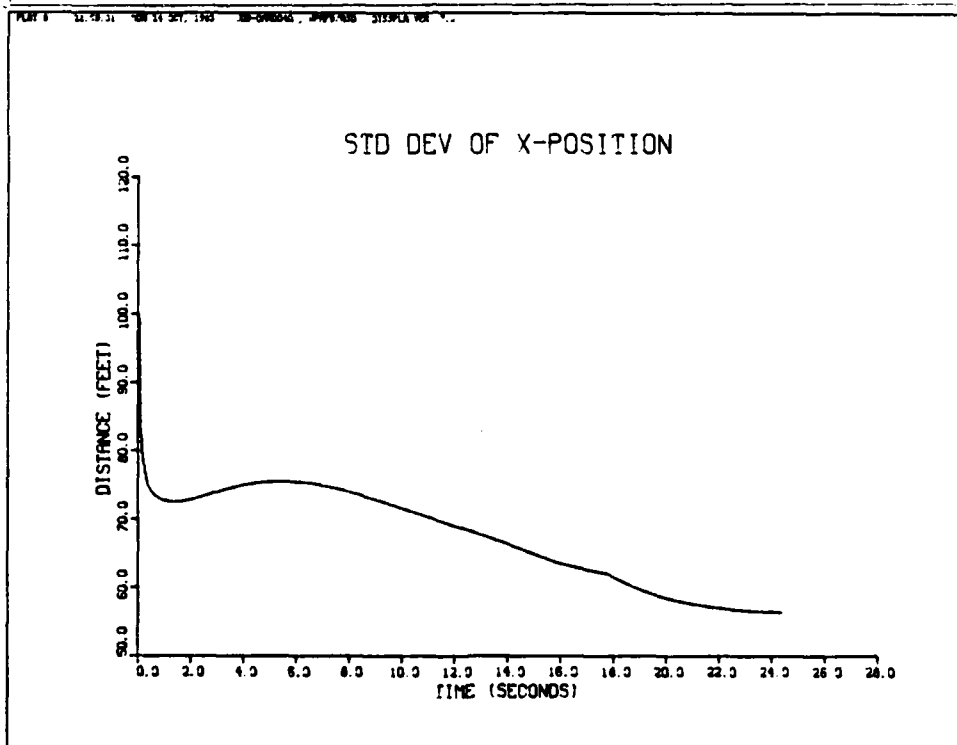
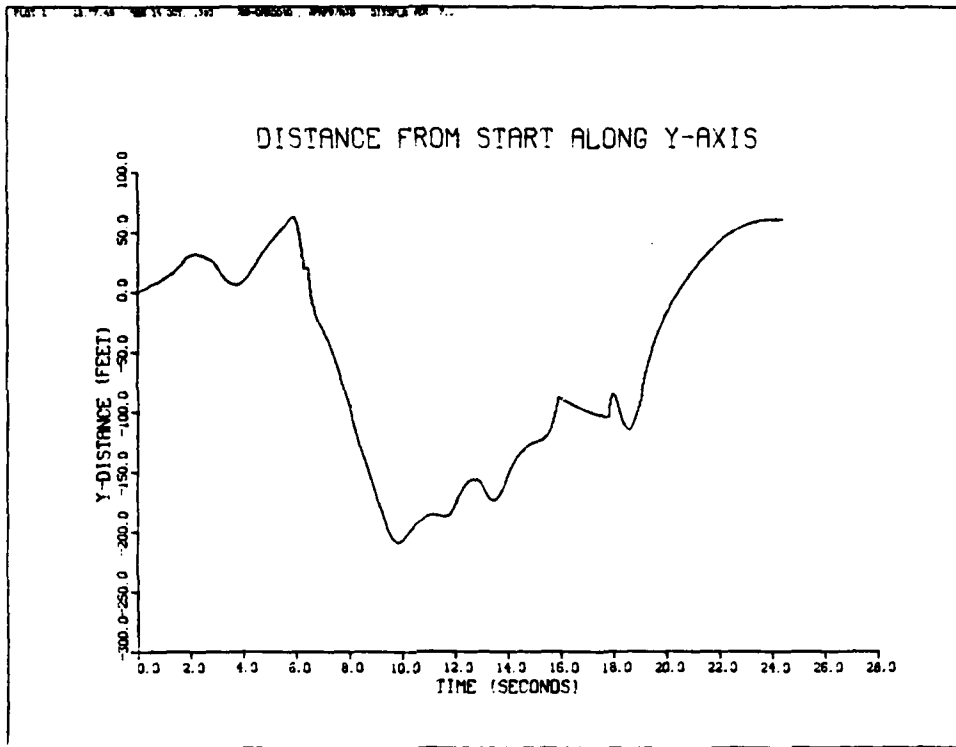


Fig. 4.17(a),(b) Extended Kalman filter - Range and azimuth

(a)



(b)

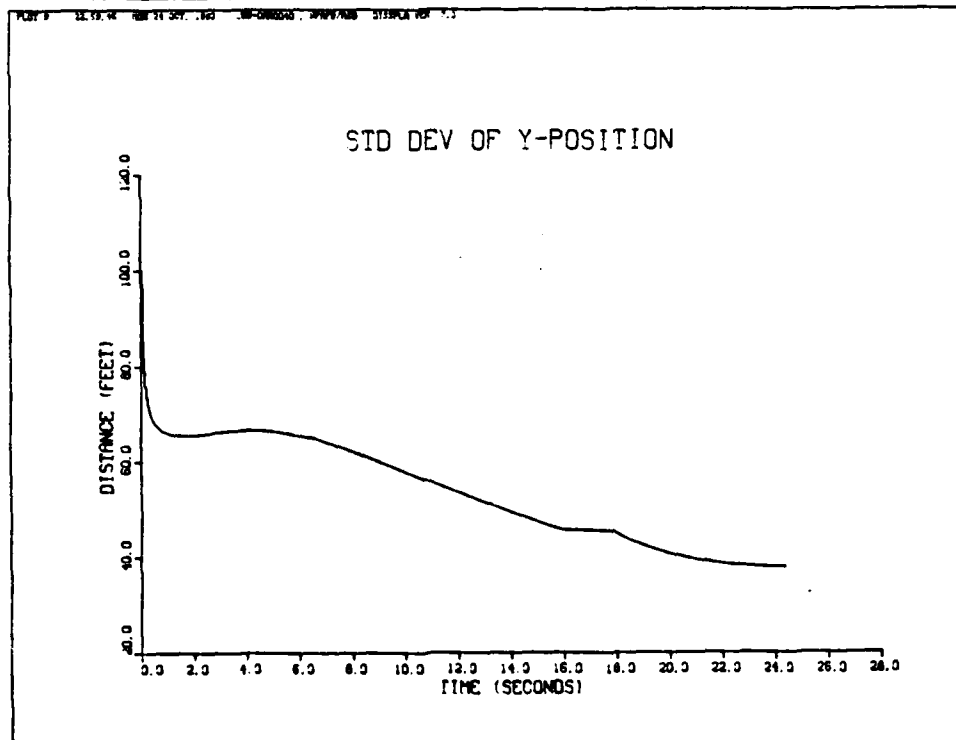
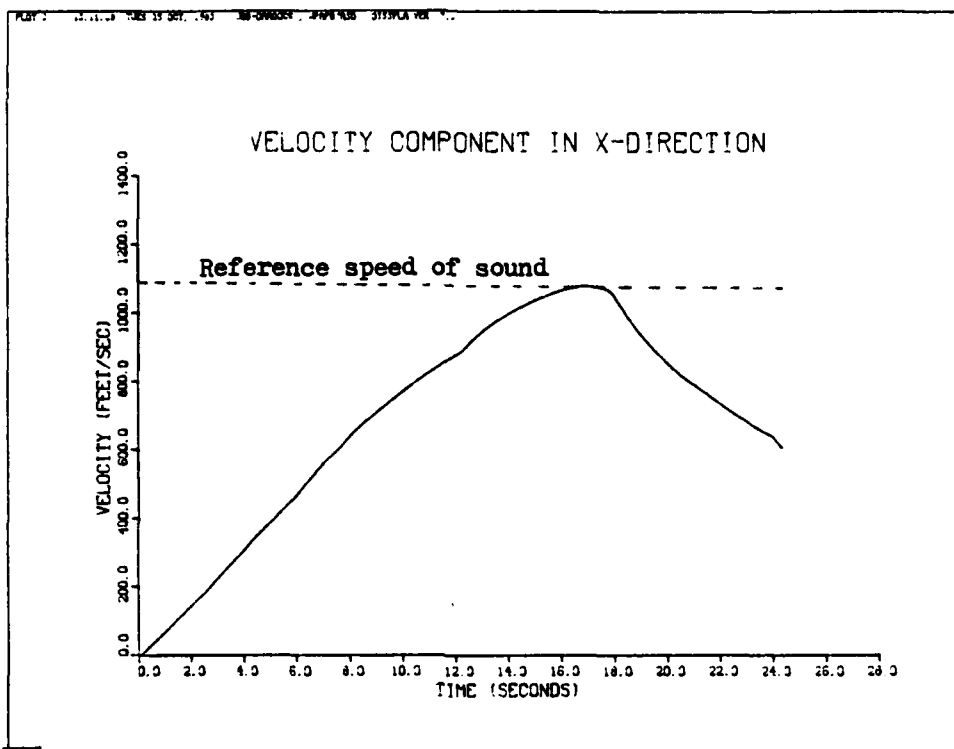


Fig. 4.18(a),(b) Extended Kalman filter - Range and azimuth



(a)



(b)

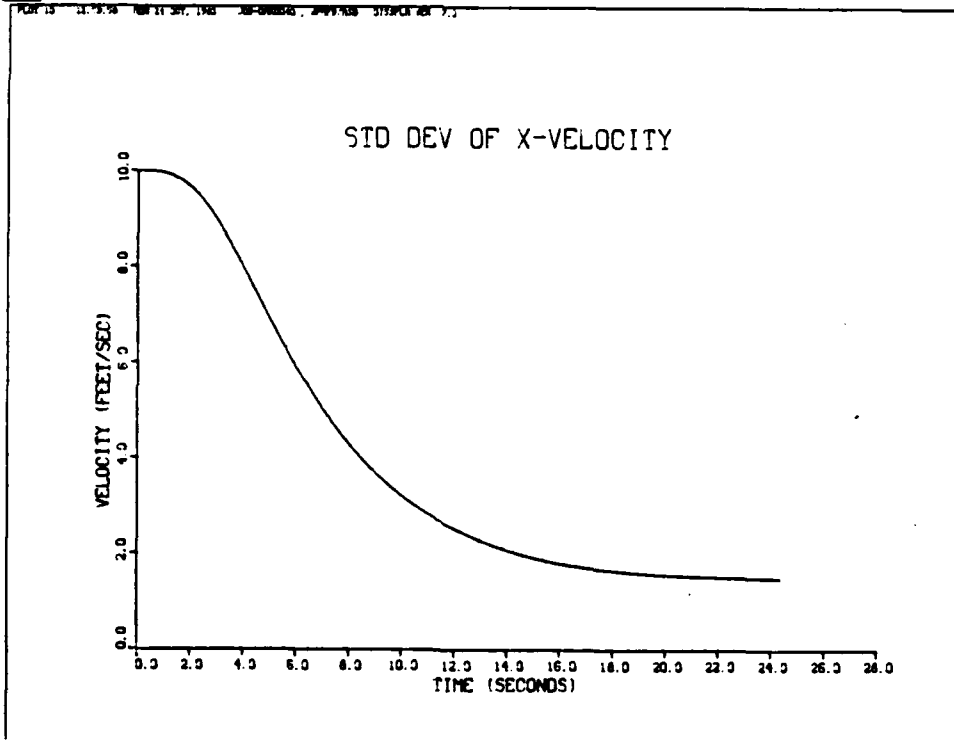
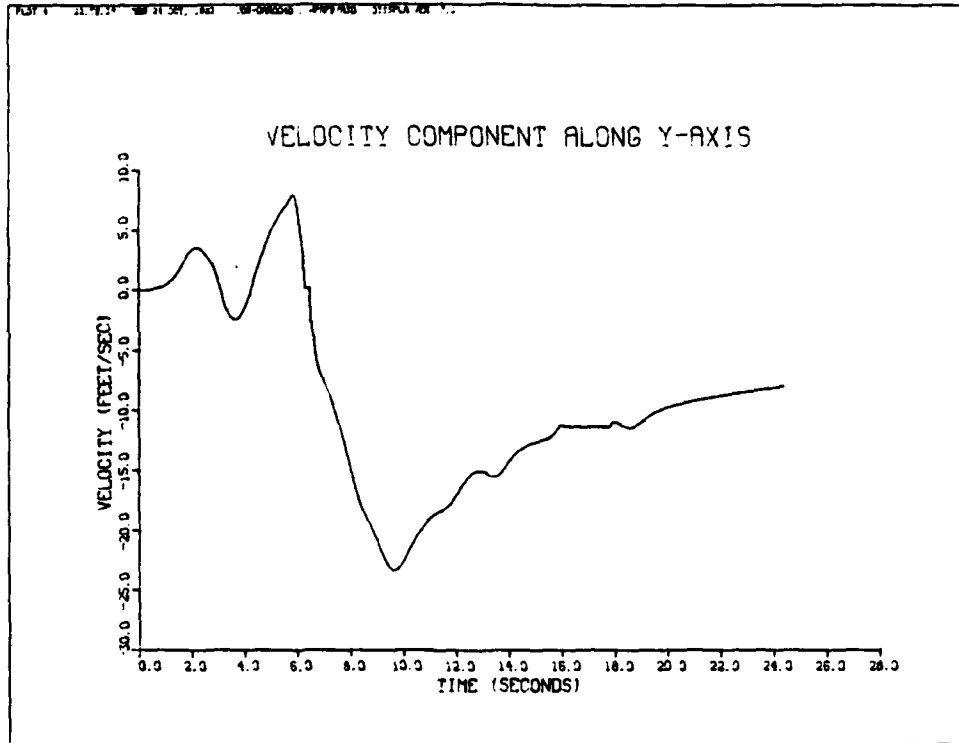


Fig. 4.19(a),(b) Extended Kalman filter - Range and Azimuth

(a)



(b)

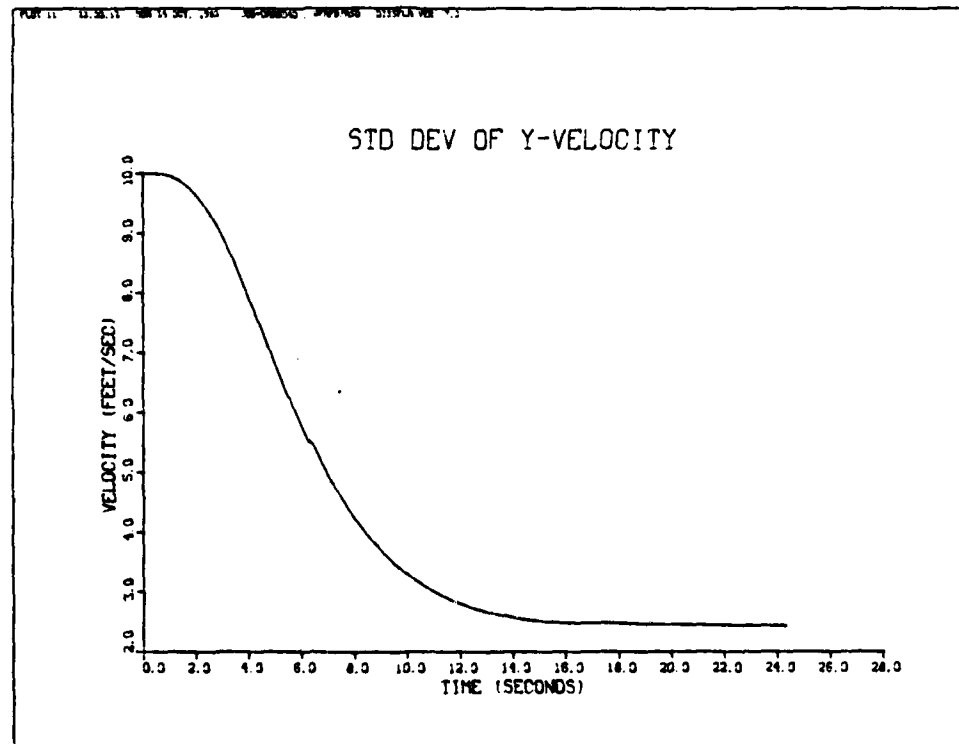


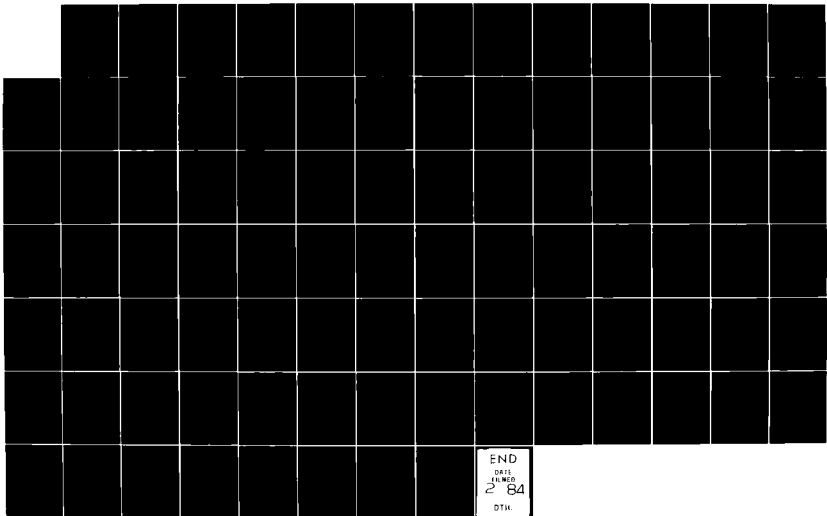
Fig. 4.20(a),(b) Extended Kalman filter - Range and Azimuth

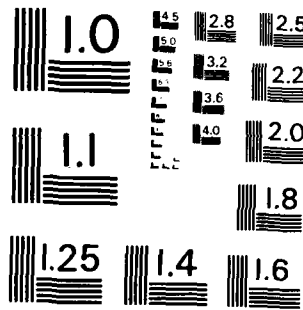
22

AD A13G 919

STOCHASTIC ESTIMATION APPLIED TO THE LAND SPEED OF  
SOUND RECORD ATTEMPT B. (U) AIR FORCE INST OF TECH  
WRIGHT PATTERSON AFB OH SCHOOL OF ENGI... D A REINHOLZ  
DEC 83 AFIT/GAE/AA/83D-19 F/G 13/6 NI

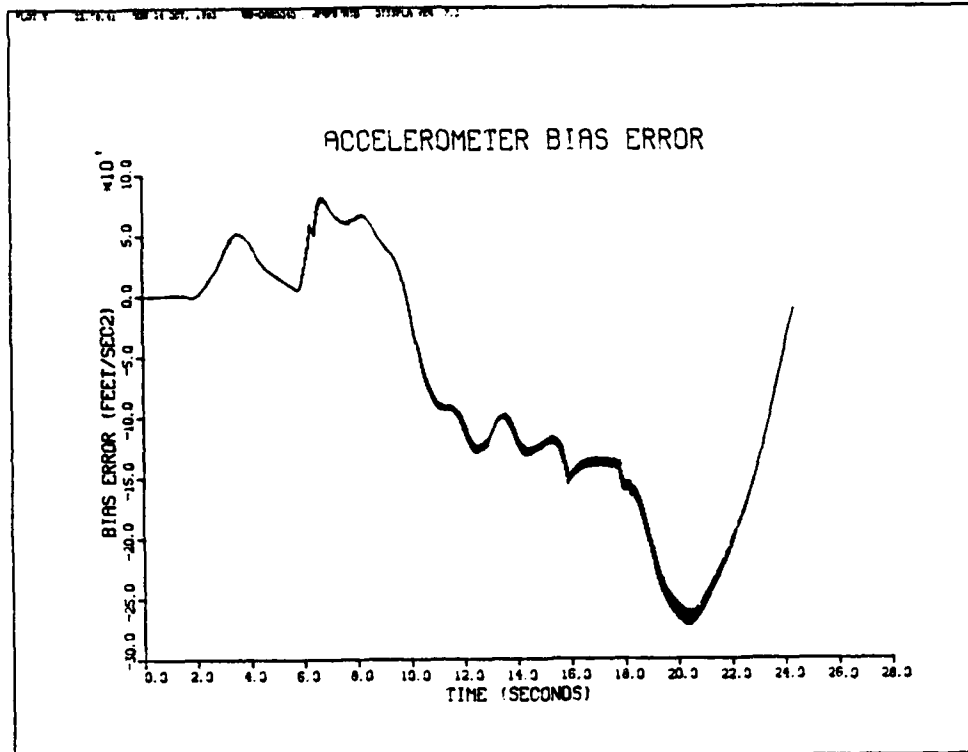
UNCLASSIFIED





MICROCOPY RESOLUTION TEST CHART  
NATIONAL BUREAU OF STANDARDS - 1963-A

(a)



(b)

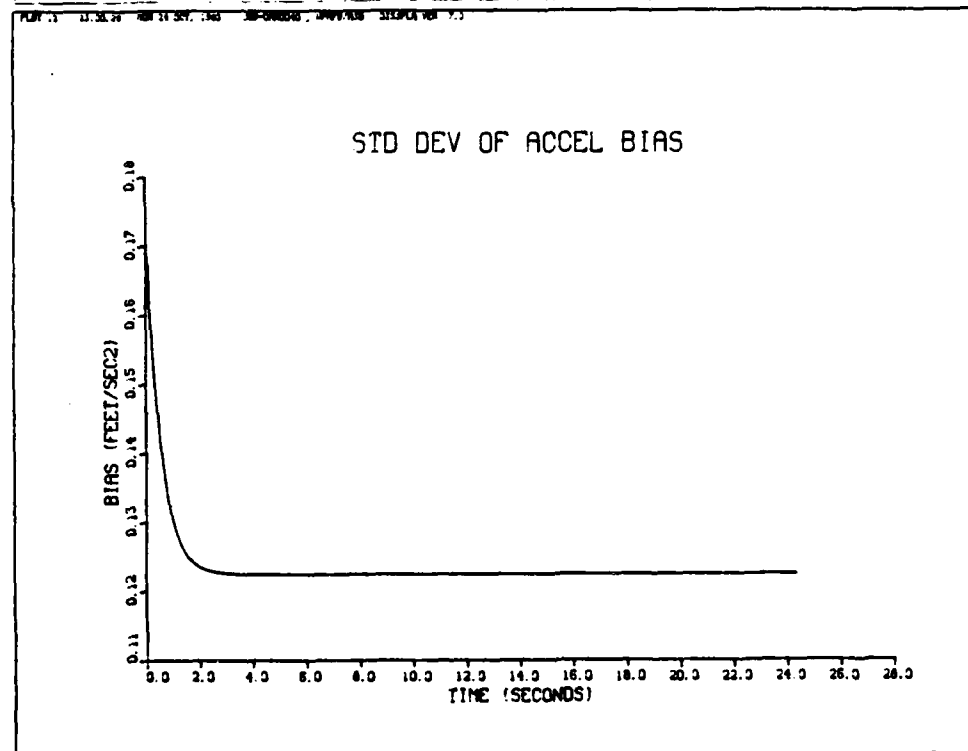
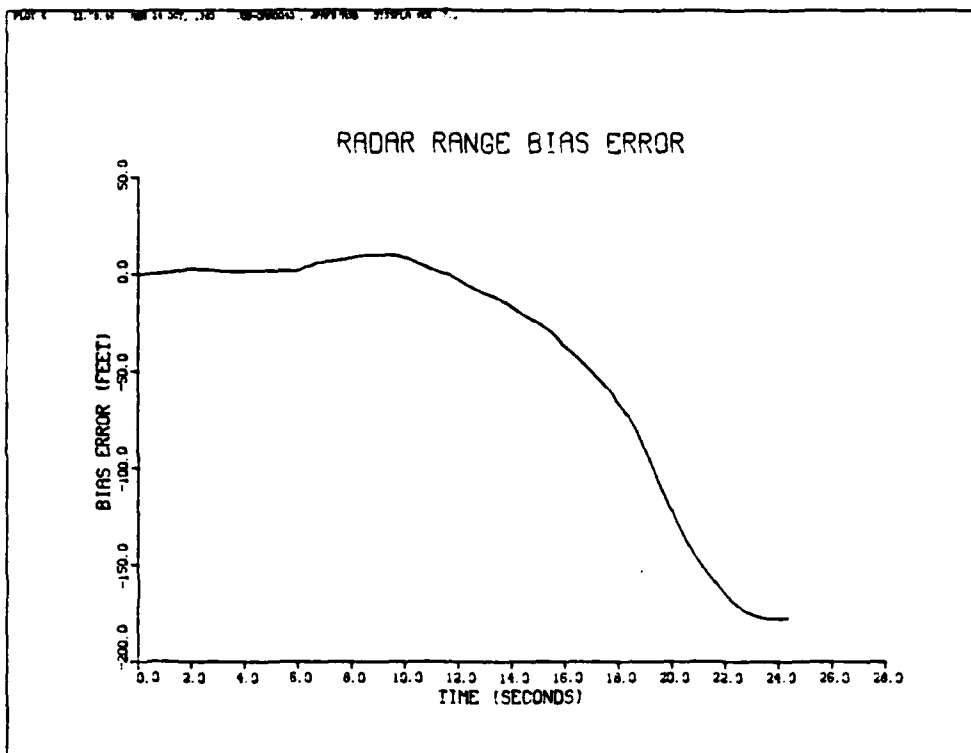


Fig. 4.21(a),(b) Extended Kalman filter - Range and Azimuth

(a)



(b)

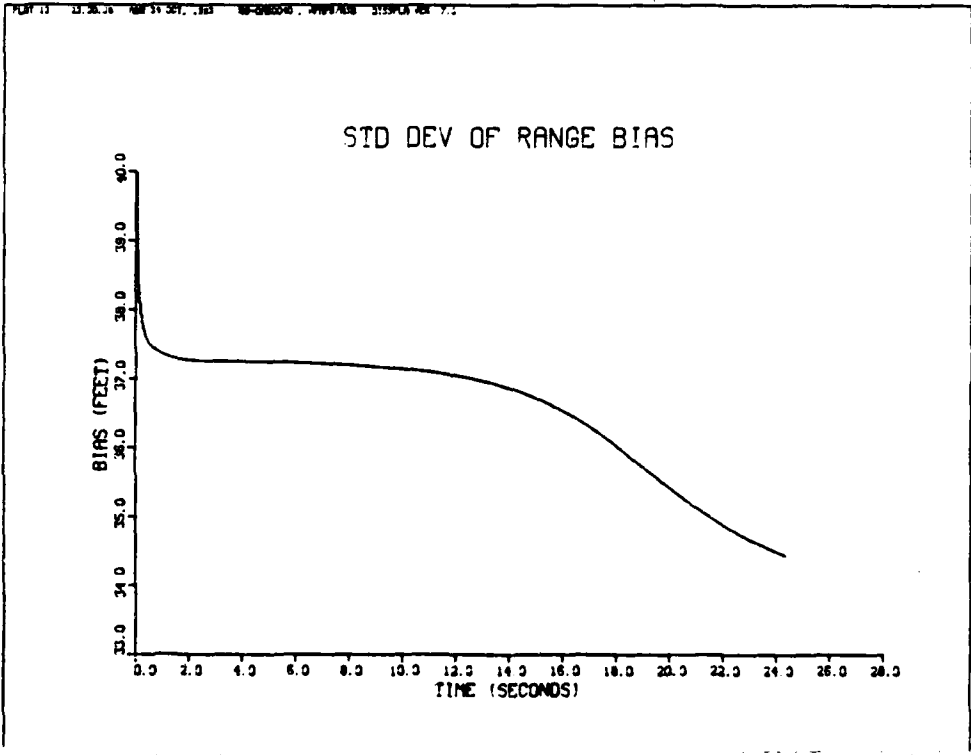
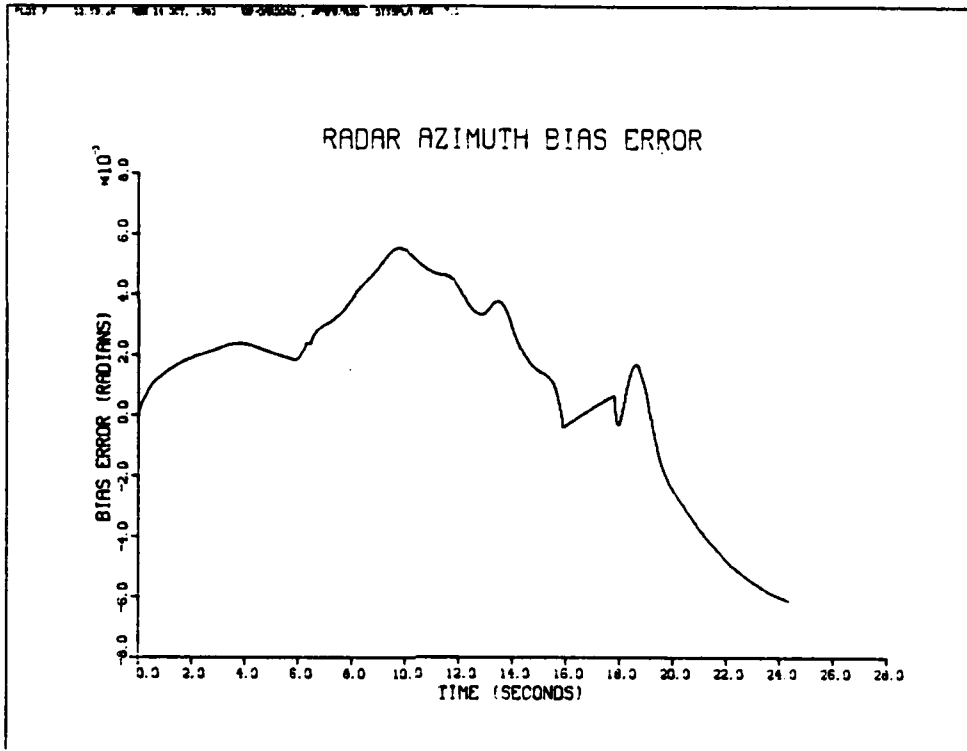


Fig. 4.22(a),(b) Extended Kalman filter - Range and Azimuth

(a)



(b)

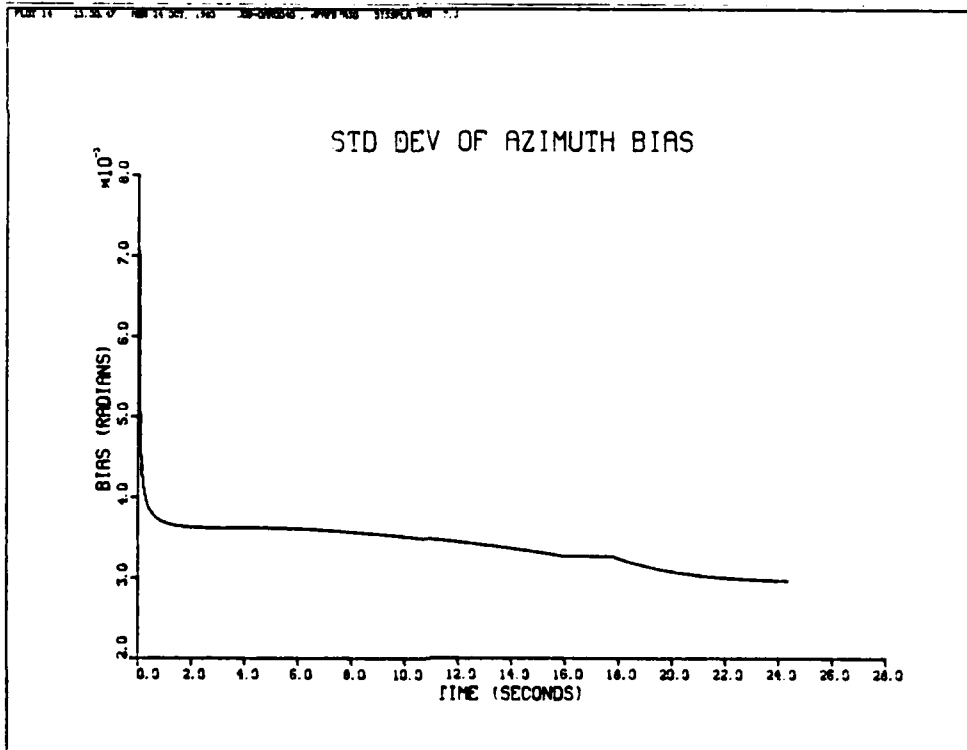
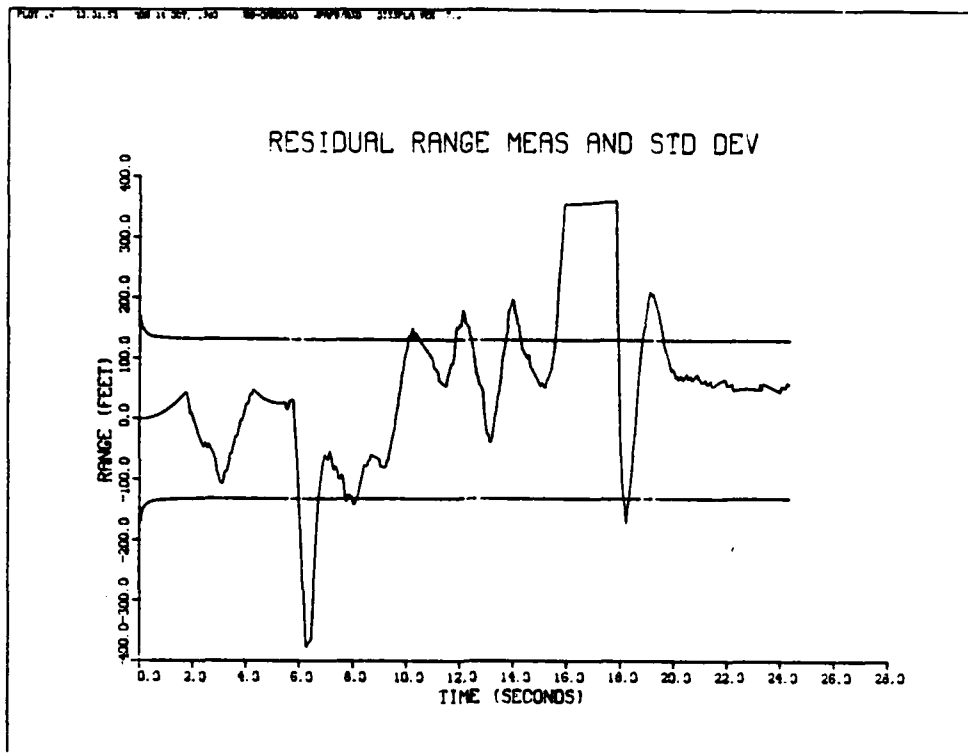


Fig. 4.23(a),(b) Extended Kalman filter - Range and Azimuth

(a)



(b)

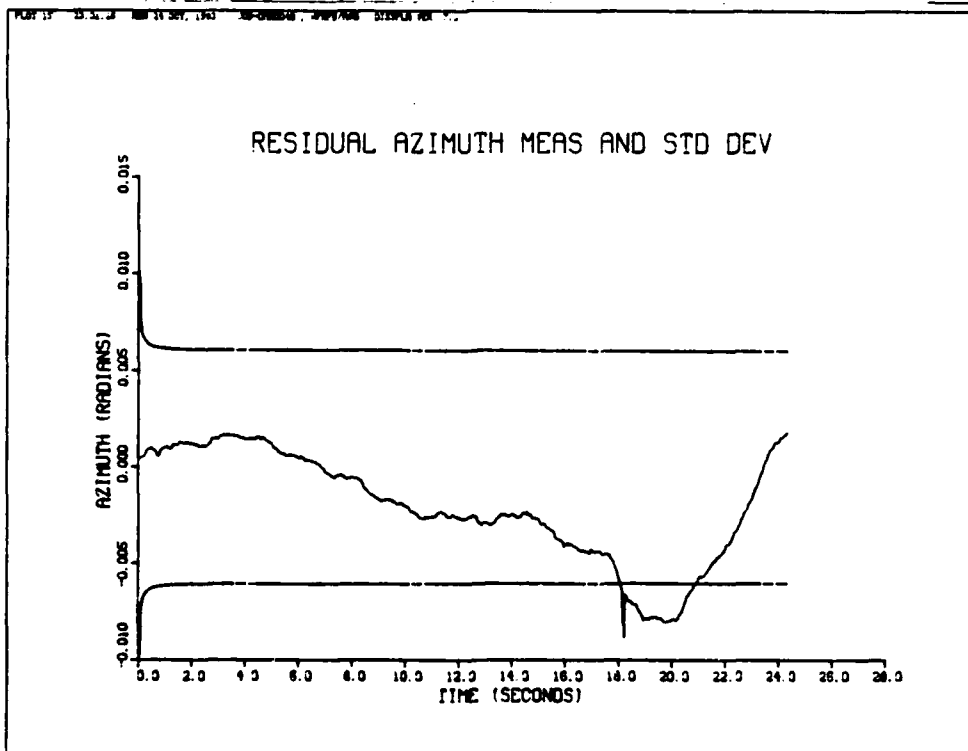
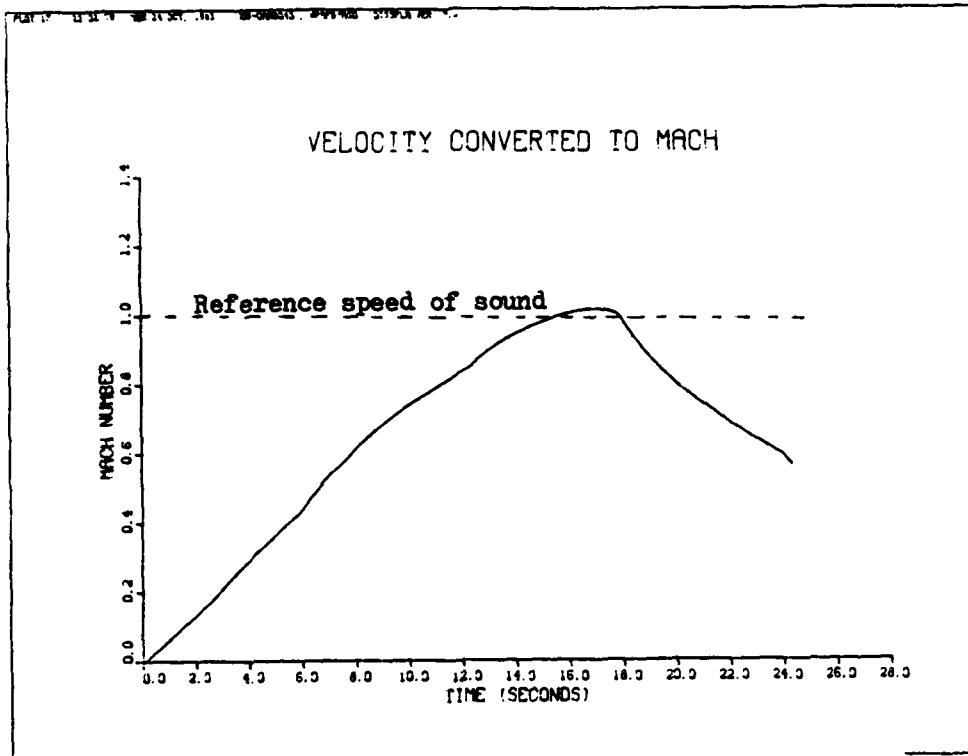


Fig. 4.24(a),(b) Extended Kalman filter - Range and Azimuth



(a)



(b)

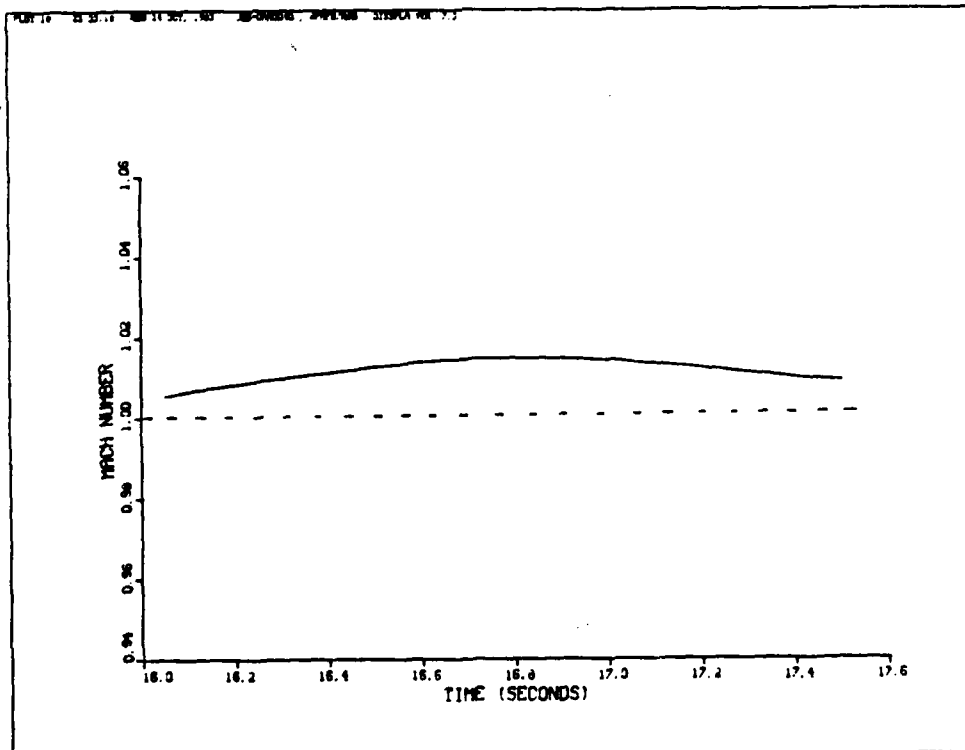


Fig. 4.25(a),(b) Extended Kalman filter - Range and Azimuth

monitoring, 40 measurements between 16-18 seconds, and three measurements near six seconds, are ignored.

Figure 4.25 (b) is a "blown up" version of Fig. 4.25 (a) which is the magnitude of the velocity vector converted to Mach number.

The plots of standard deviation for range bias and azimuth bias indicate weak convergence of the standard deviation for these states. As mentioned previously, this is due to limited observability of these states. The standard deviations of the other state estimates show good convergence and indicate that even the "noisy" range measurement provides some information on state values which can be used to improve state estimation. From the plot of range residual standard deviation it should be apparent that the residual monitoring routine is rejecting measurements of range which have a residual value greater than  $3\sigma_{res}$ , or approximately 390 feet. The straight line segment between 16-18 seconds and the "spike" at six seconds in Fig. 4.24 (a) show where the range measurements have been ignored.

The large deviation in y position shown in Fig. 4.18 (a) at approximately 10 seconds is due to range measurement errors which are significant between 6-10 seconds. The filter weights these measurements lightly due to relatively high measurement noise, but does not totally reject them. Thus, the estimated y position shows unrealistic values for this state due to inaccuracies in the range measurement. It appears from Fig. 4.11 (b) that during this four second

interval between 6-10 seconds, the range is indicating short of actual vehicle position.

The extended Kalman filter indicates a peak speed estimate at 16.85 seconds of

$$\hat{x}_{3\max} = 1089.49 \text{ ft/sec}$$

$$\hat{x}_{4\max} = -11.3765 \text{ ft/sec}$$

Calculating the scalar speed of the vehicle from

$$V = (\hat{x}_3^2 + \hat{x}_4^2)^{\frac{1}{2}}$$

we find a maximum scalar velocity of

$$V_{\max} = 1089.55 \text{ ft/sec}$$

resulting in a maximum Mach number of

$$M_{\max} = 1.015$$

when referenced to the speed of sound,  $a$ ,

$$a = 1073.536213 \text{ ft/sec}$$

The extended Kalman filter indicates that the rocket car was above the reference speed of sound for approximately 1.9 seconds.

A run of the extended Kalman filter using only azimuth measurements was made to check the influence of incorporating the inaccurate range measurement. The estimate of velocity from this run is much closer to the estimate of  $x$  velocity,  $x_3$ , obtained from integrating accelerometer data without incorporating any measurements. This reconfirms the

observability problems previously mentioned associated with estimating  $x_3$  from range measurements. The azimuth only run of the extended Kalman filter indicates the following vehicle performance:

$$\hat{x}_{3\max} = 1080.26 \text{ (16.85 sec)}$$

$$\hat{x}_3 = 977.081 \text{ (18.65 sec, trap entry)}$$

$$\text{Time above Mach 1} = 1.30 \text{ sec}$$

The azimuth only run, however, does not provide very good estimates of y position or velocity due to the observability of these states from azimuth measurements alone. It should be noted, that the apparent error in x velocity caused by observability problems using range measurements is corrected by using the fixed-interval smoother algorithm. The time history of state estimates and error variances from the run of the extended Kalman filter incorporating both measurements is stored for use in the smoother algorithm. The results of the smoother analysis will be presented in the next chapter.

## V. Optimal Smoother Results

Chapter II describes the Meditch form of the optimal "fixed-interval" smoother algorithm in detail. A simple FORTRAN program was written by the author to incorporate this smoother algorithm. The output of the extended Kalman filter, detailed in the previous chapter, is stored for use by the smoother program. The FORTRAN code used in the smoother program is listed for reference in Appendix B. The results obtained from this program are presented in this chapter.

The output of the optimal smoother at the initial time,  $t_0$ , is used to correct the initial conditions for another iteration of the forward extended Kalman filter. Such a "forward-backward" iteration scheme is used to correct model errors and initial conditions of the extended Kalman filter. After each iteration of the forward-backward estimator a comparison of state values is made. When the difference in state estimates from one iteration to the next is less than some arbitrarily specified value,  $\epsilon$ , the estimator is said to have "converged". Since our main area of concern is in the estimate of vehicle speed, we compare the peak estimates of velocity for each run of the smoother. When the difference between peak speed estimates from one iteration to the next is less than 2 ft/sec and the standard deviation of this estimate allows at least a 99 percent confidence that the vehicle exceeded the speed of sound, we stop the iterations. The latter requirement for standard deviation

becomes the driving factor due to time limitations and sufficient confidence after two iterations.

#### One Iteration of Smoother

The plots of the "smoothed" state estimates after one smoother iteration are presented in Figs. 5.1 (a) to 5.7 (a). The variance for each state estimate calculated by the smoother are presented in Figs. 5.1 (b) to 5.7 (b). Note that the smoother works "as advertised" in reducing the error variance of state estimates when compared to the standard deviation plots of the extended Kalman filter in Chapter IV. Some very interesting results are obtained and need to be discussed. The plot of y position, Fig. 5.2 (a) indicates that the vehicle track is indeed a straight line. However, the figure indicates that y position begins approximately 250 feet east of the assumed origin and decreases in a linear-manner to 60 feet east of centerline. This indicates that the starting position of the vehicle is displaced east of the earth-fixed coordinate frame and that the assumed track heading of 179 degrees true is incorrect by approximately .209 degrees. The smoother estimated state values and variances of x and y position at the start of the run,  $t_o$ , are shown to be

$$\hat{x}_1(t_o/t_f) = 167.78 \text{ ft} \quad P_{11}(t_o/t_f) = 3746.5 \text{ ft}^2$$

$$\hat{x}_2(t_o/t_f) = 255.85 \text{ ft} \quad P_{22}(t_o/t_f) = 3649.5 \text{ ft}^2$$

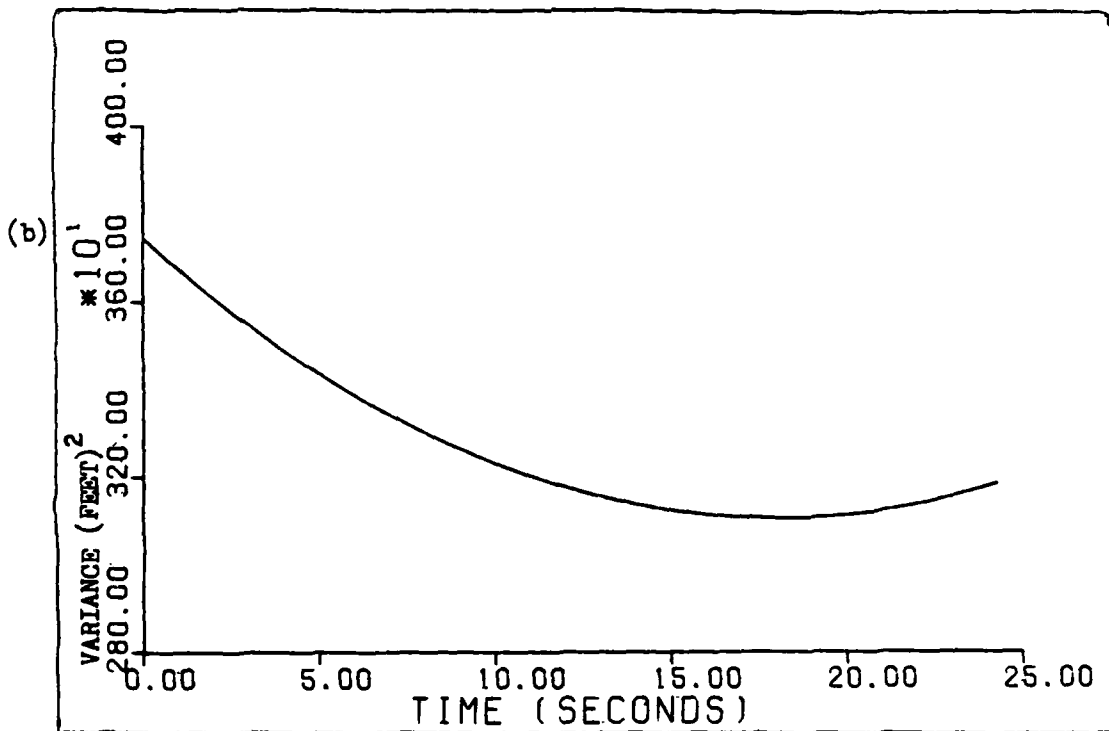
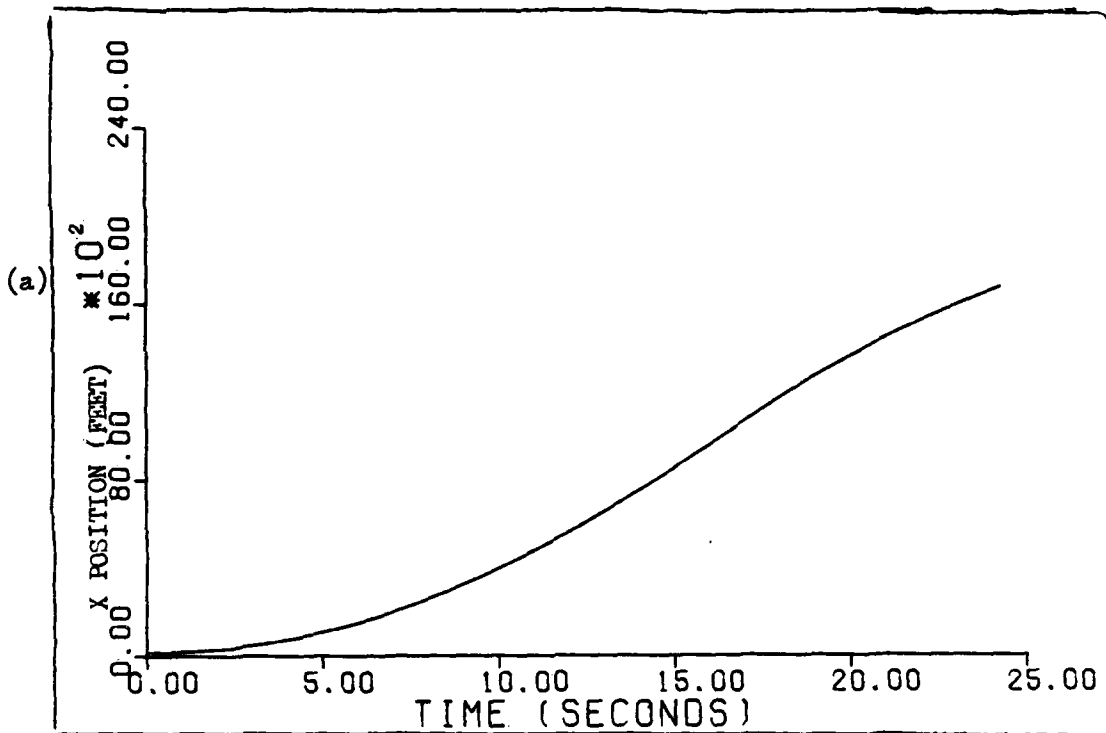


Fig. 5.1(a),(b) Smoother estimate and variance of x-position after one iteration.

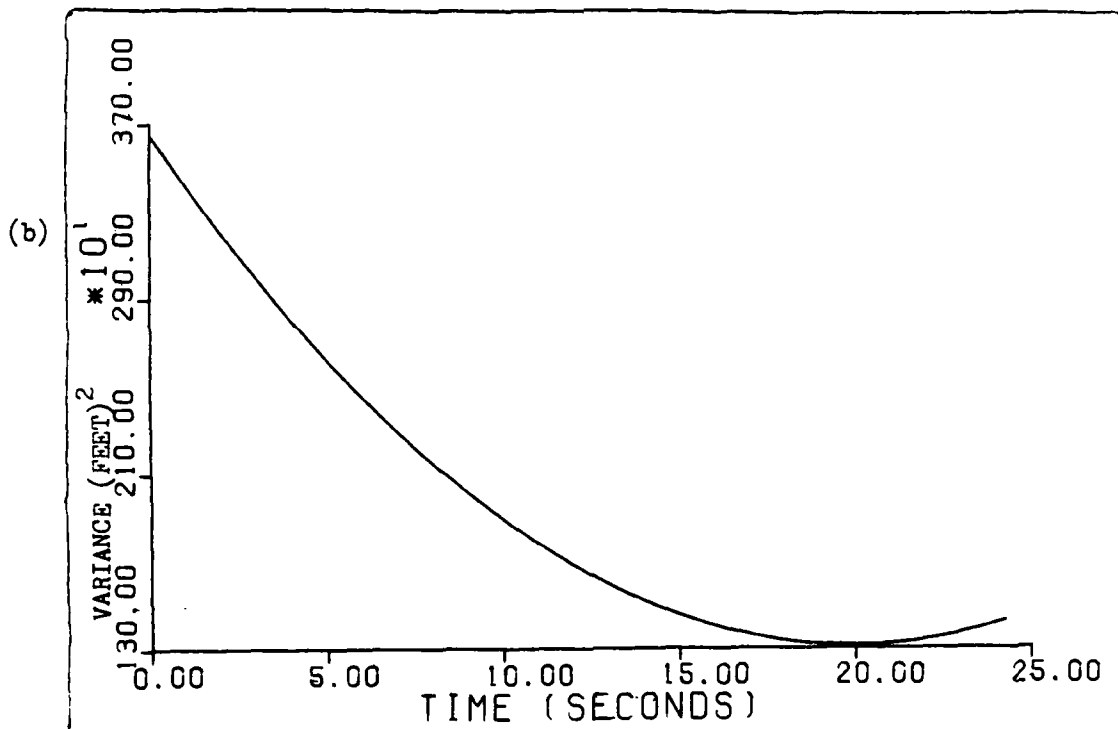
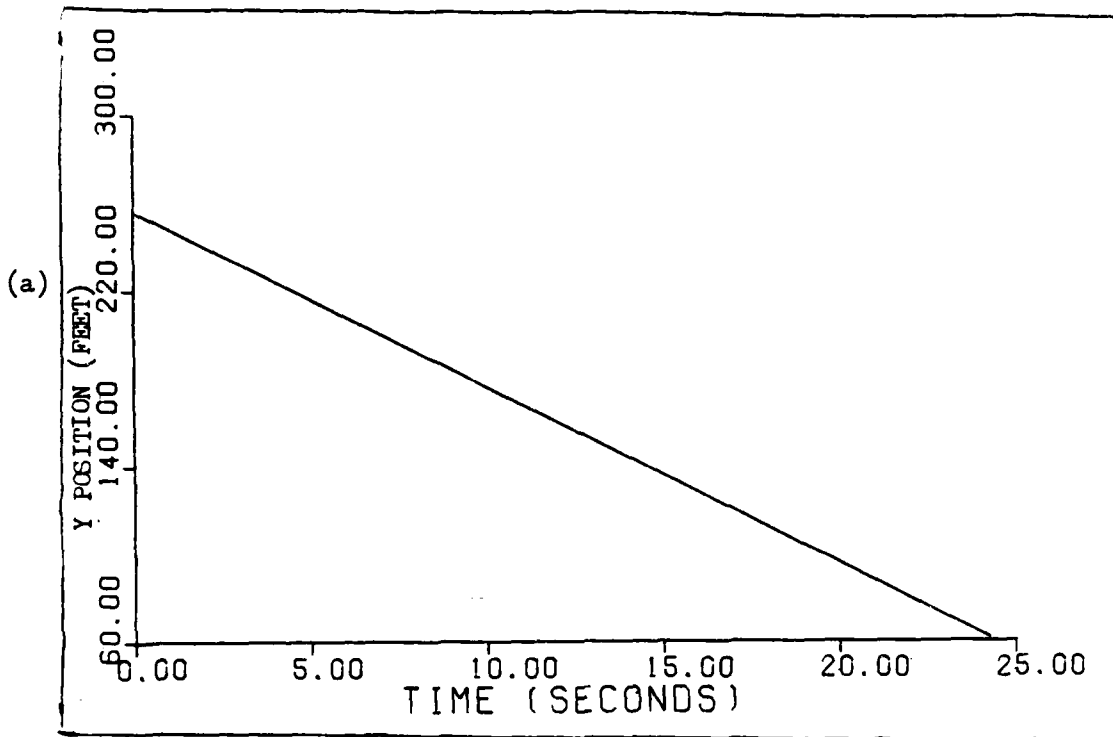


Fig. 5.2(a),(b) Smoother estimate and variance of y-position after one iteration.



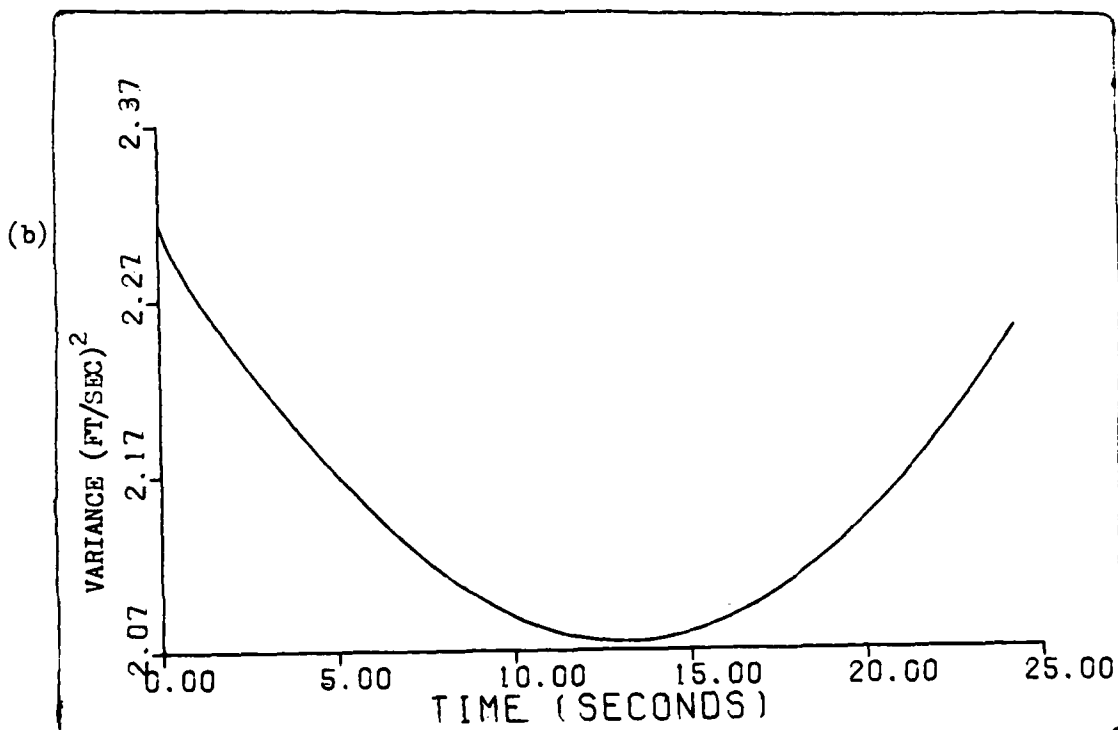
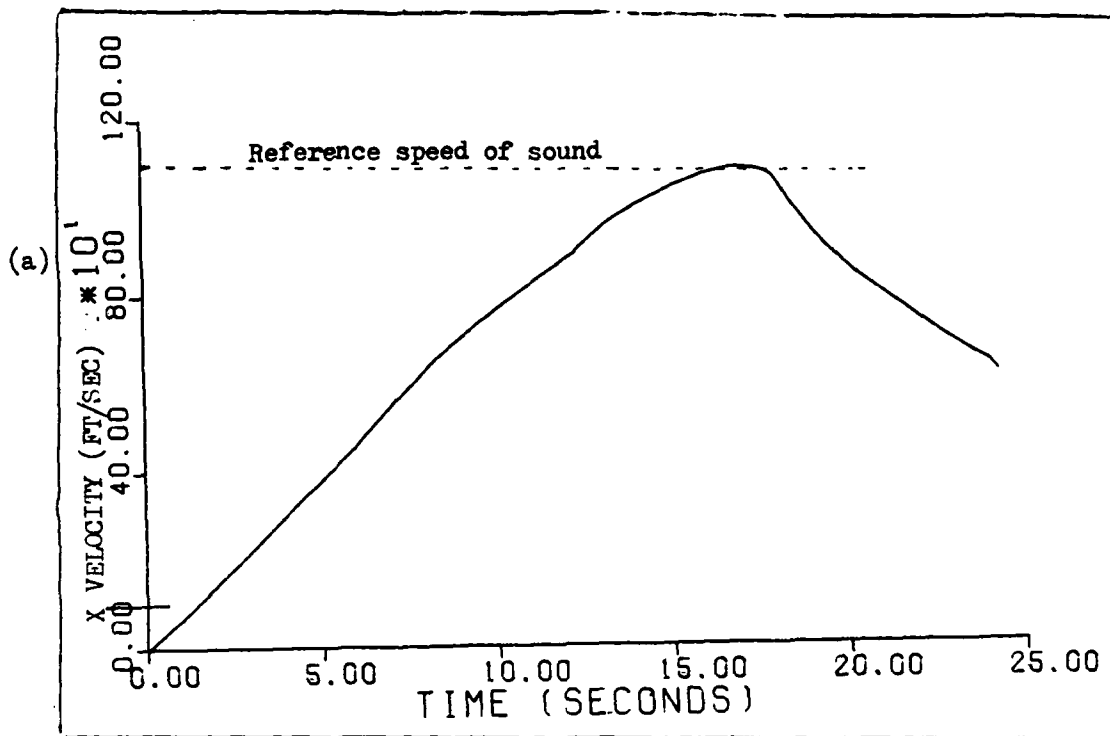


Fig. 5.3(a),(b) Smoother estimate and variance of x-velocity after one iteration.

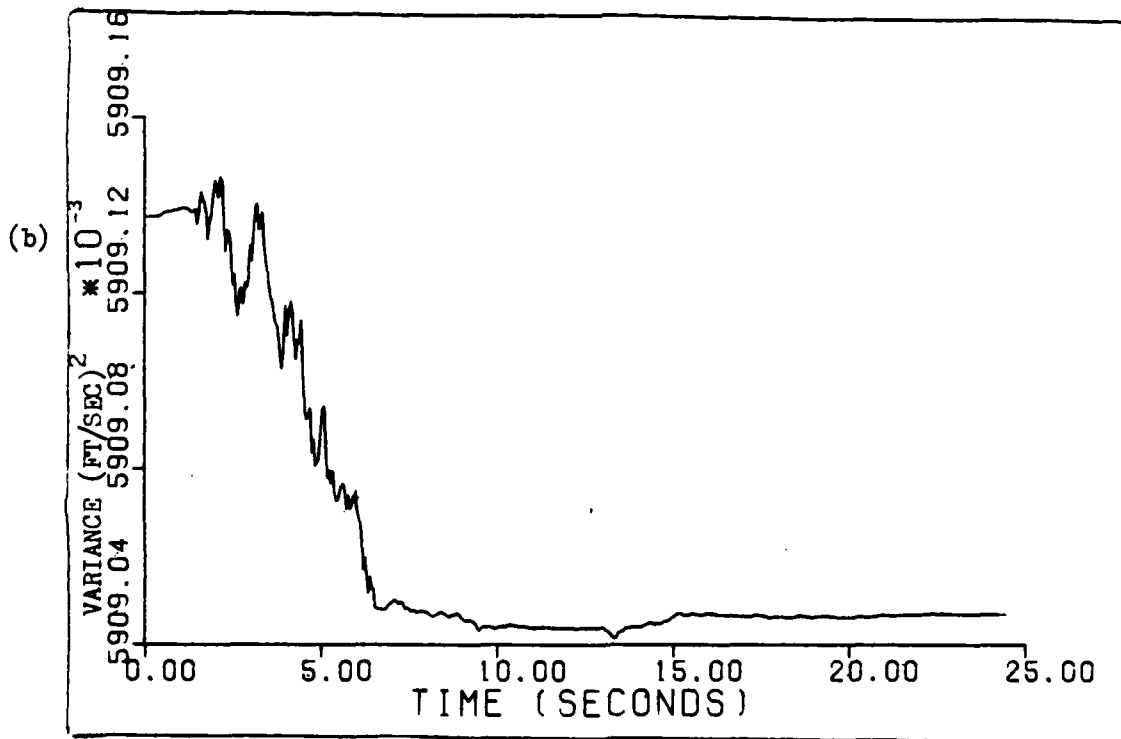
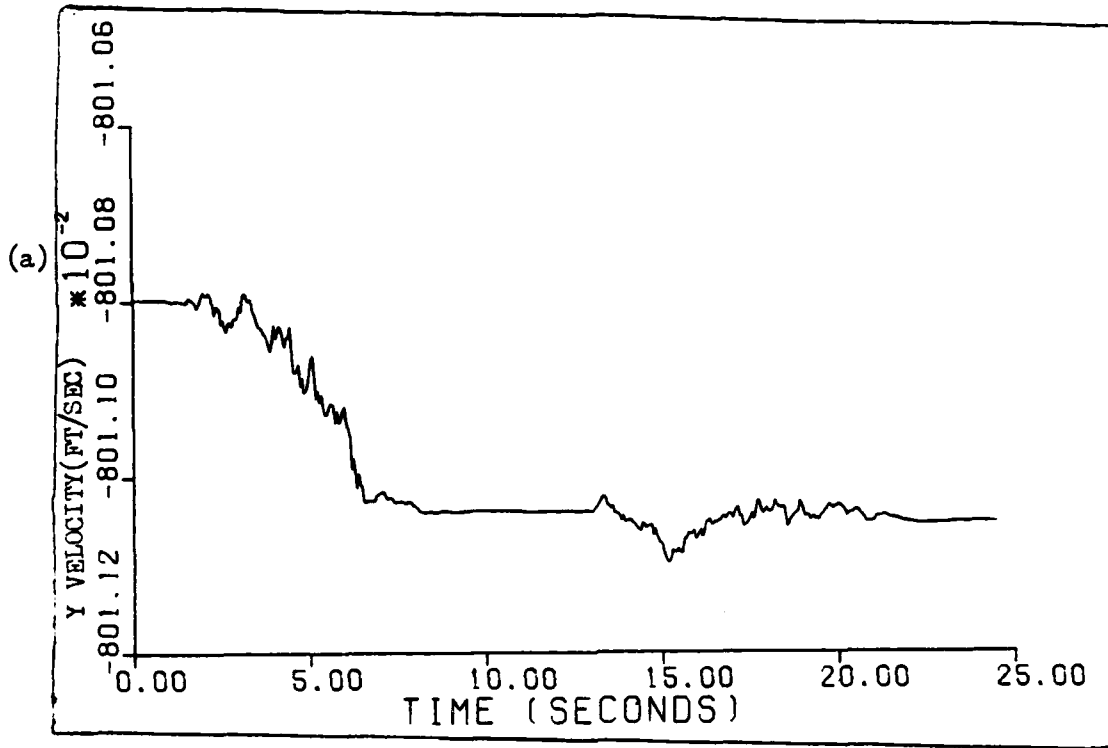


Fig. 5.4(a),(b) Smoother estimate and variance of y-velocity after one iteration.

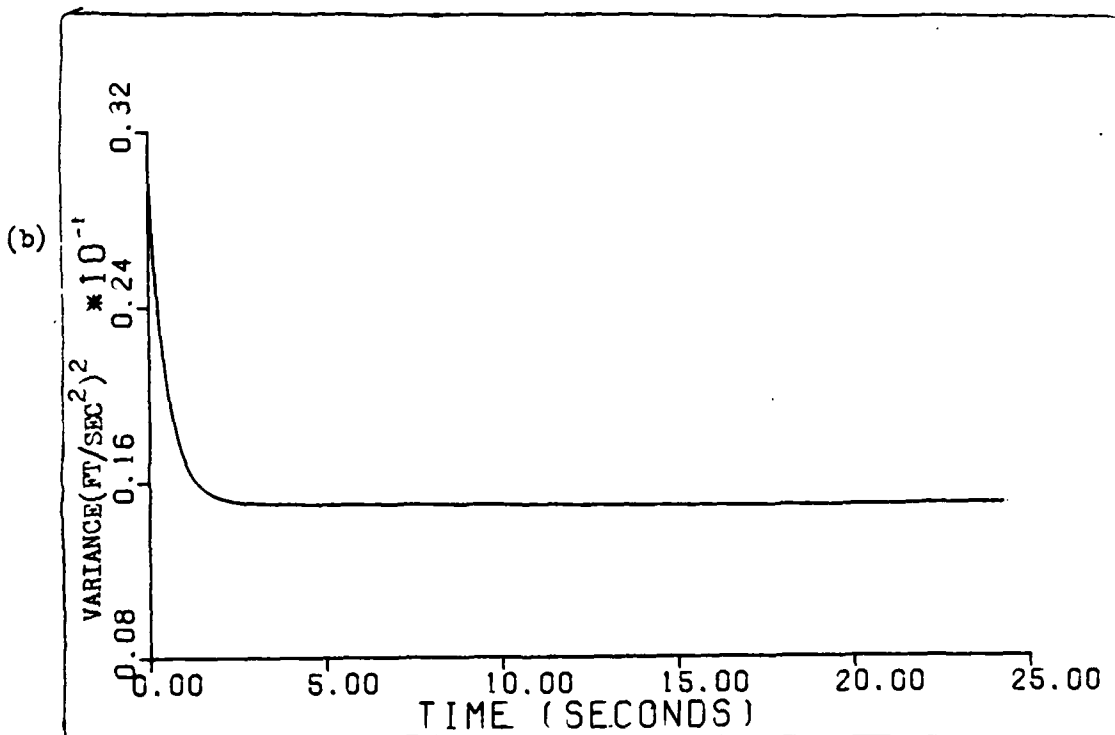
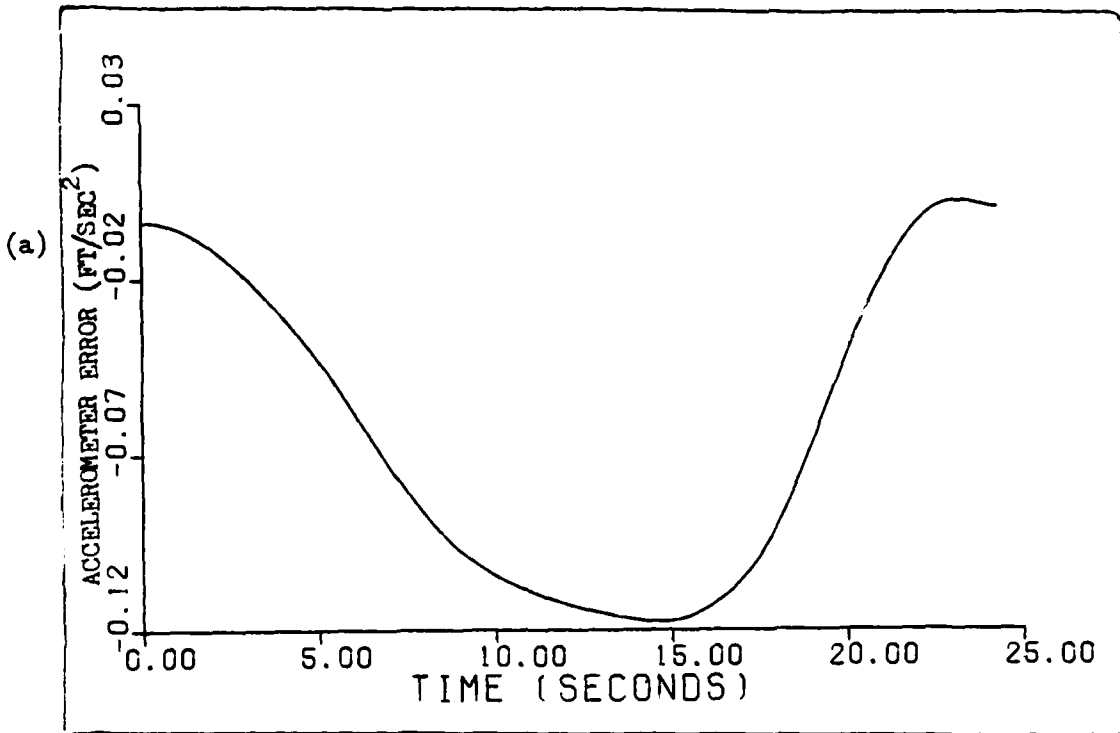


Fig. 5.5(a),(b) Smoother estimate and variance of accelerometer error after one iteration.

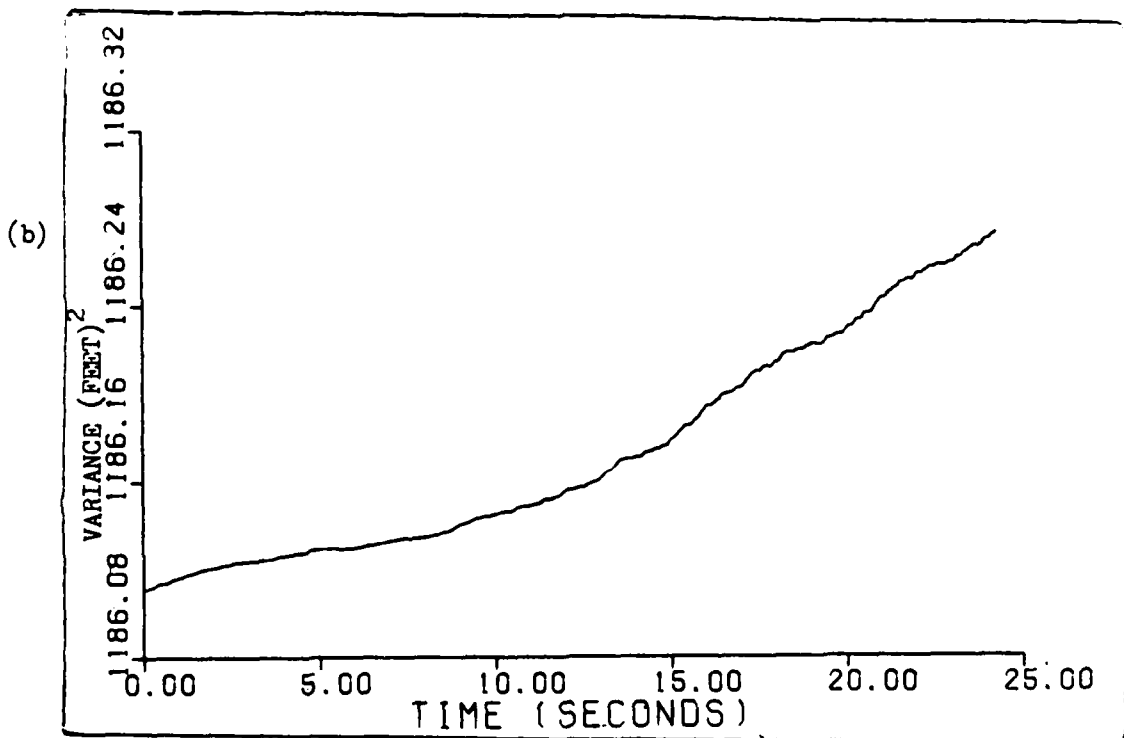
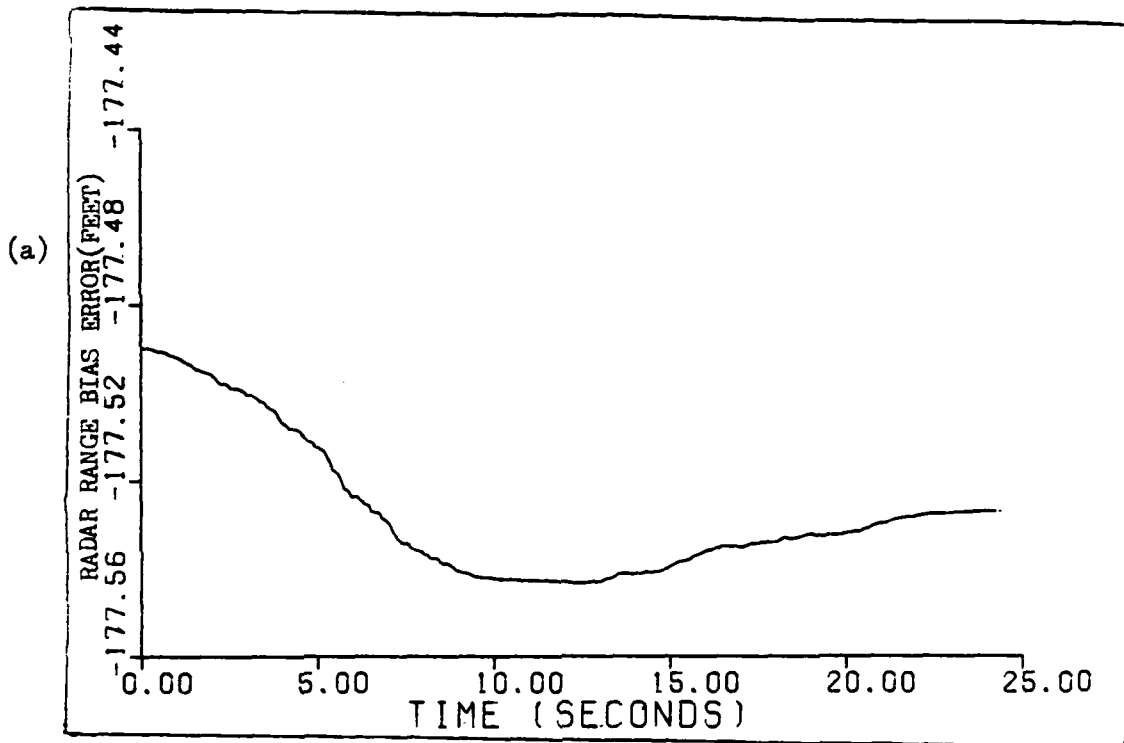


Fig. 5.6(a),(b) Smoother estimate and variance of range bias error after one iteration.

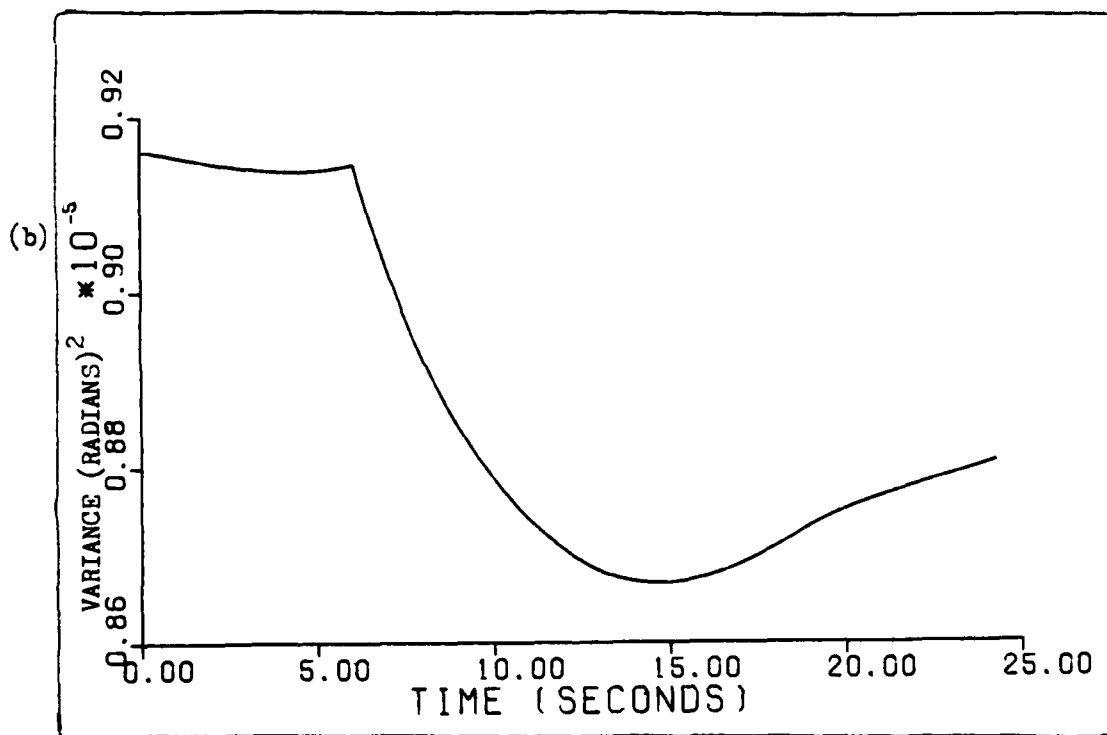
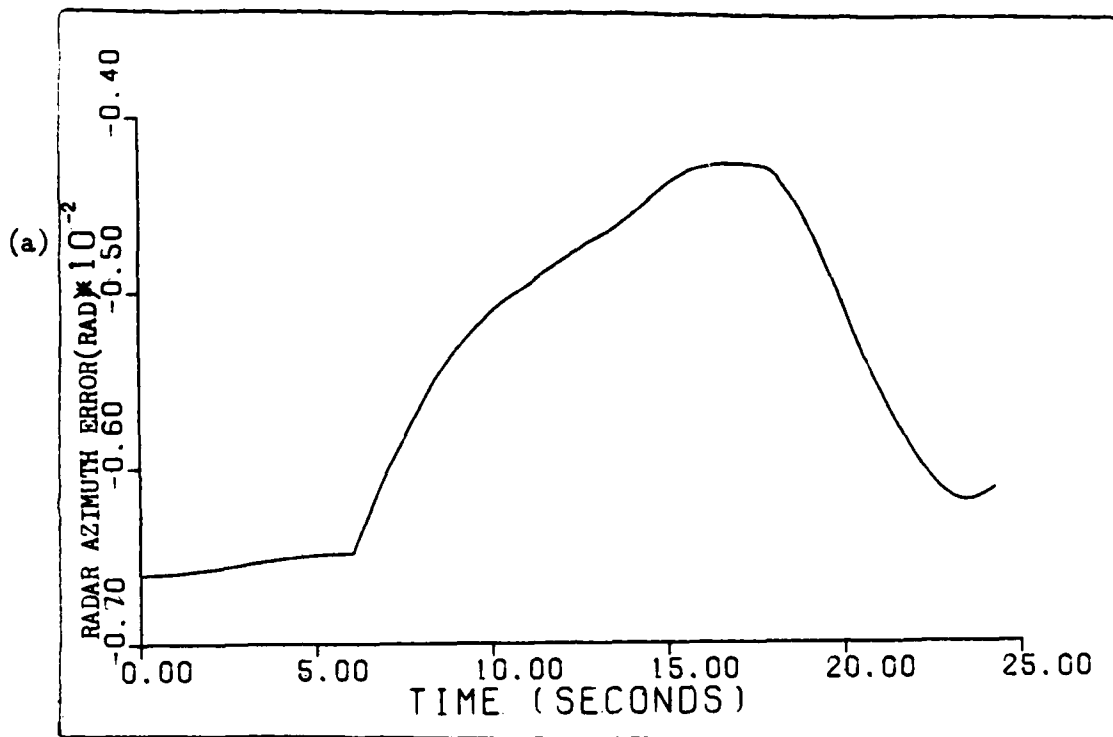


Fig. 5.7(a),(b) Smoother estimate and variance of azimuth bias error after one iteration.

and at the final time,  $t_f = 24.3$  seconds:

$$\hat{x}_1(t_f/t_f) = 16771 \text{ ft} \quad P_{11}(t_f/t_f) = 3186.3 \text{ ft}^2$$

$$\hat{x}_2(t_f/t_f) = 61.21 \text{ ft} \quad P_{22}(t_f/t_f) = 1428.0 \text{ ft}^2$$

Figure 5.2 (a) indicates that the vehicle track is indeed a straight line but not aligned with the x-axis we have chosen. The estimate of y position at the final time is used to re-correct the track heading of 179 degrees. The y position at  $t_f$  is 61.21 feet. This deviation in position indicates that we have "over-corrected" track heading previously by:

$$\tan^{-1} \left[ \frac{\hat{x}_2(t_f/t_f)}{\hat{x}_1(t_f/t_f)} \right] = \tan^{-1} \left[ \frac{61.21}{16771} \right] = .209 \text{ degree}$$

The corrected track heading now becomes 179.209 degrees. We can apply this corrected heading to the measurement relation (4-5) and (4-6) so that the bracketed terms in these equations now become:

$$(\text{DELX} - .9999x_1 + .0138x_2)$$

$$(\text{DELY} + .0138x_1 + .9999x_2)$$

By adjusting the track heading by this amount and recalculating the residual variance, as in Chapter IV, we should be able to reduce the amount of measurement noise,  $R(t_i)$ .

These adjustments should help reconfirm our knowledge of vehicle trajectory and allow the next forward-backward iterations to converge to the "true" state values.

In addition to resetting the initial covariance matrix,  $\underline{P}_0$ , to reflect smoother covariance  $\underline{P}(t_0/t_f)$ , we also correct the initial conditions of the state vector and adjust the amount of driving noise,  $\underline{Q}(t)$ . We should note here that several methods are available to adjust  $\underline{Q}(t)$ . The backward-recursive smoother can be used to generate an estimate of system noise at each sample time,  $\hat{\underline{Q}}(t_i/t_f)$  (4). One can also "tune"  $\underline{Q}(t)$  in an "off-line" manner and allow the system noise to vary over the time interval of interest. If one has knowledge of the time-varying nature of a particular state, this knowledge can be used to adjust the strength of driving noise. For example, we might desire to relate the amount of driving noise on the azimuth bias error state to incorporate our knowledge of radar operator tracking performance versus vehicle acceleration. As a side note, we should also mention that the smoother algorithm can be used to generate an estimate of the applied controls,  $\hat{\underline{u}}(t_i/t_f)$ . An estimate of the controls applied to the system at any time,  $t_i$ , is not the concern of this analysis. We also choose to iteratively adjust  $\underline{Q}(t)$  and use constant noise levels over the time interval of interest. Such an iterative adjustment to  $\underline{Q}(t)$  provides adequate smoother performance and simplifies the algorithm.

Figure 5.4 (a) is a plot of the y component of velocity obtained after one iteration of the smoother algorithm. It is apparent from this plot that the y velocity indeed behaves as a constant with a value of approximately -8.0 ft/sec.

This constant negative velocity is caused by the erroneous initial conditions we used in the extended Kalman filter. As seen in Fig. 5.4 (a) the smoother is able to detect small deviations from the constant y velocity. This is seen as small "bumps" in the plot of y velocity. Thus, our model of random walk with small driving noise is reconfirmed and will be used for the next forward-backward iteration.

The smoother estimated value for accelerometer error,  $\hat{x}_5(t_i/t_f)$ , can be seen in Fig. 5.5 (a). The error appears to grow with time and seems to be related to velocity (i.e., the higher the velocity, the more error). The error does appear to be time-correlated and does not behave as a constant bias error. Thus, the time-correlated model for accelerometer bias appears to be valid. We can, however, adjust the driving noise on the propagation of this state by using the smoother calculated steady state variance. Figure 5.5 (b) shows a constant variance of  $0.14937(\text{ft}/\text{sec}^2)^2$  after only a very short transient period. We can adjust the driving noise on this state by using this steady-state variance:

$$q_5 = P_5(\infty)2/T = .029874 (\text{ft}/\text{sec}^2)^2/\text{sec}$$

The initial variance value for this state,  $P_{05}$ , is also set to  $.014937 (\text{ft}/\text{sec}^2)^2$  to insure a stationary accelerometer error state process.

Figure 5.6 (a) is a plot of smoother estimated radar range bias error,  $\hat{x}_6(t_i/t_f)$ . This figure indicates that this state indeed behaves as a constant with only slight



variations from the initial estimate,  $\hat{x}_6(t_o/t_f) = -177.49$  ft. Thus, a reduction in the amount of driving noise on this state appears valid. We now reduce the strength of driving noise on this state to indicate more confidence in its behavior as a constant. The value of  $q_6$  for the next iteration of the extended Kalman filter-smoother combination is obtained by "tuning" the extended Kalman filter in a sensitivity analysis. The new value for  $q_6$  is determined to be:

$$q_6 = .0001 \text{ ft}^2/\text{sec}$$

This amount of driving noise is two orders of magnitude less than the value used in the first iteration. The new initial variance for  $x_6$  becomes:

$$P_{o6} = 1186.1 \text{ ft}^2$$

and the new initial condition on this state obtained from the smoother becomes:

$$\hat{x}_{o6} = -177.49 \text{ ft}$$

Referring to Fig. 5.7 (a) we see that the azimuth bias error,  $\hat{x}_7(t_i/t_f)$ , does not behave entirely as a constant. It appears that during the first five seconds of the run the bias error is greatest and reduces to a minimum value as the vehicle achieves peak speed (minimum acceleration). As the vehicle begins to decelerate, the azimuth bias error again grows to a larger value. This result is consistent with our knowledge of radar operator tracking error. The

amount of driving noise on this state appears adequate to allow the filter to track deviations in its value. Thus,  $q_7$  is left unchanged for the next iteration of the forward-backward estimator. We adjust the initial condition and variance of this state, as before:

$$P_{07} = .91619 \text{ E-5 rad}^2$$

$$\hat{x}_{07} = .0066051 \text{ rad}$$

The extended Kalman filter and smoother are used again with new initial conditions on the states and adjusted initial variance. The amount of driving noise on accelerometer error,  $x_5$ , and range bias,  $x_6$ , are also adjusted for the next iteration of the forward-backward estimator. As a result of the first iteration of the smoother we make the following adjustments to our model for measurements and initial conditions:

1) The track heading is corrected to 179.209 degrees true.

2) Based on the corrected model for measurement incorporation, we recalculate measurement residual variance to reduce the estimate for  $\underline{R}(t_i)$ ,  $\hat{\underline{R}}(t_i)$ .

3) Initial conditions on the state vector are corrected to reflect the smoother calculation of  $\hat{\underline{x}}(t_0/t_f)$  such that

$$\hat{\underline{x}}_0 = \begin{bmatrix} 167.78 \\ 255.88 \\ 1.1896 \\ -8.0108 \\ -.003834 \\ -177.49 \\ -.0064 \end{bmatrix}$$

4) The initial covariance matrix,  $\underline{P}_0$ , is adjusted to reflect the smoother calculated value of  $\underline{P}(t_0/t_f)$ :

$$\underline{P}_0 = \begin{bmatrix} 3746.5 & & & & \\ & 3649.5 & & & \\ & & 2.315 & & \\ & & & 5.91 & \\ \underline{0} & & & & .015 \\ & & & & & 1186.1 \\ & & & & & & .916E-5 \end{bmatrix}$$

5) Finally, the system noise matrix,  $\underline{Q}(t)$  is corrected to indicate increased confidence in our model for range bias, and adjusted steady-state variance on the accelerometer error:

$$\underline{Q}(t) = \begin{bmatrix} 0 & & & & \\ & 0 & & & \\ & & 0 & & \\ \underline{0} & & & 0 & \\ & & & & .1E-7 \\ & & & & & .02987 \\ & & & & & & .1E-3 \\ & & & & & & & .1E-7 \end{bmatrix}$$

The residual variance analysis detailed in Chapter IV now produces an estimated measurement noise matrix,  $\hat{\underline{R}}(t_i)$ , such that:

$$\hat{\underline{R}}(t_i) = \begin{bmatrix} 16235.4 & 0 \\ 0 & .3900685E-4 \end{bmatrix}$$

The range residual variance is calculated from 415 of 487 total measurements which have a residual magnitude less than 300 feet. These variance values result in calculated RMS errors for the range and azimuth measurements of 127.42 ft and .006245 radian, respectively.

Incorporating updated values for measurement noise, initial state and variance conditions, and system noise, we

rerun the extended Kalman filter. The results of this run are shown in Appendix A. The state and covariance time histories are stored for use in a second iteration of the smoother algorithm.

### Second Iteration of Smoother

The second iteration of the optimal smoother algorithm provides refined state estimates as shown in Figs. 5.8 (a) to 5.14 (a). The basic behavior and values of these states remain unchanged from the first iteration of the smoother. The smoother state estimates at the initial time,  $t_0$ , are refined from those obtained in the first iteration.

To illustrate the convergent properties of the smoother, we present a comparison of state estimates and variances between the first and second smoother iterations in Table II. This table includes the percentage difference between the two iterations for each state and variance value and the overall percentage change between the second and first iteration. We choose to compare these values at the time of peak vehicle speed at 16.85 seconds. Table II indicates good reduction in error variance for all the states. This is due to the improved initial conditions supplied to the extended Kalman filter after the first run of the smoother. The smoother is able to reduce error variance from the first to second iterations due to improved state estimates from the forward filter. The convergence of the velocity state estimates and reduction in error variance on these states is

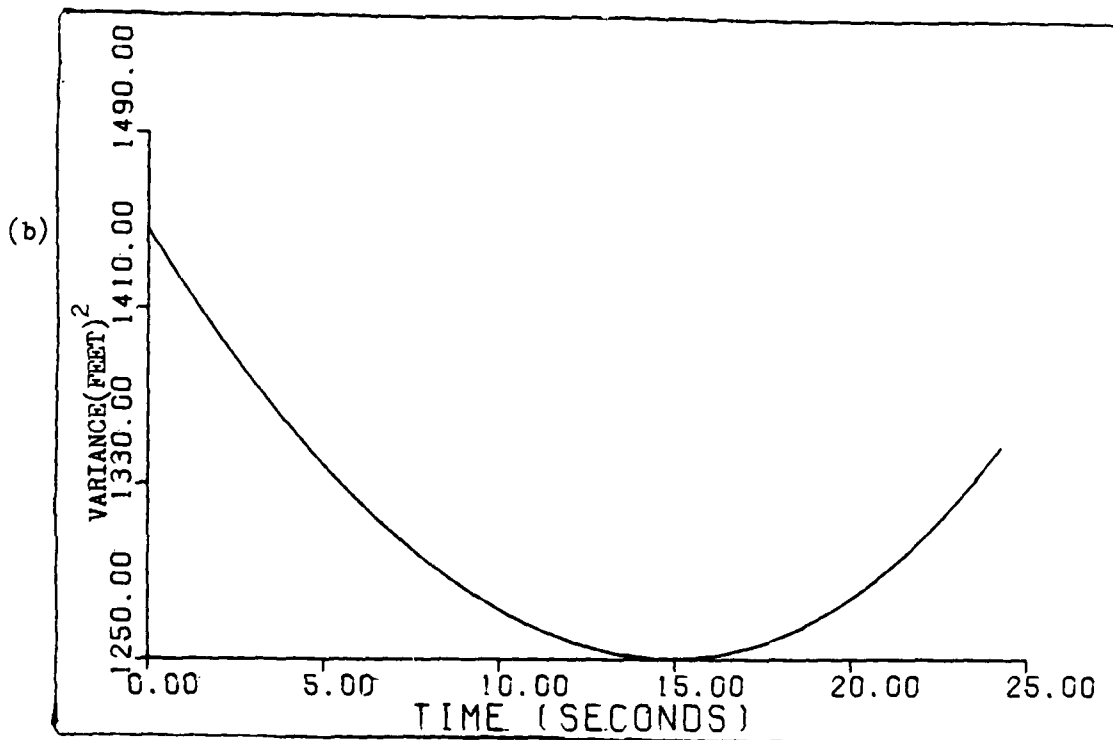
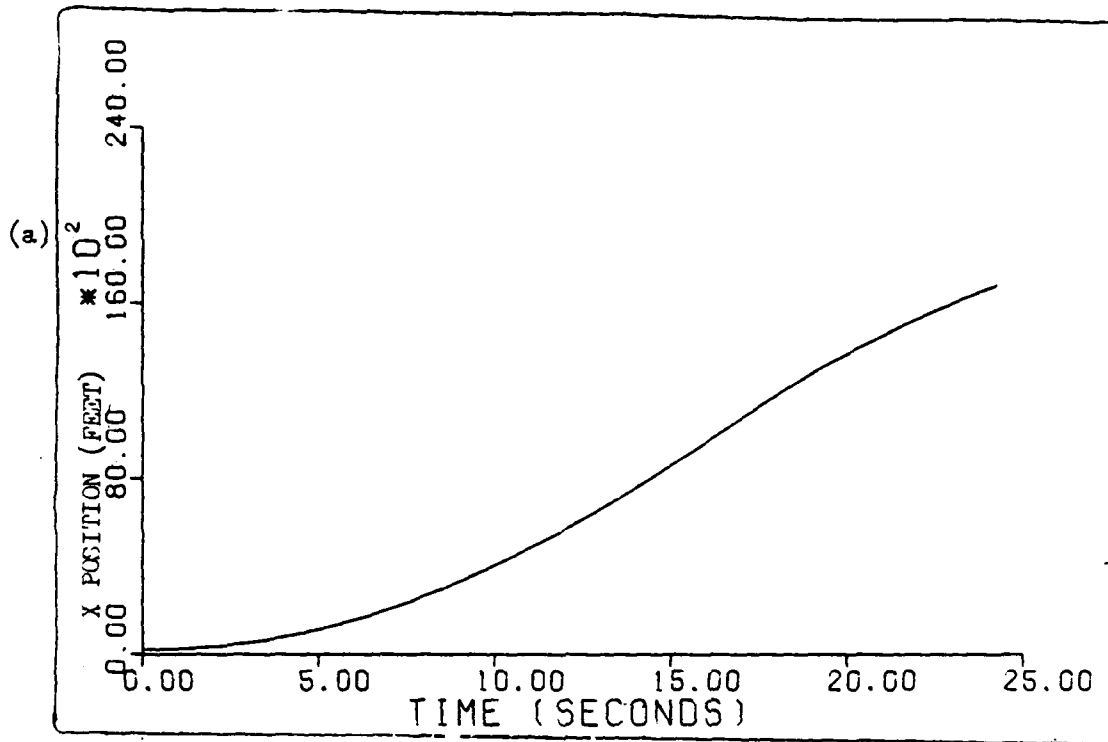


Fig. 5.8(a),(b) Smoother estimate and variance of x-position after two iterations.

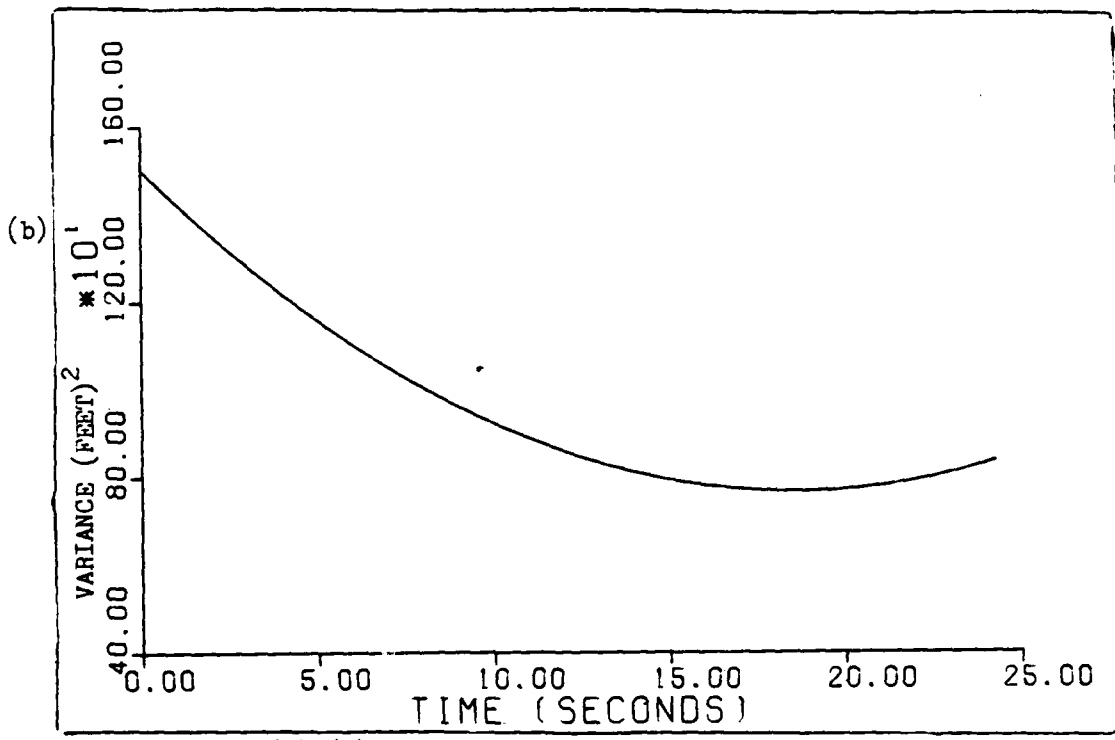
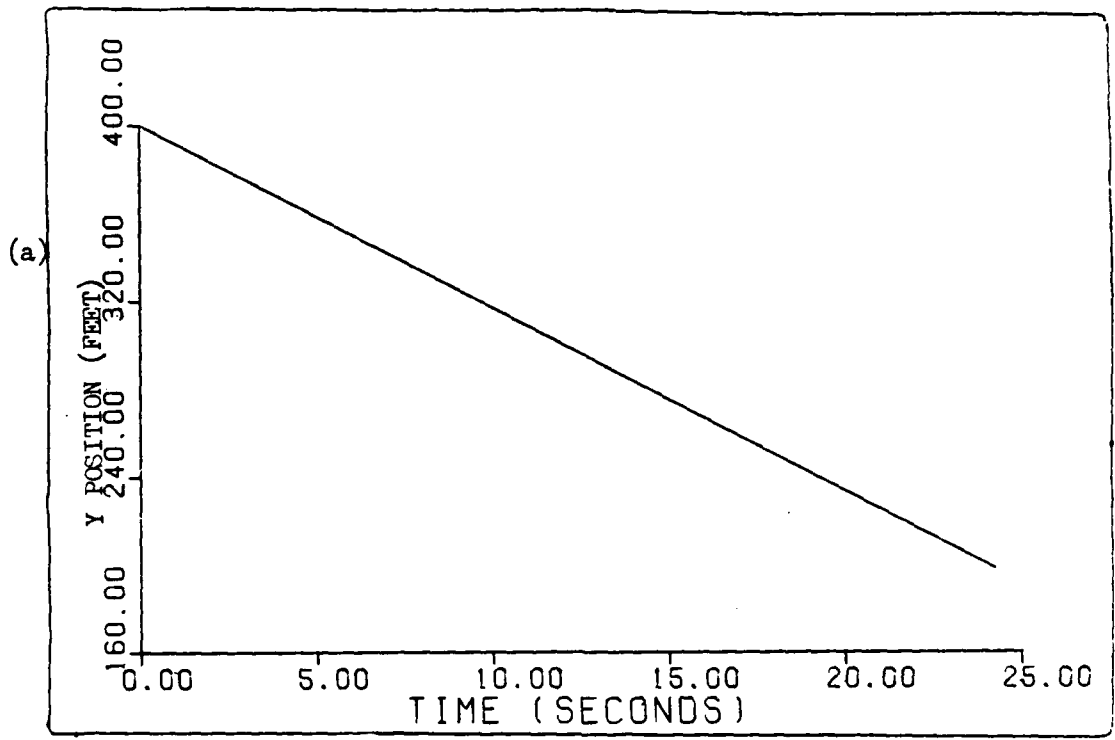


Fig. 5.9(a),(b) Smoother estimate and variance of y-position after two iterations.

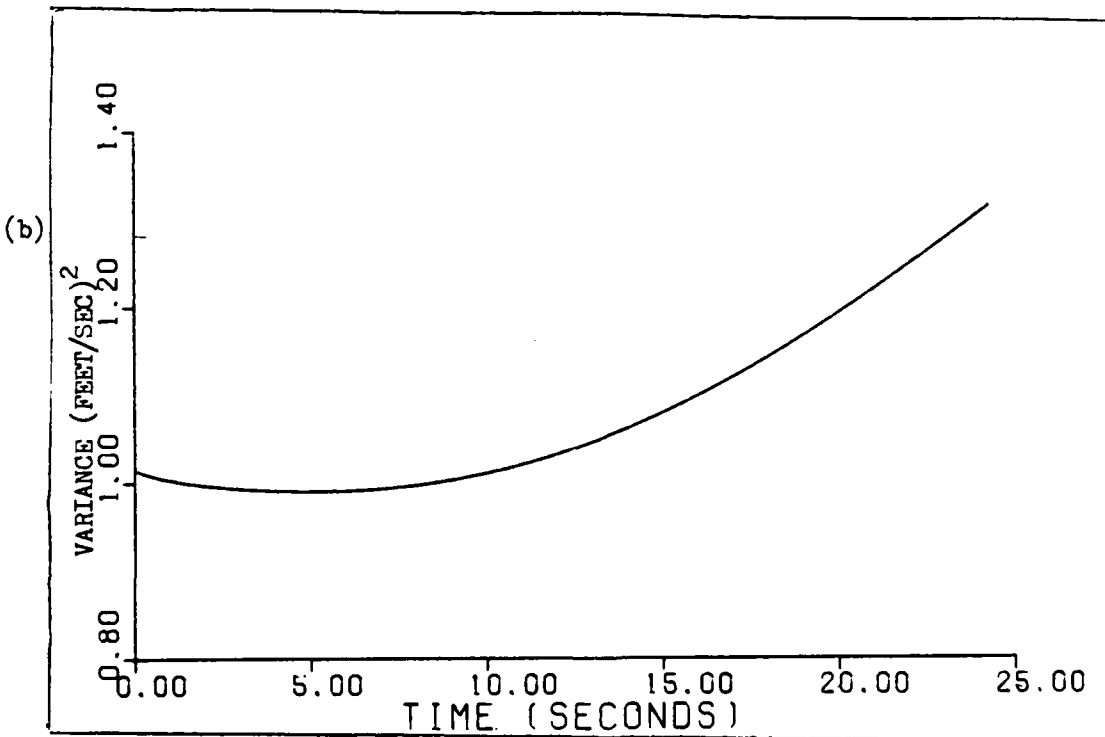
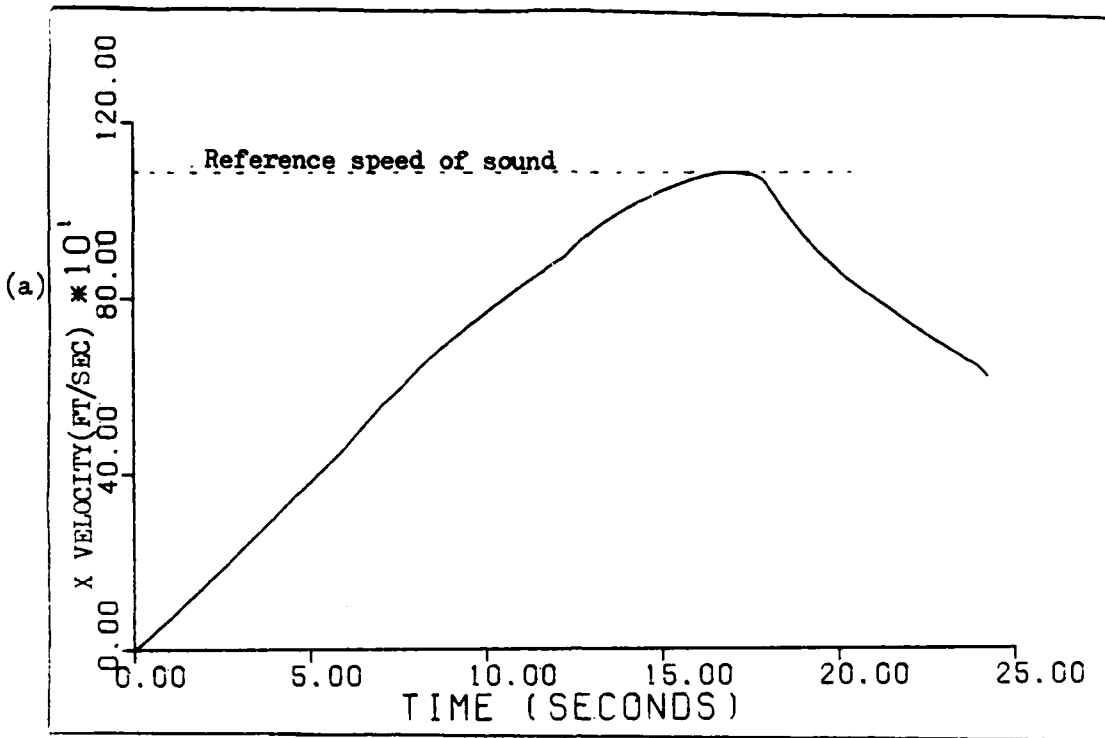


Fig. 5.10(a),(b) Smoother estimate and variance of x-velocity after two iterations.

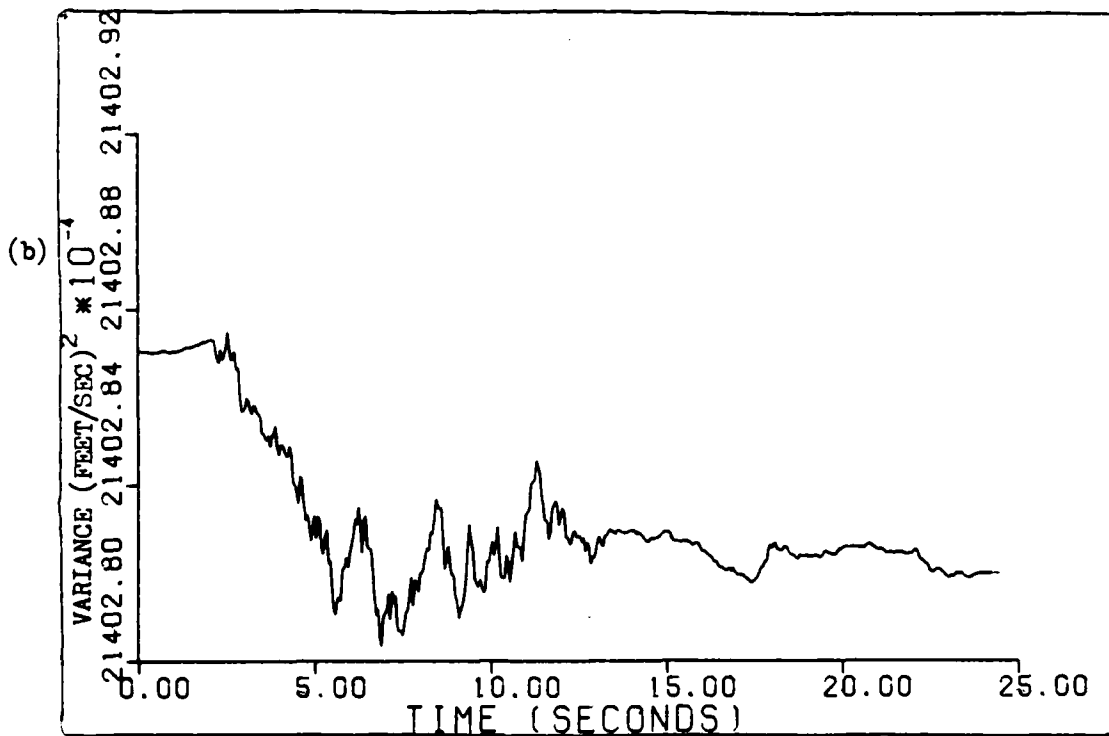
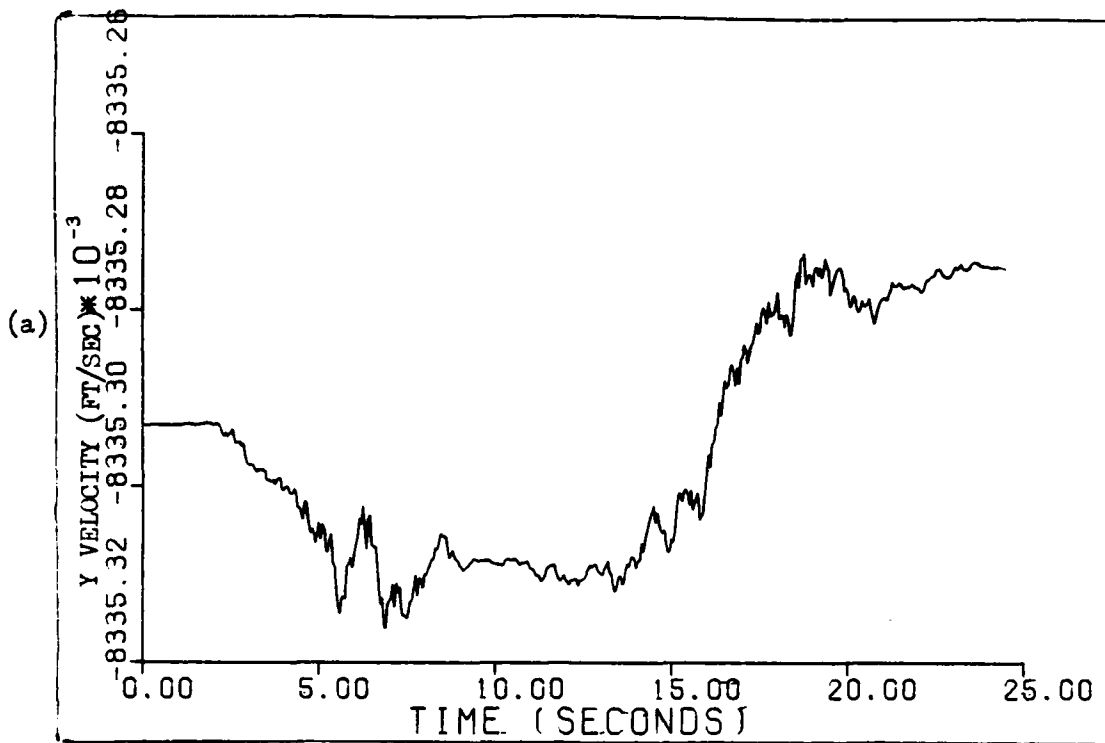


Fig. 5.11(a),(b) Smoother estimate and variance of y-velocity after two iterations.



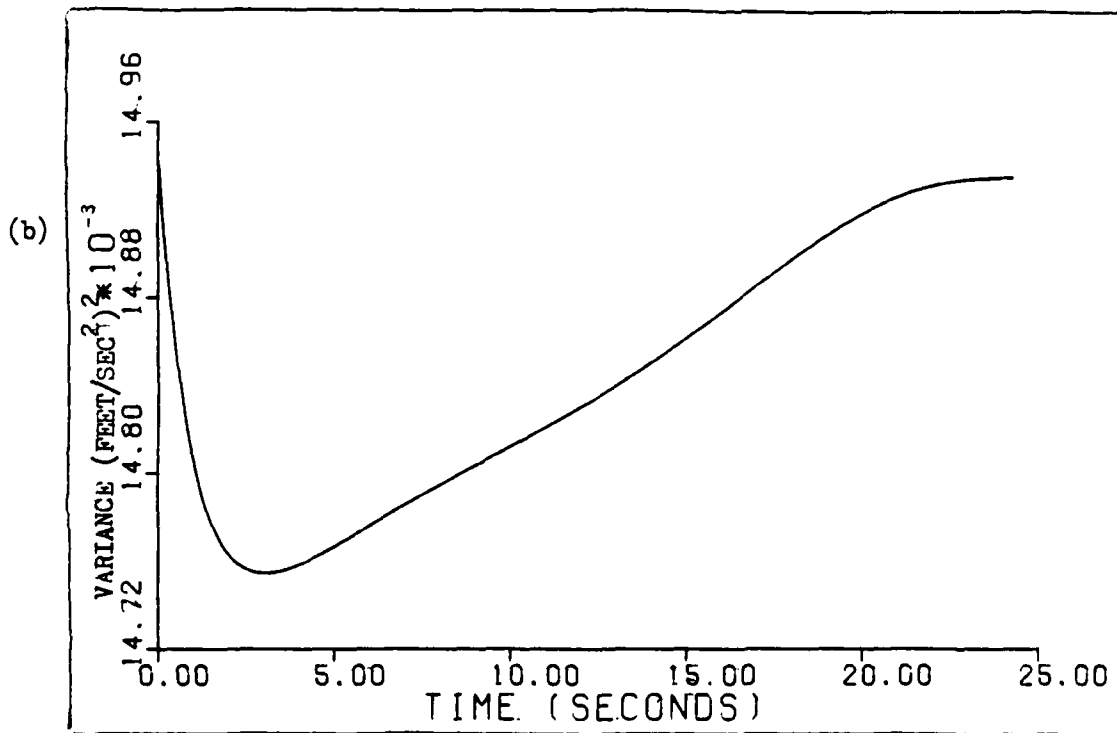
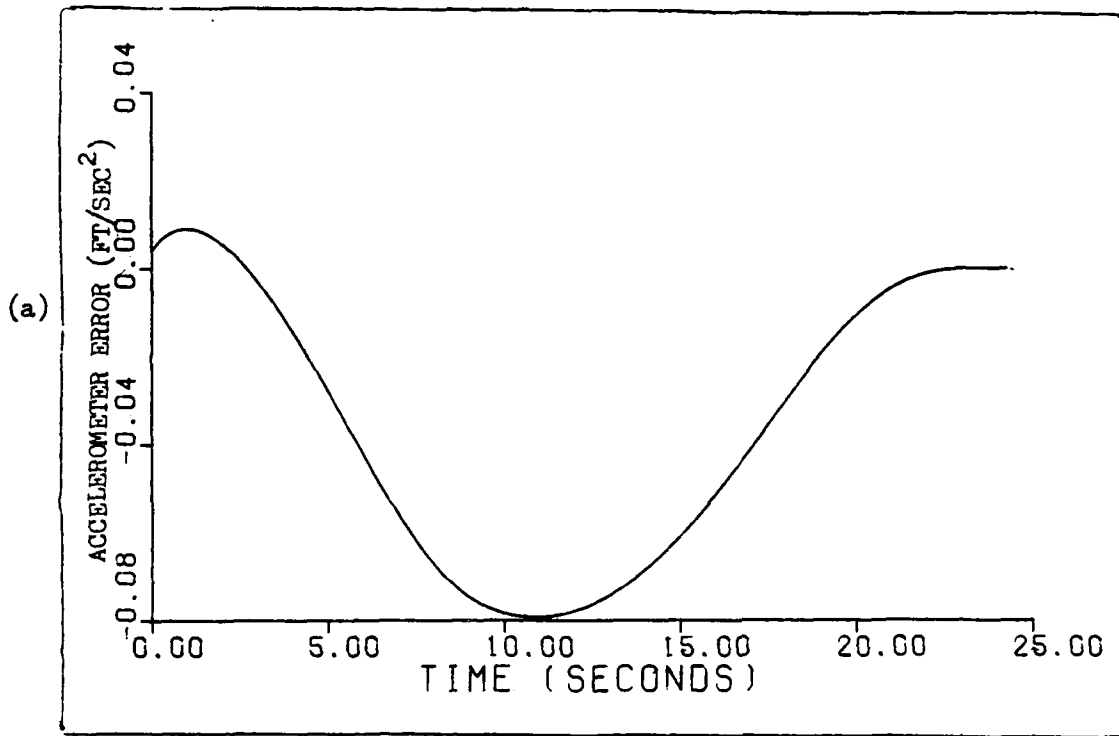


Fig. 5.12(a),(b) Smoother estimate and variance of accelerometer error after two iterations.

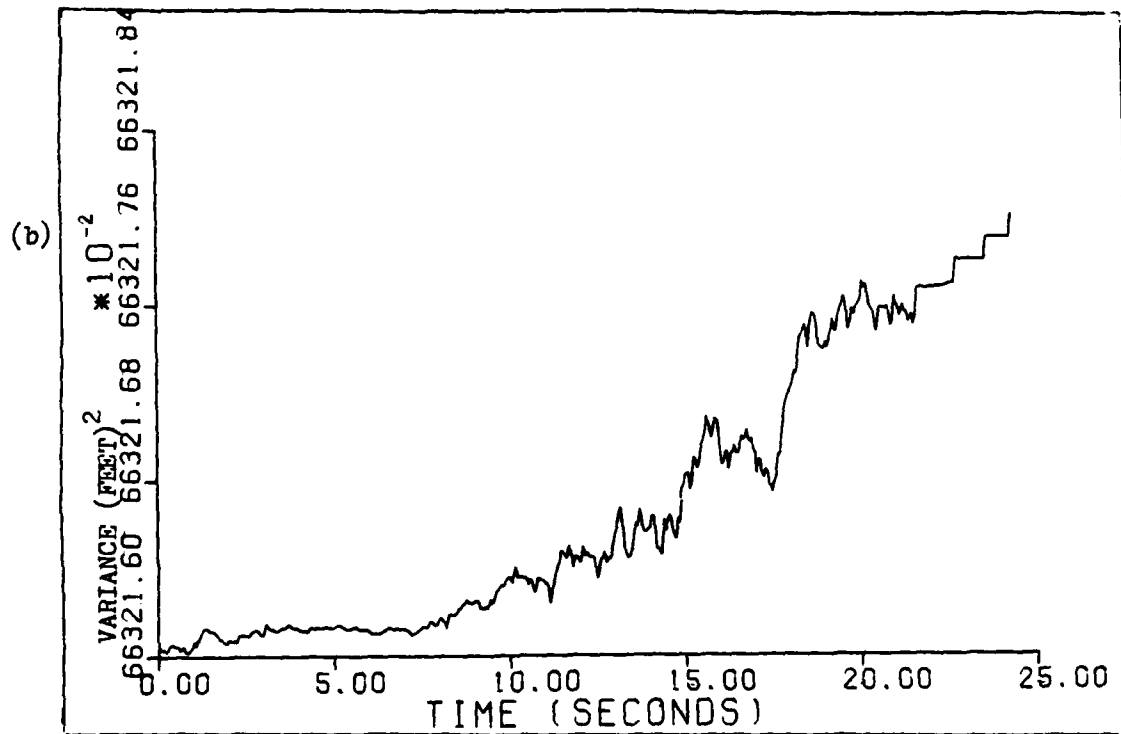
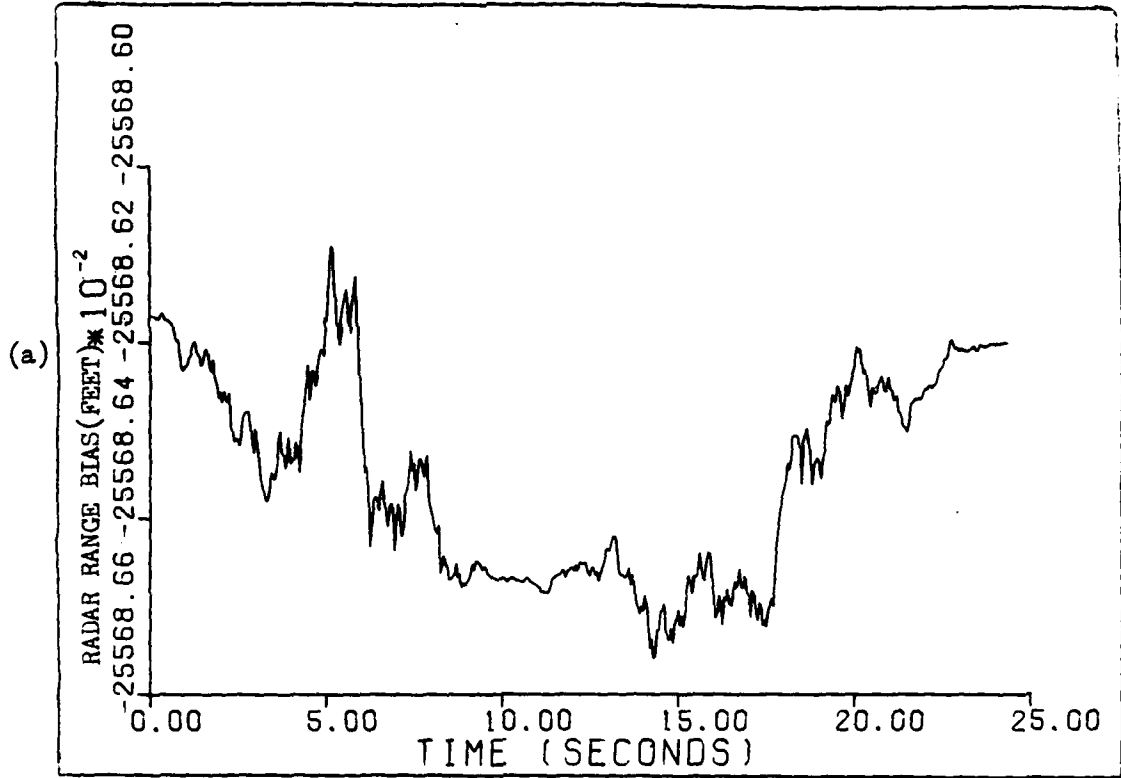


Fig.5.13(a),(b) Smoother estimate and variance of range bias error after two iterations.

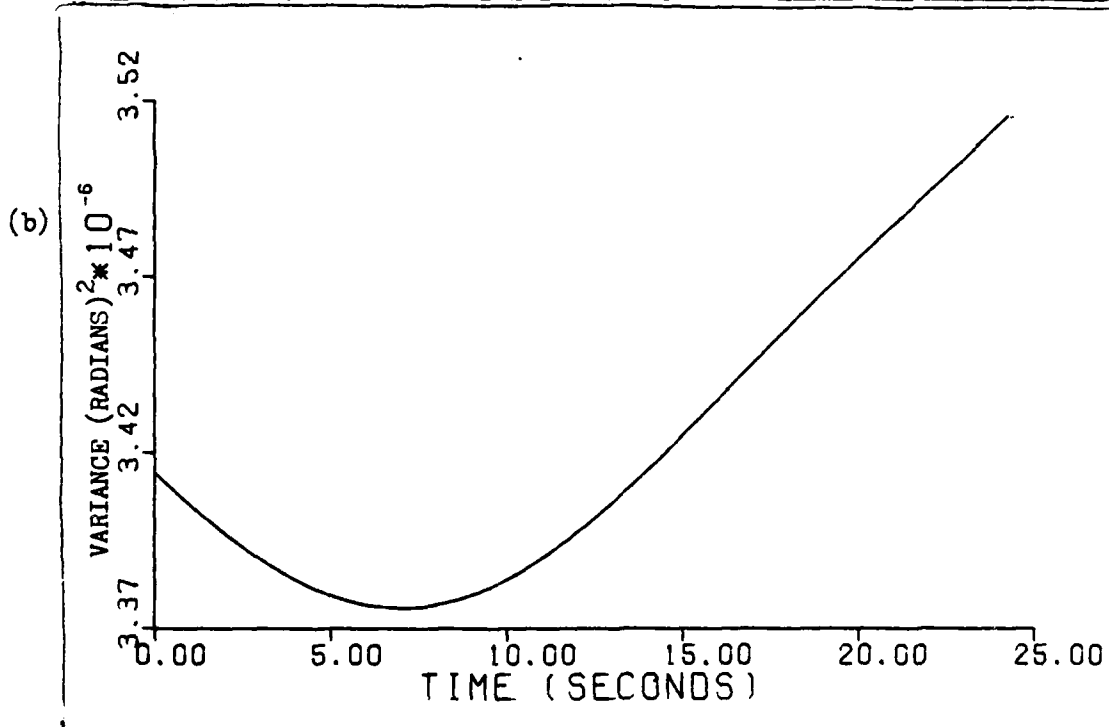
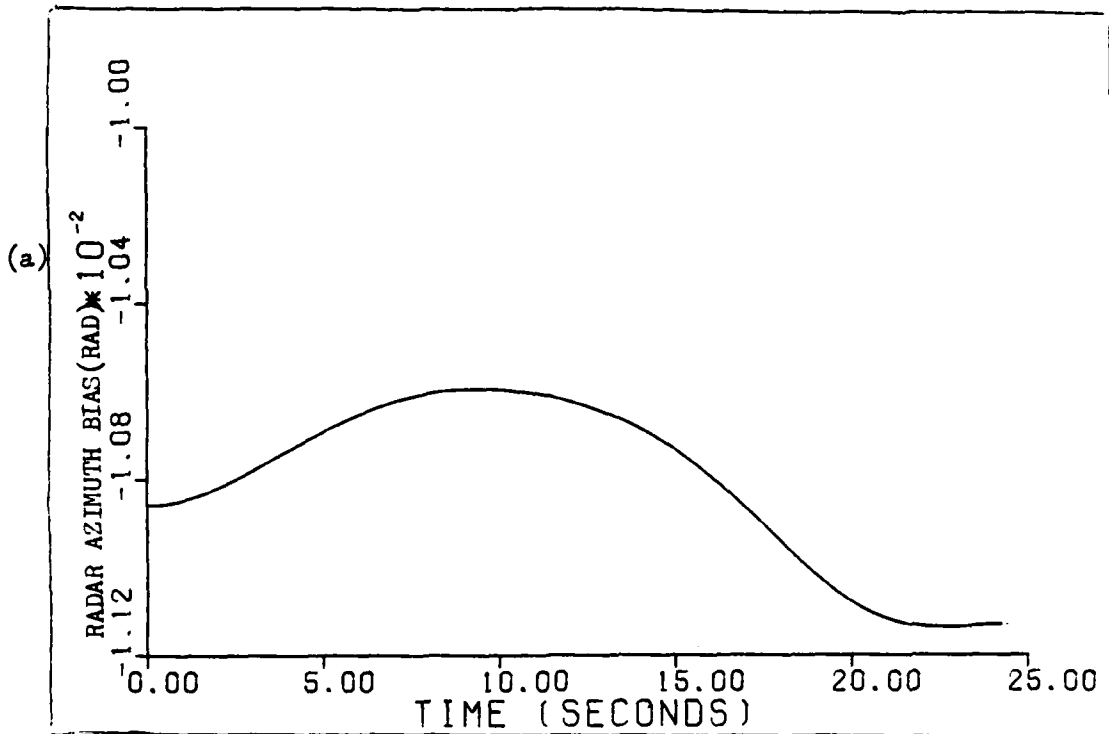


Fig. 5.14(a),(b) Smoother estimate and variance of azimuth bias error after two iterations.

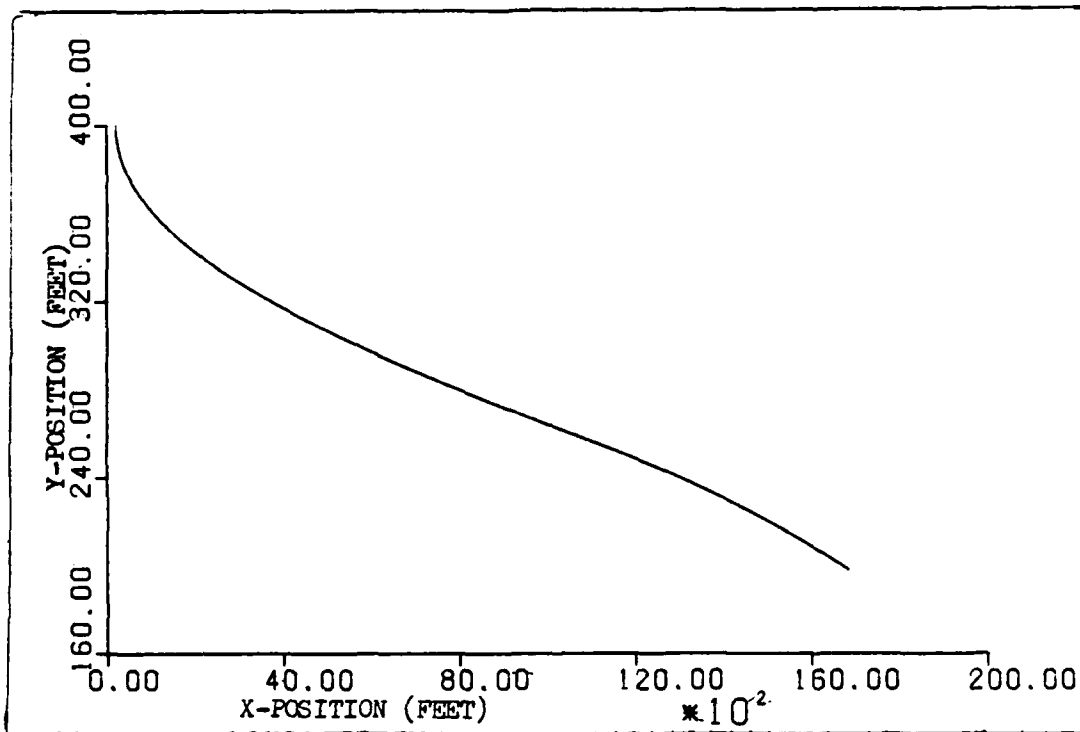


Fig. 5.15 Vehicle trajectory in earth-fixed coordinate frame of reference ( $x_2$  plotted against  $x_1$  - feet)

TABLE II

Comparison of First and Second Smoother Iterations

State	$x(16.85/t_f)^*$	$x(16.85/t_f)^{**}$	Difference(%)	$P(16.85/t_f)^*$	$P(16.85/t_f)^{**}$	Difference(%)
$x_1$	10502.3	10577.3	+ .71	3107.5	1254.2	-59.64
$x_2$	120.89	259.72	+114.84	1367.3	772.7	-43.49
$x_3$	1080	1082	+ .185	2.096	1.117	-46.71
$x_4$	-8.01	-8.33	-4.0	5.909	2.14	-63.78
$x_5$	-.1073	-.0427	+60.2	.01488	.01488	0
$x_6$	-177.53	-255.7	-44.03	1186.2	663.22	-44.08
$x_7$	-.00429	-.0108	-151.75	.8687E-5	.3444E-5	-60.35

Average change = -3.4%

Average change = -45.44%

\* First Iteration

\*\* Second Iteration

sufficient to stop the iterations at two. Another iteration of the smoother using refined initial conditions for the extended Kalman filter based on  $\hat{\underline{x}}(t_0/t_f)$  and  $\underline{P}(t_0/t_f)$  was not made due to time limitations and sufficient confidence in our estimate of vehicle performance. A third iteration of the smoother would provide only limited refinement of state estimates and better reduction in error variance. However, it will be shown in Chapter VI that only two iterations meet our confidence level requirements.

Figures 5.8 (a) and 5.9 (a) show the starting position of the vehicle to be approximately 400 feet east and 200 feet north of the assumed coordinate origin. The x velocity estimate (Fig. 5.10 (a)) at  $t_0$  again indicates that the vehicle has already started down the track at the assumed initial time. The smoother estimate of x velocity at  $t_0$  is 2.72 ft/sec. Comparing this to the accelerometer only run, the point in the radar data chosen as  $t_0$  appears to be in error by approximately one sample period or .05 second. The y velocity estimate again shows a constant value of approximately -8.33 ft/sec. This constant negative velocity is caused by the orientation of the test track with respect to the chosen coordinate frame of reference. To illustrate the actual vehicle track in the assumed frame of reference, Fig. 5.15 shows smoother estimated y position plotted against x position. This plot indicates the estimated trajectory of the vehicle in the earth-fixed coordinate frame of reference. The trajectory is indeed a straight line, but not along the

x-axis we have used. However, an exact starting position and track orientation are not the goals of this analysis. Our main interest is to obtain a good estimate of peak vehicle speed along the track. We are not concerned with where this peak speed occurs but more with the value and error of this estimate.

The second iteration of the smoother yields a maximum velocity of 1082.028 ft/sec at 16.85 seconds from chosen initial time. The scalar speed estimate at 18.65 seconds, FIM trap entry time, is 975.043 ft/sec. The reason we do not get better agreement between the smoother and FIM estimates of velocity at the trap is due to the time skew in the radar data previously discussed. The time scale we have used shows trap entry between 18.60 to 18.70 seconds but we are not sure exactly where trap entry occurs in this interval.

The behavior of the error states indicated by the first iteration of the smoother is reconfirmed by the second iteration. The radar range bias error behaves very much as a constant with only slight deviations from a steady value of -255.68 ft. The smoother estimate of range error is plotted in Fig. 5.13 (a). Radar azimuth error in Fig. 5.14 (a) is again shown to be "slowly-varying" over the 24 second interval. Our initial assumptions about the radar operator azimuth tracking error are again reconfirmed. The error in azimuth starts out high as the operator lags behind the vehicle due to rapid acceleration, decreases as the operator "catches up"

to the car near peak speed, and again increases upon vehicle deceleration as the operator "jumps" ahead of the car.

The accelerometer error state estimate shown in Fig. 5.12 (a) indicates that this state varies between approximately 0 to  $0.08 \text{ ft/sec}^2$  or 0 to .0025 g's. Maximum error in the accelerometer occurs at approximately ten seconds into the run and the error decreases to near zero by 24 seconds. Perhaps the behavior of this error state can be explained by referring to Fig. 3.2 which is a plot of raw accelerometer data in g's versus time. Figure 3.2 indicates that maximum sustained g's on the vehicle occur between 0 to 10 seconds and slowly decrease from that time on. It appears from Fig. 5.12 (a) that the accelerometer error is a function of the time of application and level of sustained g's on the vehicle. This figure indicates a time-correlated behavior of the accelerometer. Such behavior may have been adequately modeled as a random walk. One way to model this behavior might be to relate the amount of driving noise on the accelerometer error state to the level of acceleration units at any given time. Thus,  $q_5$ , could be modeled as time-varying for use in a random walk model of accelerometer error. Certainly, it can be argued that a correlation time of one second is too short from the behavior of the accelerometer error shown in Fig. 5.12 (a). Nevertheless, the forward-backward iterations have provided better information on the "true" behavior of the states of interest. Another iteration of the smoother could be made with updated initial conditions and perhaps a



different model for accelerometer error, but two iterations have provided sufficient reduction in variance values for our purposes.

Figures 5.8 (b) through 5.14 (b) are plots of smoother calculated error variances for each state. These plots show that the backward filter is able to reduce the errors in state estimates from those obtained from the first iteration of the smoother. After two iterations of the forward-backward estimator, the error in state estimation is reduced by an average of 45% over that obtained in the first iteration of the smoother.

The results of this second iteration of the smoother are now used to test the hypothesis that the rocket car did, in fact, exceed the reference speed of sound. This will be shown in detail in the next chapter.

## VI. Hypothesis Testing

The previous chapter presented the results of the extended Kalman filter - fixed interval smoother estimation scheme. The resulting state estimates and error covariance after two iterations of the smoothing method will now be evaluated to yield the best estimate of peak rocket car speed and a confidence level for this estimate. Before we can analyze a hypothesis test of the peak vehicle speed, it is necessary to calculate the scalar speed estimate standard deviation.

### Development of Scalar Speed Standard Deviation

The values for  $x_3$  and  $x_4$ ,  $x$  and  $y$  velocity, are given in terms of mean values,  $\hat{x}_3(t_i/t_f)$  and  $\hat{x}_4(t_i/t_f)$  and variances  $P_{33}(t_i/t_f)$  and  $P_{44}(t_i/t_f)$  and the covariance  $P_{34}(t_i/t_f)$ . Under our assumptions of approximately Gaussian error models, these mean and variance values completely describe a two-dimensional Gaussian probability density function which propagates forward in time from the initial to final time. The state estimates of  $x$  and  $y$  velocity provide the components of a two-dimensional conditional mean vector,  $\underline{m}$ , the magnitude of which is the estimate of scalar speed at any time,  $t_i$ . This mean vector in the  $x$ - $y$  plane, shown in Fig. 6.1, locates the peak of the density function. Surfaces of "constant likelihood" (4) are generated by passing planes through the density function parallel to the  $x$ - $y$  plane. These surfaces are

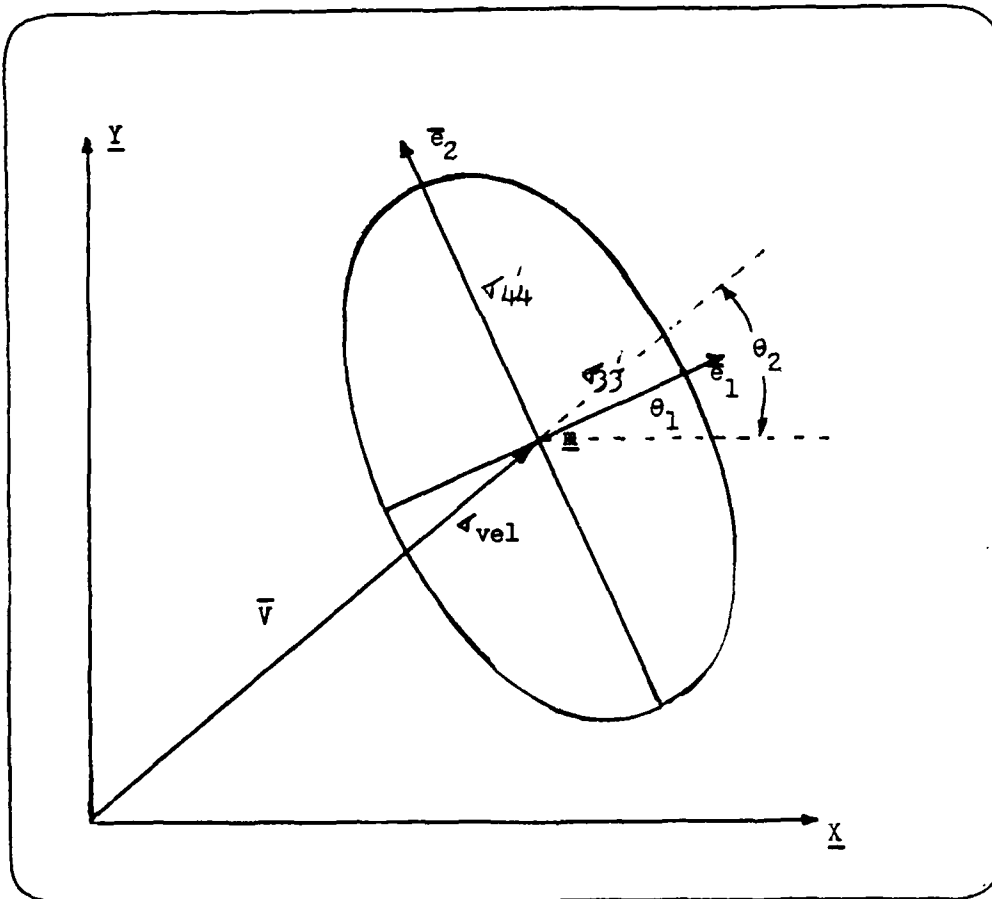


Fig. 6.1 Velocity vector and one sigma ellipse of constant likelihood

ellipses parallel to the x-y plane and when viewed from above, the one sigma surface of constant likelihood appears as in Fig. 6.1.

The covariance matrix for the two-dimensional velocity density function determines the spread of the density about  $\underline{m}$  as in the figure. This covariance matrix also determines the angular orientation of the "principal axes" (4) of the ellipses of constant likelihood.

$$\underline{P}_{34}(t_i) = \begin{bmatrix} \sigma_{33}^2 & \rho_{34}\sigma_{34}\sigma_{43} \\ \rho_{43}\sigma_{43}\sigma_{34} & \sigma_{44}^2 \end{bmatrix} \quad (6-1)$$

where  $\rho$  is the correlation factor. If there were no correlation between state estimates of x and y velocity (i.e.,  $\rho_{34} = \rho_{43} = 0$ ), the covariance matrix would be diagonal, and the principal axes of the ellipse would be parallel to the x and y axes. The magnitudes of the semimajor and semiminor axes of the one sigma ellipse are determined from the eigenvalues,  $\lambda_i$ , of the covariance matrix

$$\sigma_{33}' = \sqrt{\lambda_1} \quad (6-2)$$

$$\sigma_{44}' = \sqrt{\lambda_2} \quad (6-3)$$

where the primed notation indicates the lengths are defined in the principal axes frame of reference. We desire to relate the calculated scalar speed estimate from the optimal smoother:

$$\left[ \bar{v}(t_i/t_f) \right] = \left[ (\hat{x}_3(t_i/t_f))^2 + (\hat{x}_4(t_i/t_f))^2 \right]^{1/2} \quad (6-4)$$

to its associated standard deviation. To do this we must find the associated representation of the normalized velocity vector estimate in the frame of the principal axes of the one sigma ellipse shown in Fig. 6.1. The velocity vector in the x-y coordinate frame can be represented by:

$$\bar{v}_{xy} = v_x \bar{i}_x + v_y \bar{i}_y \quad (6-5)$$

The same vector can be specified using the unit vectors,  $\bar{e}_1$  and  $\bar{e}_2$ , in the principal axes frame of reference:

$$\bar{v}_{e_1 e_2} = v_{e_1} \bar{e}_1 + v_{e_2} \bar{e}_2 \quad (6-6)$$

From the smoother-generated variances and covariances for x and y velocity we solve for the associated eigenvalues and eigenvectors of this matrix. The square root of the eigenvalues of this 2-by-2 matrix will be shown to be the length of the semiminor and semimajor axis of the one sigma ellipse. The associated eigenvectors determine the angular orientation of the principal axes of the one sigma ellipse.

We solve for eigenvalues and eigenvectors in the following manner. For simplification, we define the covariance matrix of the velocity states at any time,  $t_i$ , as:

$$\underline{P}_{34}(t_i) = \begin{bmatrix} P_{33} & P_{34} \\ P_{43} & P_{44} \end{bmatrix} \quad (6-7)$$

Forming the matrix  $[\lambda \underline{I} - \underline{P}]$  and solving for the determinant we can find the eigenvalues of  $\underline{P}_{34}$ :

$$|\lambda \underline{I} - \underline{P}| = \begin{vmatrix} \lambda - P_{33} & -P_{34} \\ -P_{43} & \lambda - P_{44} \end{vmatrix} = \lambda^2 - (P_{33} + P_{44})\lambda + (P_{33}P_{44} - P_{34}P_{43}) \quad (6-8)$$

This "characteristic polynomial" is set equal to zero and the resulting roots are the eigenvalues,  $\lambda_1$  and  $\lambda_2$ , of the velocity covariance matrix. Noting that this covariance matrix is symmetric so that:

$$P_{34} = P_{43} \quad (6-9)$$

we define the characteristic polynomial as:

$$\lambda^2 - (P_{33} + P_{44})\lambda + (P_{33}P_{44} - P_{34}^2) = 0 \quad (6-10)$$

The resulting eigenvalues are

$$\lambda_{1,2} = [(P_{33} + P_{44}) \pm \sqrt{(P_{33} + P_{44})^2 - 4(P_{33}P_{44} - P_{34}^2)}] / 2 \quad (6-11)$$

Substituting these eigenvalues,  $\lambda_i$ , into the matrix  $[\lambda_i \underline{I} - \underline{P}]$  and noting that the eigenvectors are in the "null space" of this matrix, so that

$$\begin{bmatrix} \lambda_i - P_{33} & -P_{34} \\ -P_{34} & \lambda_i - P_{44} \end{bmatrix} \begin{bmatrix} e_{i1} \\ e_{i2} \end{bmatrix} = \underline{0} \quad (6-12)$$

results in two equations for each eigenvector of the form:

$$a e_{i1} + b e_{i2} = 0 \quad (6-13)$$

either one of which is related to the other by a constant.

Thus, we have one equation and two unknowns from which to solve for the eigenvector,  $\bar{e}_i$ , for a given eigenvalue,  $\lambda_i$ .

We need another relation between the components of the eigenvector in order to solve for the individual elements. Noting that the "normalized" eigenvector is the unit vector we find the other equation:

$$e_{i1}^2 + e_{i2}^2 = 1 \quad (6-14)$$

With two equations and two unknowns we can solve for the individual components of each eigenvector.

The resulting eigenvectors determine the angular orientation of the principal axes of the one sigma ellipse. The angle,  $\theta_1$ , between the x-axis and the semiminor axis of the ellipse (associated with x velocity error variance) can be found from:

$$\theta_1 = \tan^{-1} (e_{12}/e_{11}) \quad (6-15)$$

where  $e_{12}$  and  $e_{11}$  are the components of the eigenvector which describes the orientation of the semiminor axis. This angle specifies a coordinate transformation matrix,  $\underline{L}$ , for a rotation about the z axis, such that:

$$\underline{L} = \begin{bmatrix} \cos\theta & \sin\theta & 0 \\ -\sin\theta & \cos\theta & 0 \\ 0 & 0 & 1 \end{bmatrix} \quad (6-16)$$

This coordinate transformation matrix is used to relate the orientation of the normalized velocity vector to the principal axes of the one sigma ellipse. Transforming this velocity unit vector into the frame of reference of the principal axes, we obtain a length from ellipse center to the one sigma ellipse in the direction of the velocity vector. It is the magnitude of this length,  $\sigma_{vel}$  in Fig. 6.1, which determines scalar speed standard deviation.

#### Calculation of Peak Scalar Speed and Standard Deviation

After two iterations of the smoother algorithm we arrive at the following estimates of x and y velocity at 16.85

seconds. As in the previous iteration, this time is found to be the point at which peak x velocity is obtained. The associated error variances and covariances for  $x_3$  and  $x_4$  at this time are also given:

<u>Velocity State Estimates</u>	<u>Covariances</u>
$\hat{x}_3(16.85/t_f) = 1081.996 \text{ fps}$	$P_{33} = 1.117148 \text{ (fps)}^2$
$\hat{x}_4(16.85/t_f) = -8.335287 \text{ fps}$	$P_{44} = 2.140282 \text{ (fps)}^2$
	$P_{34} = P_{43} = .071 \text{ (fps)}^2$

The magnitude of the velocity vector or scalar speed estimate is:

$$|\bar{v}| = 1082.028 \text{ fps} \quad (6-17)$$

From the covariances for the velocity state estimates at 16.85 seconds we form the two-dimensional covariance matrix:

$$P_{34} = \begin{bmatrix} 1.117148 & .071 \\ .071 & 2.140282 \end{bmatrix} \quad (6-18)$$

The eigenvalues and associated eigenvectors for this matrix are found from (6-11), (6-13), and (6-14):

$$\begin{aligned} \lambda_1 &= 1.11328 & \bar{e}_1 &= \begin{bmatrix} .99852 \\ .0544 \end{bmatrix} \\ \lambda_2 &= 2.14453125 & \bar{e}_2 &= \begin{bmatrix} .06894 \\ .99762 \end{bmatrix} \end{aligned} \quad (6-19)$$

The lengths of the semiminor and semimajor axes of the one sigma ellipse of constant likelihood become:



$$\begin{aligned}\sqrt{\lambda_1} &= 1.05512 \text{ ft/sec} \\ \sqrt{\lambda_2} &= 1.464422 \text{ ft/sec}\end{aligned}\quad (6-20)$$

The eigenvector associated with  $\lambda_1$  determines the angular orientation of the semiminor axis of the one sigma ellipse in the x-y coordinate frame of reference:

$$\theta_1 = \tan^{-1}(.0544/.99852) = 3.11843 \text{ degrees} \quad (6-21)$$

This angle,  $\theta_1$ , defines a direction cosine matrix,  $\underline{L}$ , in order to transform the normalized velocity vector

$$\bar{v} = 1081.996\bar{i}_x - 8.335287\bar{i}_y \Rightarrow .99997\bar{i}_x - .0077\bar{i}_y \quad (6-22)$$

into the frame of reference of the one sigma ellipse such that

$$\underline{L} = \begin{bmatrix} .99852 & .0544 & 0 \\ -.0544 & .99852 & 0 \\ 0 & 0 & 1 \end{bmatrix} \quad (6-23)$$

and

$$\begin{aligned}\bar{i}_x &= .99852\bar{e}_1 + .0544\bar{e}_2 \\ \bar{i}_y &= -.0544\bar{e}_1 + .99852\bar{e}_2\end{aligned}\quad (6-24)$$

The normalized velocity vector in the principal axes frame becomes

$$\begin{aligned}\bar{v}_{\bar{e}_1\bar{e}_2} &= .99997(.99852\bar{e}_1 + .0544\bar{e}_2) - .0077(-.0544\bar{e}_1 + .99852\bar{e}_2) \\ &= .9989\bar{e}_1 + .0467\bar{e}_2\end{aligned}\quad (6-25)$$

The angle of this normalized vector with respect to the x-axis becomes:

$$\theta_2 = \tan^{-1}(.0467/.9989) = 2.6767 \text{ degrees} \quad (6-26)$$

Subtracting (6-26) from (6-21) we find the angle between the  $\bar{e}_1$  eigenvector and the velocity vector in the principal axes frame:

$$\theta_1 - \theta_2 = .44172 \text{ degrees} \quad (6-27)$$

This knowledge will become helpful in a moment.

We need to find the distance from the one sigma ellipse center to the ellipse itself, in the direction of the velocity vector,  $\bar{v}_{\bar{e}_1 \bar{e}_2}$ . To accomplish this, we have the general equation for any point  $(x_1, x_2)$  on the ellipse:

$$\frac{x_1^2}{\lambda_1} + \frac{x_2^2}{\lambda_2} = c \quad (6-28)$$

where  $c$  is a constant. For the one sigma ellipse  $c$  is equal to one. We also have the familiar relationship between two vectors  $\bar{v}_1, \bar{v}_2$ :

$$\frac{\bar{v}_1 \cdot \bar{v}_2}{|\bar{v}_1| |\bar{v}_2|} = \cos \gamma \quad (6-29)$$

where  $\gamma$  is the angle between the vectors. Let  $x_1$  and  $x_2$  describe the coordinates of the point where the line from ellipse center in the direction of the transformed velocity unit vector intersects the ellipse. We apply (6-28) and (6-29) to the point on the ellipse described by these points  $x_1$  and  $x_2$ . In (6-29) we are interested in the  $\bar{e}_1$  eigenvector direction of length  $\sqrt{\lambda_1}$ , and the transformed velocity vector

$$\bar{v} = x_1 \bar{e}_1 + x_2 \bar{e}_2 \quad (6-30)$$

of length  $\sqrt{x_1^2 + x_2^2}$ . It is this length which describes the one sigma deviation of the scalar speed estimate. From (6-28)

$$\frac{x_1^2}{\lambda_1} + \frac{x_2^2}{\lambda_2} = 1 \quad (6-31)$$

and from (6-29)

$$\frac{\sqrt{\lambda_1} \bar{e}_1 \cdot [x_1 \bar{e}_1 + x_2 \bar{e}_2]}{|\sqrt{\lambda_1} \bar{e}_1| |x_1 \bar{e}_1 + x_2 \bar{e}_2|} = \cos \gamma = \cos(.44172) = .99997$$

$$\frac{x_1}{\sqrt{x_1^2 + x_2^2}} = .99997$$

$$x_1 = 129.095572x_2 \quad (6-32)$$

From (6-31)

$$\frac{16665.67x_2^2}{\lambda_1} + \frac{x_2^2}{\lambda_2} = 1 \quad (6-33)$$

we find

$$x_2 = .008173$$

and from (6-32)

$$x_1 = 1.055098$$

Thus,

$$\sqrt{x_1^2 + x_2^2} = 1.05513 \quad (6-33)$$

This value is the standard deviation of the scalar speed estimate, 1082.028 ft/sec. Note that we expected the standard deviation of the velocity estimate to be only slightly higher than the one sigma deviation of the x velocity estimate due

to the small off-diagonal terms of the  $P_{34}$  matrix, and relative magnitudes of the x and y velocities.

Hypothesis Test of Peak Speed and Confidence Level

We are now prepared to apply a hypothesis test of the peak vehicle speed. We wish to test the hypothesis that the peak speed estimate is above the reference speed of sound, a:

$$a = 1073.536213 \text{ fps}$$

From our assumptions of Gaussian models, the estimate of peak speed and associated covariance describe a conditional normal distribution. The appropriate one-sided "confidence interval" (8) for this hypothesis test is given by (8):

$$\bar{x} - z (\text{confidence level}) \sigma(\bar{x}) \geq \mu \quad (6-34)$$

where

$\bar{x}$  - mean of normal distribution = 1082.028

$z$  - area under the standard normal distribution curve

$\sigma(\bar{x})$  - standard deviation of normal distribution = 1.05513

$\mu$  - lower bound of confidence interval = 1073.536213

For  $\bar{x} = 1082.028$  fps,  $\mu = 1073.536213$ ,  $\sigma(\bar{x}) = 1.05513$ :

$$z(\text{confidence}) = \frac{\bar{x} - \mu}{\sigma} = 8.048 \quad (6-35)$$

To eight significant figures (6-35) yields a probability that the vehicle was below Mach one of:

$$1 - P(x) = 3.4346578 \text{ E-15} \quad (6-36)$$

from which  $P(x)$ , the probability that the vehicle was above Mach one, is found to be:

$$P(x) = .9999999999999965653422 \quad (6-37)$$

For all intents and purposes, we have achieved a probability or confidence level of one that the vehicle exceeded the reference speed of sound. Of course, this confidence level is based on the assumptions and modeling techniques we have used in this analysis. Such a high confidence after only two iterations of the forward-backward estimator illustrates the power of optimal smoothing theory in post-run data analysis.

## VII. Conclusions and Recommendations

### Conclusions

Two iterations of the forward-backward estimator have provided improved state estimates and lower error variance than is possible with a forward filter only. The backward recursive fixed-interval smoother provides updated initial state and variance values which yield improved state estimates from the forward extended Kalman filter. The forward-backward estimation method has reduced the error variance from the forward filter by more than half after only two iterations. Based on the second iteration of the smoothing algorithm we make some general comments.

The improved initial time conditions from the smoother indicate an inaccurate assumption of the starting position of the run. We used an origin based on very inaccurate range measurements. It appears that the initial x and y position are, in fact, displaced approximately 200 feet north and 400 ft east of the assumed starting position. The vehicle is also already moving at our assumed initial time. This can be explained by an error in the initial time chosen for the radar measurements. The point in time in the radar data chosen as  $t_0$  appears to be off by approximately 0.05 second. In other words, the actual starting time of the run is about one radar data sample before the time chosen as the starting time. This causes the smoother to estimate an off-zero velocity at our declared initial time. This also explains why we do not

see exact correlation between filter estimated velocity and FIM trap speed at 18.65 seconds. On the time scale we have used, the FIM trap occurs somewhere between 18.60 and 18.70 seconds. In spite of this time skew, the estimated values are close enough to trap speed to allow the comparison shown in Table III.

The actual starting position of the vehicle is really not the information we desire. We set out primarily to get the best estimate possible of peak vehicle speed no matter at what time or where on the track this occurs. In terms of vehicle velocity, the smoothing algorithm used in this analysis after two iterations has provided excellent convergence to the "true" peak speed.

We also have come close to the maximum velocity estimate obtained on the day of the run from AFFTC radar data analysis. It appears that the AFFTC method used to correct erroneous range data was valid and even averaging only three radar points came very close to the "true" peak speed. We now summarize the estimates obtained of the peak vehicle speed by AFFTC, accelerometer data only, and one and two iterations of the forward-backward smoothing method incorporating range and azimuth measurements. These velocity estimates are converted to Mach number using the calculated reference speed of sound of 1073.536213 ft/sec. These results are summarized in Table IV.

Two iterations of the optimal smoother also provide some information on the behavior of the error states of the

TABLE III  
Speed Estimate at FIM Trap (18.65 seconds)

Method	Feet/sec	MPH
FIM Recorded Speed	977.1432	666.234
Accelerometer Data Only	978.582	667.215
First Run of Extended Kalman Filter	979.22	667.649
First Run of Smoother	972.91	663.35
Second Run of Extended Kalman Filter	978.568	667.206
Second Run of Smoother	975.043	664.802

TABLE IV  
Peak Scalar Speed Estimates

Method Used	Feet/sec	MPH	MACH	Time Above Mach 1
AFFTC Computer Analysis of Corrected Radar Data	1084.835	739.66	1.0105	N/A
Integration of Longitudinal Accelerometer Data	1080.05	736.4	1.006	1.25 sec
First Run of Extended Kalman Filter	1089.5	742.84	1.0149	2.0 sec
First Run of Smoother	1080.006	736.34	1.006	1.25 sec
Second Run of Extended Kalman Filter	1086.71	740.94	1.0123	1.8 sec
Second Run of Smoother	1082.028	737.75	1.008	1.4 sec



accelerometer and radar. The accelerometer error varies between 0 and  $.08 \text{ ft/sec}^2$  (0 to  $.0025 \text{ g's}$ ) during the 24 second time interval of interest, achieving its maximum value at approximately ten seconds into the run. From ten seconds on, this error slowly decreases to approximately zero by 24 seconds. The sustained g's on the vehicle are fairly high (Fig. 3.2) up to ten seconds and then begin to decrease after this time. It would appear the accelerometer error is a function of the length of time sustained g's are applied to the accelerometer and the magnitude of these acceleration units. Depending on one's definition of "slowing-varying", one could make a case for using a random walk model for the accelerometer error. Certainly, it could be argued that a correlation time of one second is too short for the behavior of this error. Another study of the rocket car data could use on-line "tuning" of the system noise matrix,  $\underline{Q}(t)$ , by allowing the smoother to calculate an estimate of its value over time,  $\hat{Q}(t_i/t_f)$ . One could also calculate smoother estimated inputs  $\hat{u}(t_i/t_f)$ . In terms of the rocket car analysis, such estimation of accelerometer input at any time  $t_i$  based on the entire measurement time history would yield improved state estimation. Nevertheless, the smoother has provided a better "glimpse" of the "true" behavior of this state than is available from a forward filter only, especially without more knowledge about inherent accelerometer errors.

The random walk models for radar range and azimuth bias errors prove to be very adequate. These errors are shown as

nearly constant over the 24 second interval with only slow changes from the behavior of true constants. Certainly, we are somewhat surprised at the magnitude of the radar range bias error. Considering the size of the vehicle being tracked, lack of transponder, ground clutter, and distance from the radar site, it is conceivable that the radar range has a large inherent error. The azimuth bias error behaves as we expected based on our knowledge of operator tracking performance. Perhaps "bias" is a misnomer, as most of the error in azimuth is operator-induced. The azimuth error shows that the operator lags behind the vehicle initially but is able to regain good tracking as the acceleration decreases. After engine "flame-out" at approximately 18 seconds, the azimuth error again increases, indicating the operator has probably "jumped" ahead of the vehicle. For another iteration of the estimator, a better description of the azimuth error could be used. One could relate the strength of driving noise on this state,  $q_7$ , to the acceleration of the vehicle. When acceleration is high  $q_7$  would be increased. The amount of driving noise would decrease as vehicle acceleration decreases.

This analysis has shown that state estimation can be significantly improved if the estimation algorithm has access to future measurements. This is the real benefit of a smoother algorithm in post-run data analysis. The method used in this analysis requires a straightforward incorporation of existing theory and available software with only limited additional programming required. The forward-backward

iteration scheme is a simple yet effective way to provide improved state estimates in an "off-line" application. It can be applied to almost any system of interest no matter what dimension, with only computer workload becoming a driving factor. Good dynamical and error models are a requirement, but not a necessity. The iterative method used in this analysis can help "fine-tune" very simplified models to provide improved state estimates.

The reader familiar with estimation of unknown parameters using a "maximum likelihood" estimation technique may wonder if such a technique could have been employed in this analysis. The answer is a guarded "yes" if we can make some valid assumptions. The inherent assumption in maximum likelihood estimation is that the parameters to be identified can be accurately modeled as constants over some time interval of interest. In this analysis, we are concerned with accurate estimates of state values at discrete points in time (i.e., peak speed at some time,  $t_i$ ). If we assume the parameters affecting this problem, such as accelerometer and radar errors, are constant over time, a maximum likelihood estimation algorithm will yield a best fit of a constant to the data. If the parameters are not true constants, a better (non-constant) model would inherently allow better estimation accuracy. This analysis has shown that the error states do not behave as constants. Therefore, one cannot accurately model these errors as constant unknown parameters for implementation in a maximum likelihood estimation algorithm without non-negligible

estimation performance degradation. Without a priori information on the behavior of the errors to be modeled, the decision was made to model the errors as states in the forward extended Kalman filter-backward smoother estimator.

If there is a "bottom-line" to this analysis it has to do with the peak speed of the Budweiser Rocket Car on 17 December 1979. Rather than "eyeballing" the peak speed of the car based on poor data, we are able to provide an estimate of the speed and a confidence level for our estimate. In fact, after only two iterations of the forward-backward smoothing technique, we can state with probability of nearly one that the vehicle did achieve the reference speed of sound, based on the assumptions and modeling techniques used in this analysis.

#### Recommendations

The position estimates and off-zero velocities calculated by the smoother at the initial time,  $t_0$ , indicate a rather poor choice of origin for the vehicle frame of reference. Relying on the radar to provide a good initial "fix" of vehicle position, no matter how long the radar is aimed at the vehicle, is only "wishful thinking". Perhaps a better origin could have been located at remote camera site A8 shown in Fig. 1.1. This point has been surveyed and "exact" latitude and longitude coordinates of both A8 and the radar site are known. Using these coordinates one could calculate a much better DELX and DELY from which to reference changing

radar measurements to vehicle motion in the frame of reference. If the information on track alignment with respect to A8 is correct, a frame of reference at A8 should indicate a vehicle track parallel to the x-axis. The starting position of the vehicle within a frame of reference centered at A8 is still unknown, however, and only iterative methods could "zero-in" on the "true" starting position.

An adjustment could be made in the initial time chosen in the radar data to find the "true" sample time as the vehicle starts to move. At 20 samples per second, however, one can only get within 0.05 second accuracy. Also, the radar data is constant until the azimuth suddenly increases very rapidly. We chose one sample time before the first change in azimuth as the initial time. One could "back-up" the radar data until the smoother estimate of x-velocity at  $t_0$  approaches zero.

Other possibilities for further study include some off-line tuning of system noise to account for the time-varying nature of accelerometer and azimuth errors. One way to accomplish this might be to use the smoother estimate of system noise,  $\hat{Q}(t_i/t_f)$ , based on the measurement data to provide a time history of driving noise for each of the affected states. This would provide the forward extended Kalman filter with improved knowledge of state behavior.

Finally, it might be beneficial to allow the smoother to calculate an estimate of the applied controls, in this case accelerometer specific force. This smoother estimated

control input,  $\hat{u}(t_i/t_f)$ , could be used to better determine accelerometer errors and improve state estimation. These possibilities were not explored in this analysis due to time limitations and a feeling that confirmation of peak vehicle speed was the critical area of concern.

Appendix A. Plots from Second Iteration  
of Extended Kalman Filter

This section presents the results of the second iteration of the extended Kalman filter developed in Chapter III and IV. State estimates and error variances at the initial time from the first iteration of the Meditch (5) smoothing algorithm are used to update the initial conditions of the extended Kalman filter for this run. In addition, a slight correction to the assumed test track heading provides closer filter correlation to range and azimuth measurements, allowing a reduction in the estimated measurement noise for radar range.

Figure A.1 shows a plot of estimated and actual radar range obtained with the corrected test track heading. This figure indicates that the divergence of actual and estimated range between 20 to 24 seconds has been removed.

The extended Kalman filter shows improved convergence of the standard deviations of the state estimates due to improved initial conditions from the smoother. This can be seen by comparing to part (b) of Figs. A.2 through A.8 to part (b) of Figs. 4.17 to 4.23. Figures A.9 (a) and A.9 (b) are plots of the range and azimuth measurement residuals bracketed by the residual standard deviations. From Fig. A.9 (a) it is apparent when the residual monitoring routine bypasses range measurements in excess of three times the residual standard deviation. Figure A.10 (b) is an expanded

version of Fig. A.10 (a) which is the scalar speed estimate  
(magnitude of the velocity vector) converted to Mach number.



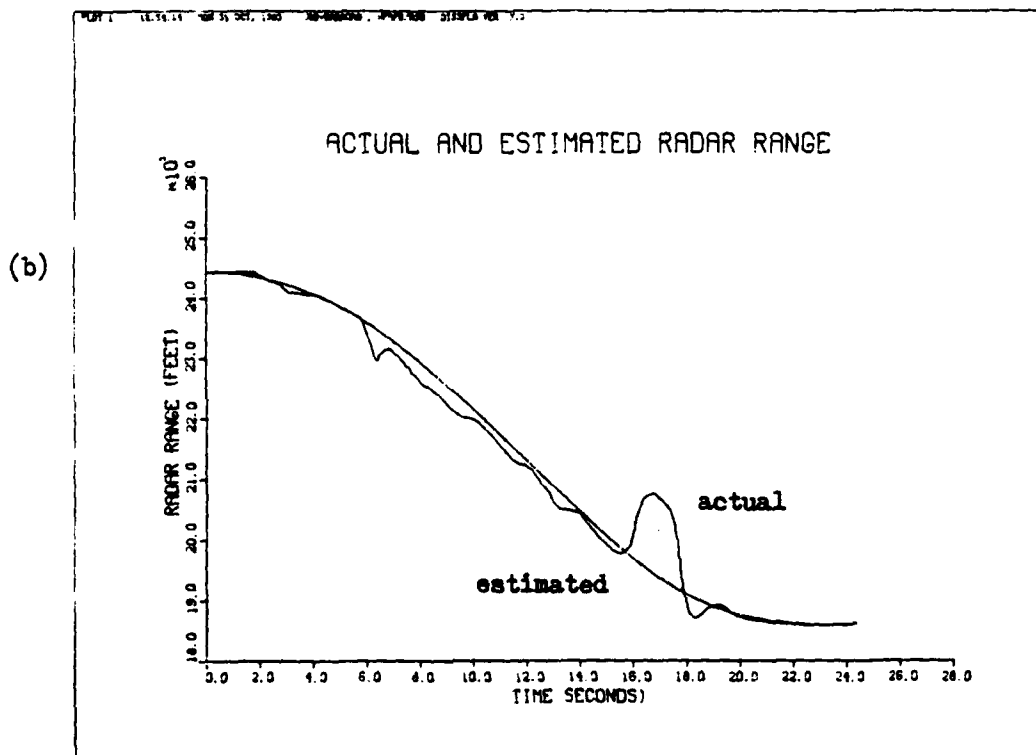
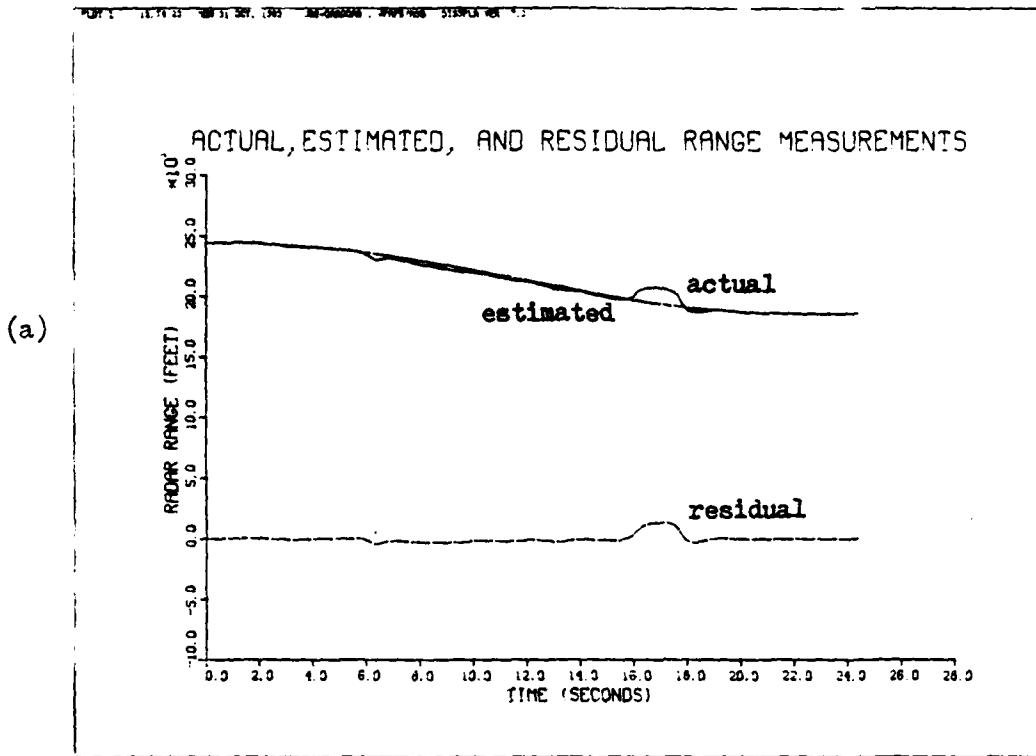
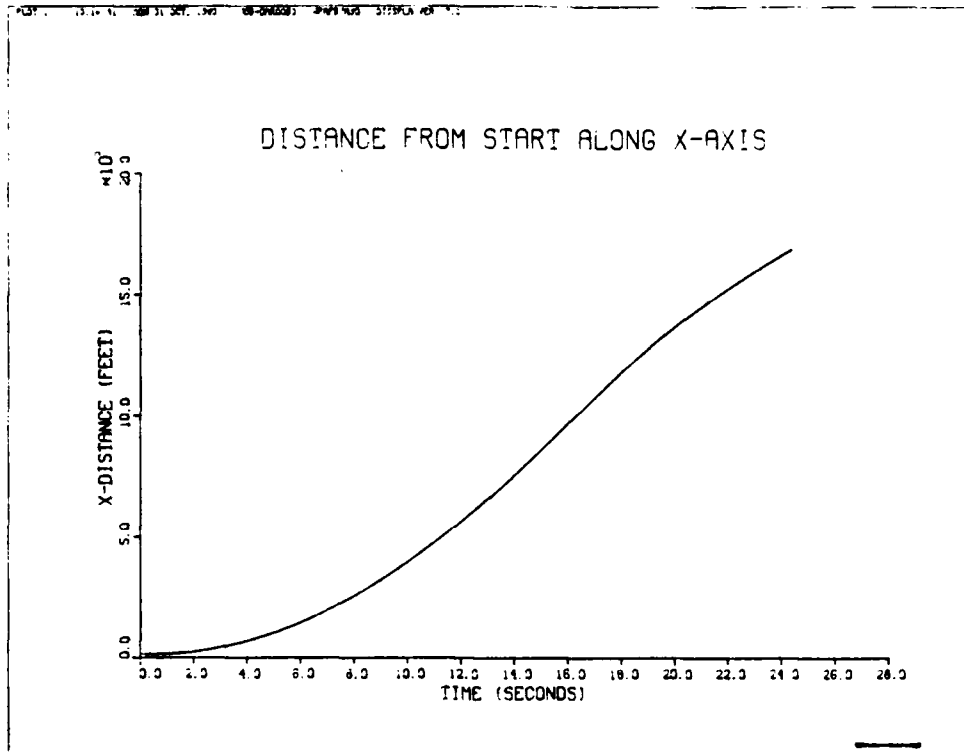


Fig. A.1(a),(b) Residual range analysis after correcting track heading to 179.209 degrees true.

(a)



(b)

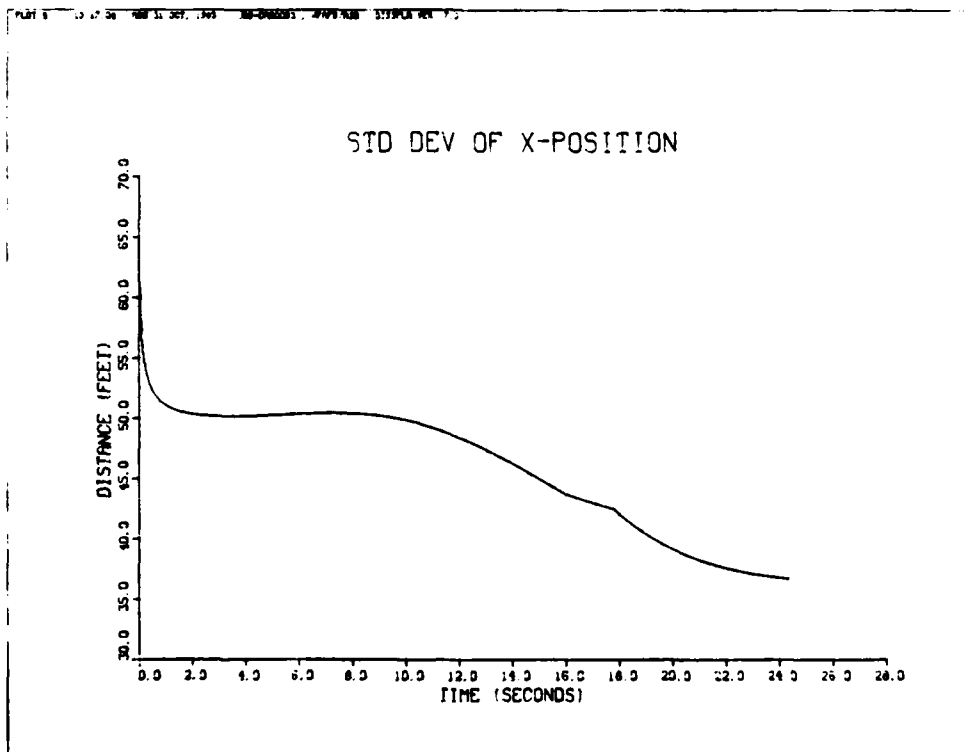
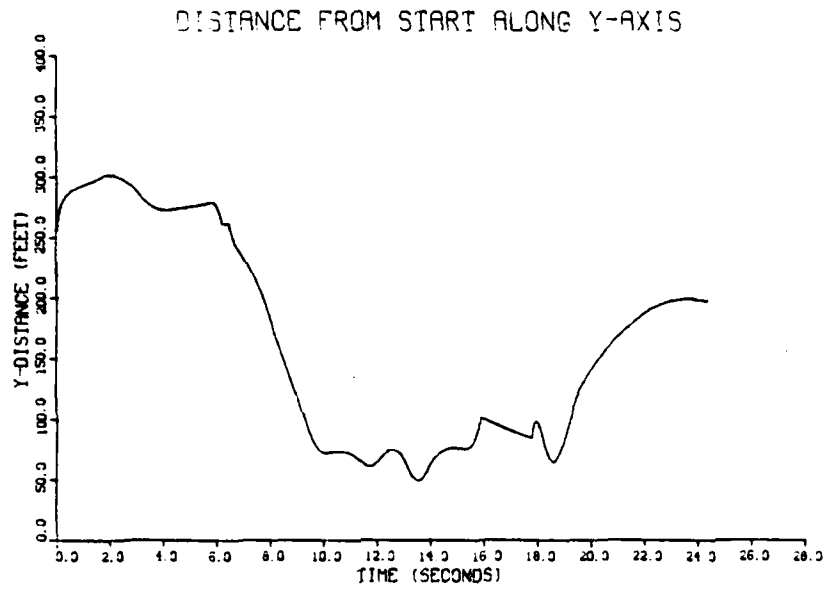


Fig. A.2(a),(b) Extended Kalman filter state estimate and standard deviation after two iterations

(a)



(b)

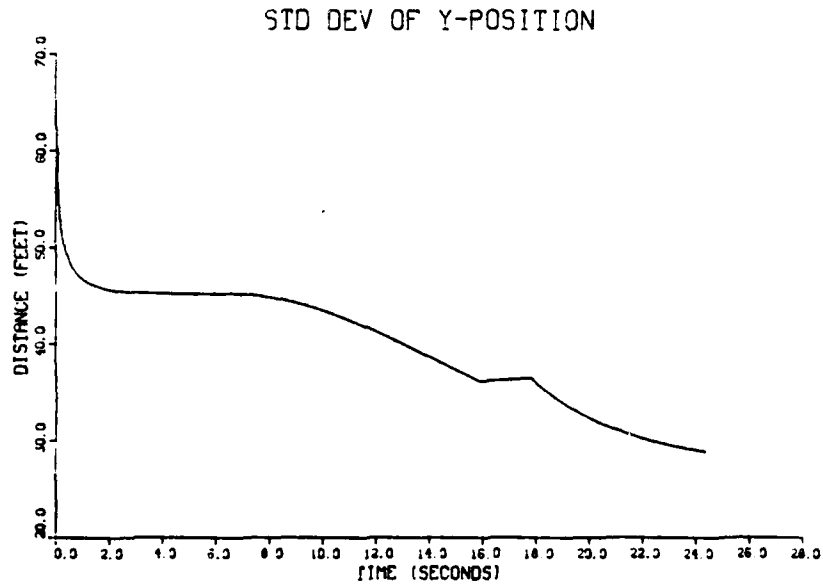


Fig. A.3(a),(b) Extended Kalman filter state estimate and standard deviation after two iterations

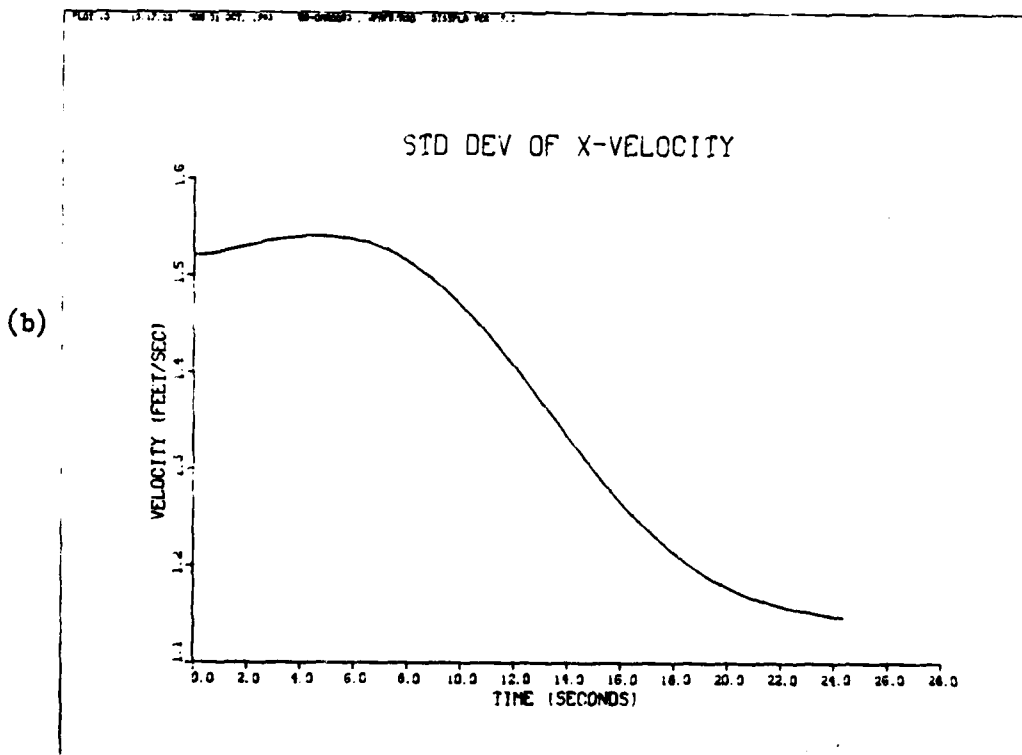
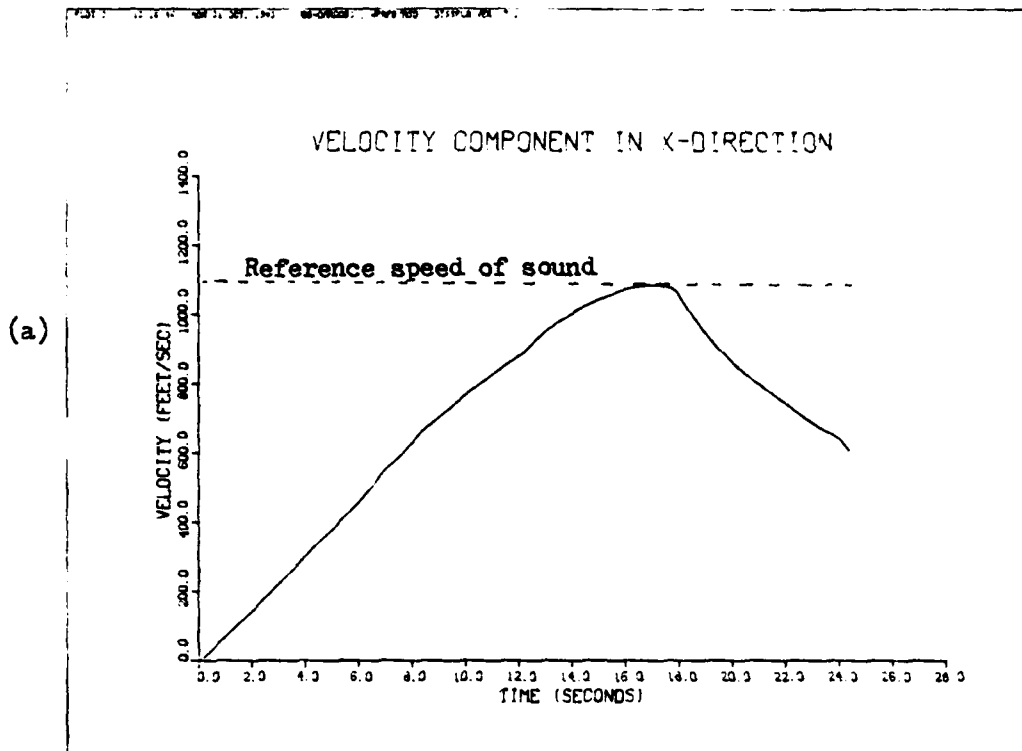
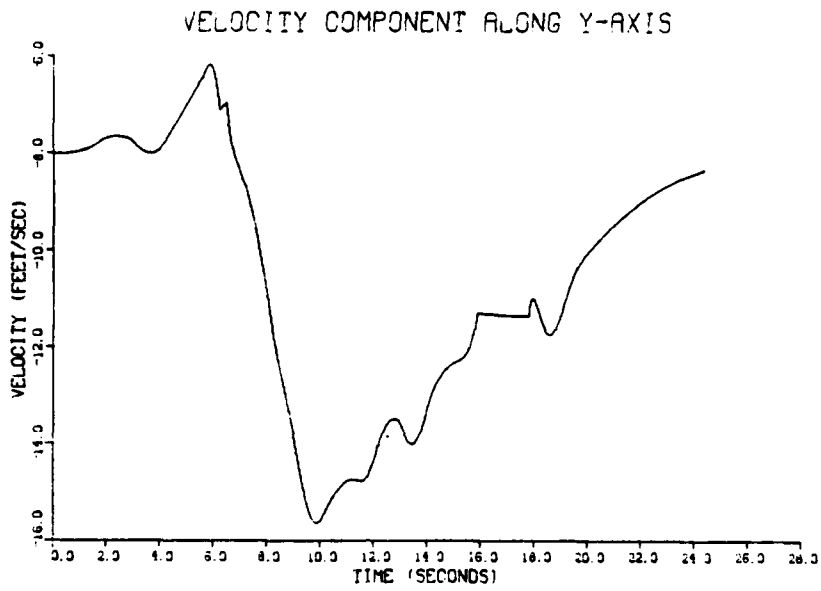


Fig. A.4(a),(b) Extended Kalman filter state estimate and standard deviation after two iterations

(a)



(b)

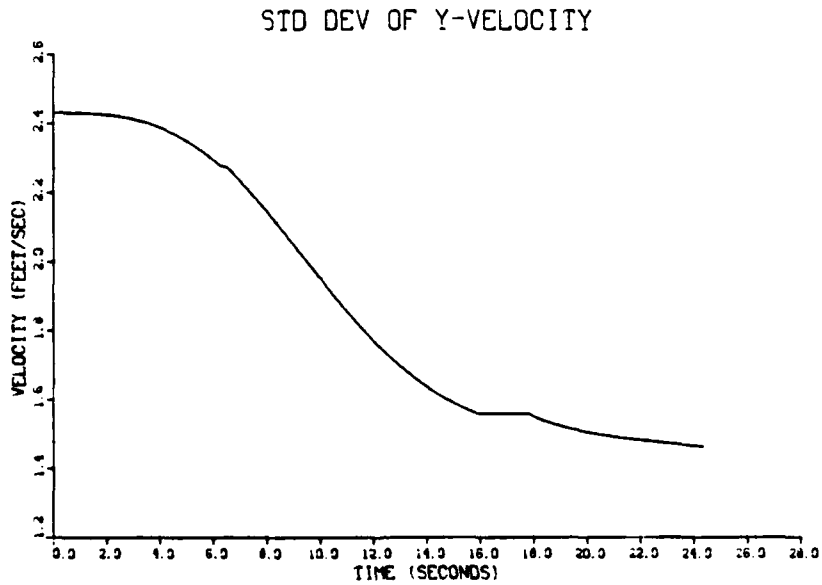
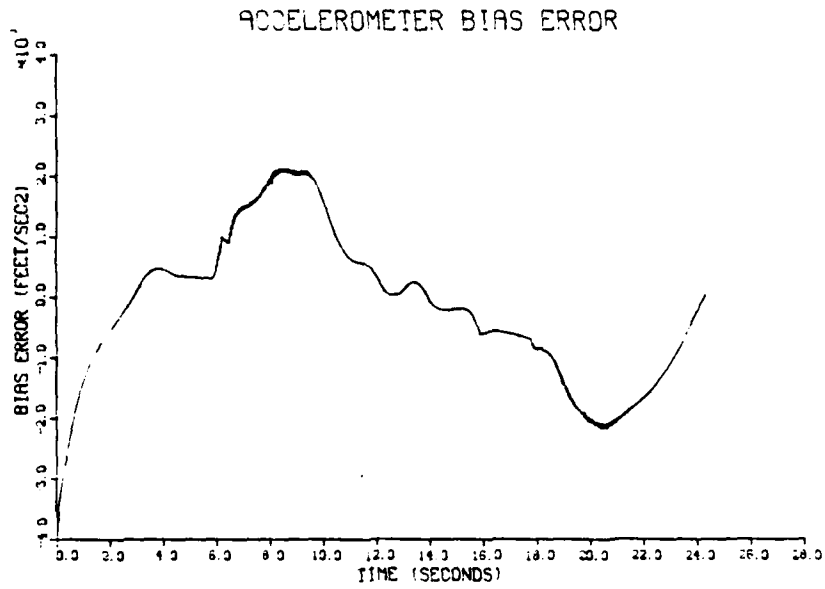


Fig. A.5(a),(b) Extended Kalman filter state estimate and standard deviation after two iterations

(a)



(b)

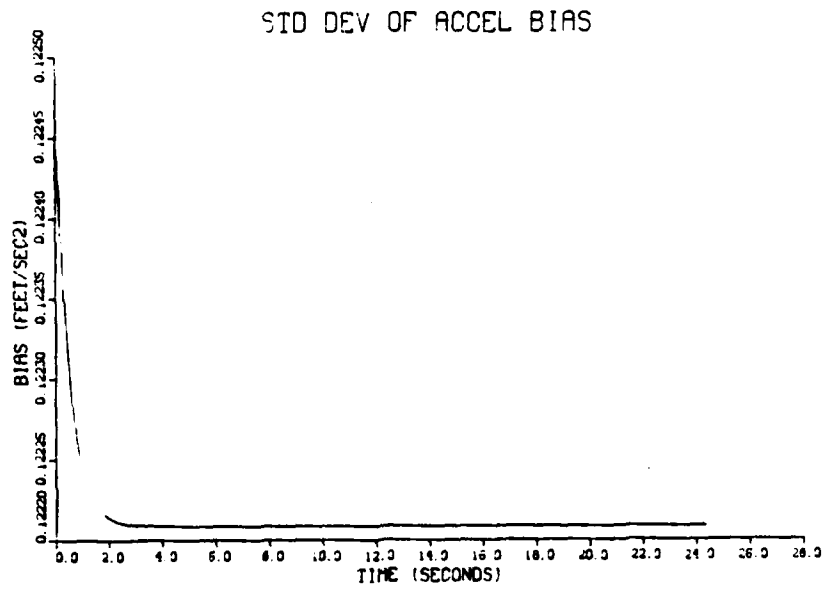
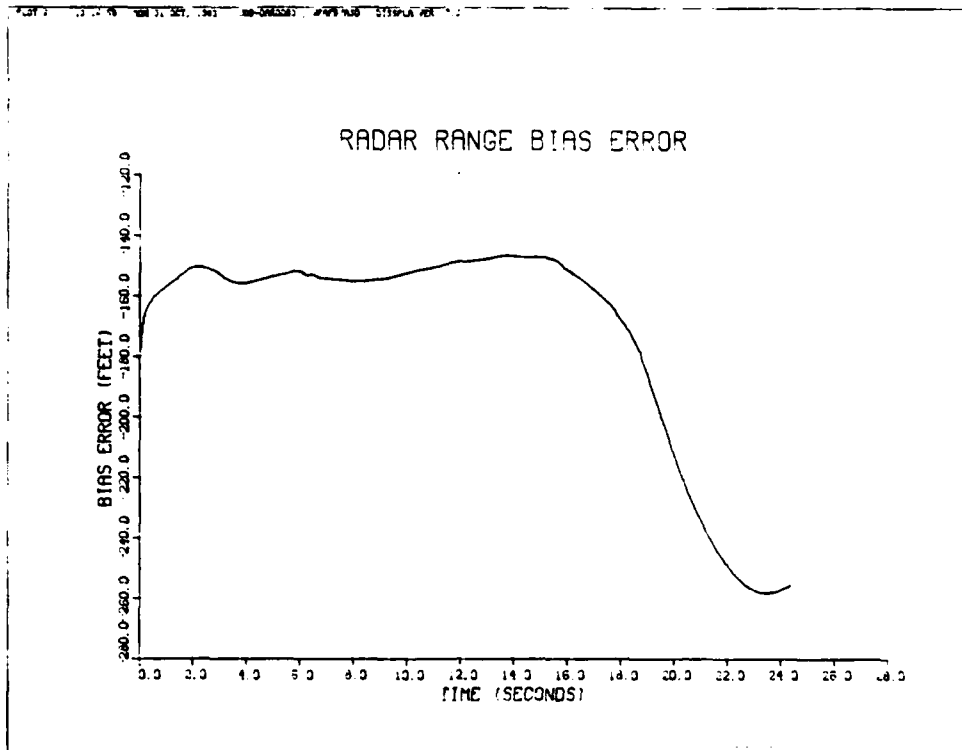


Fig. A.6(a),(b) Extended Kalman filter state estimate and standard deviation after two iterations

(a)



(b)

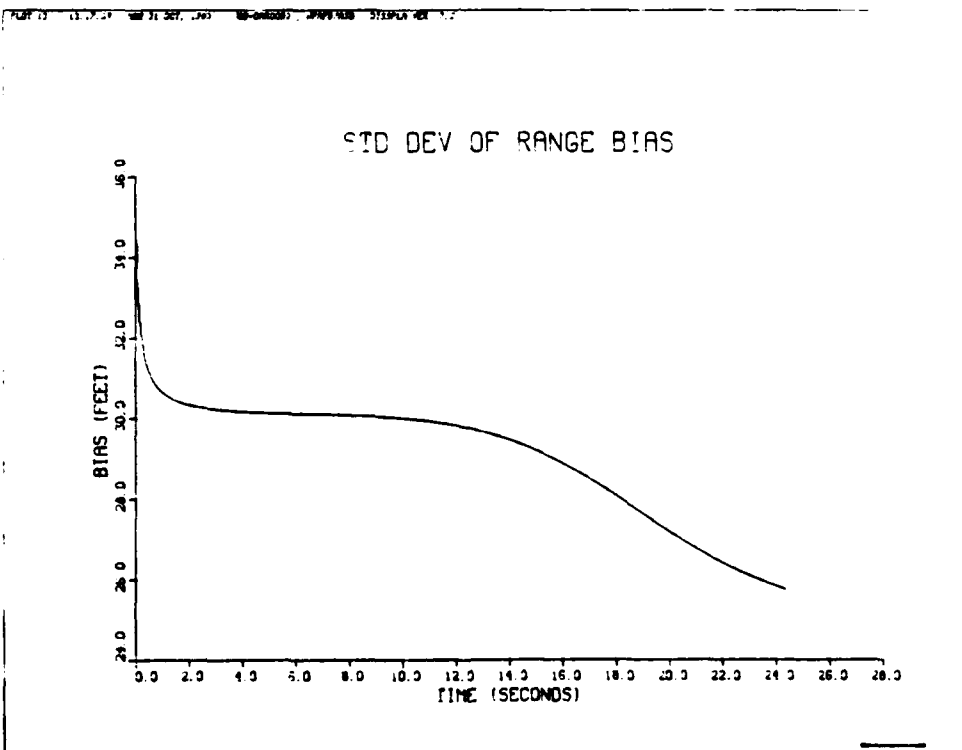
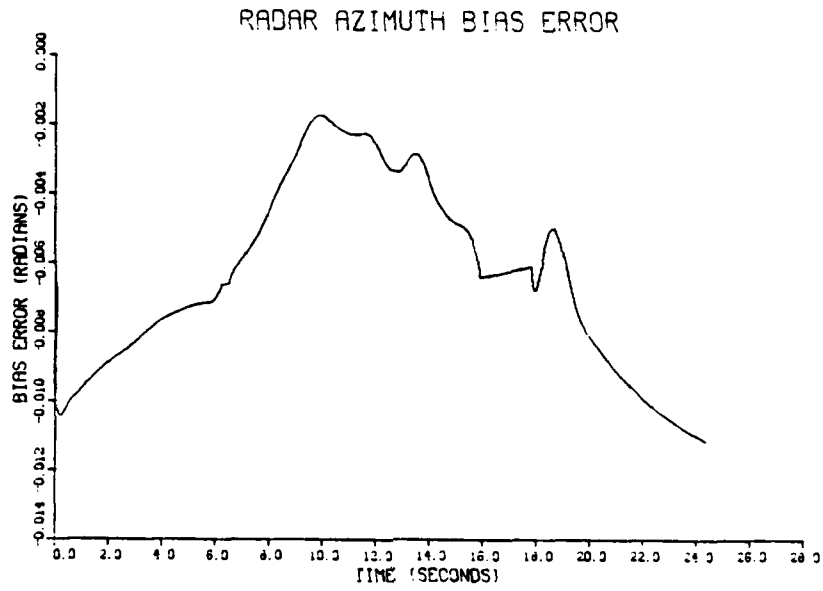


Fig. A.7(a),(b) Extended Kalman filter state estimate and standard deviation after two iterations

(a)



(b)

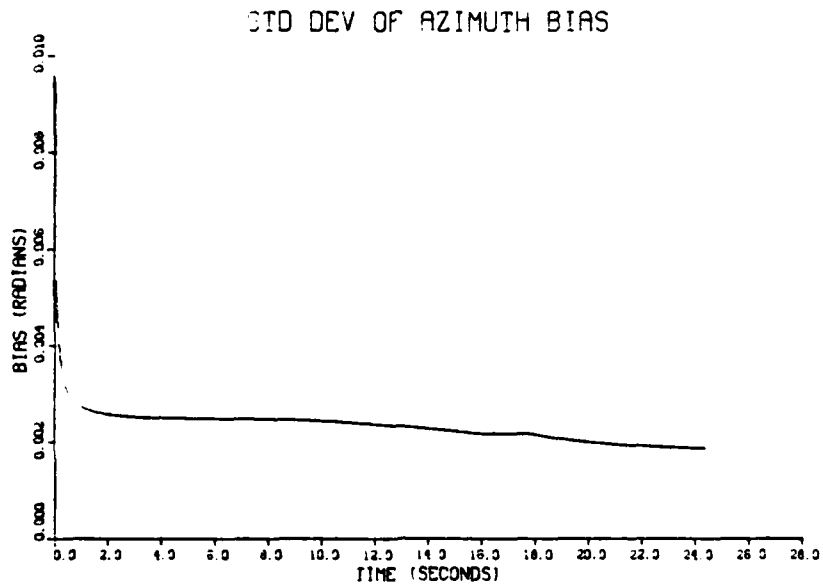
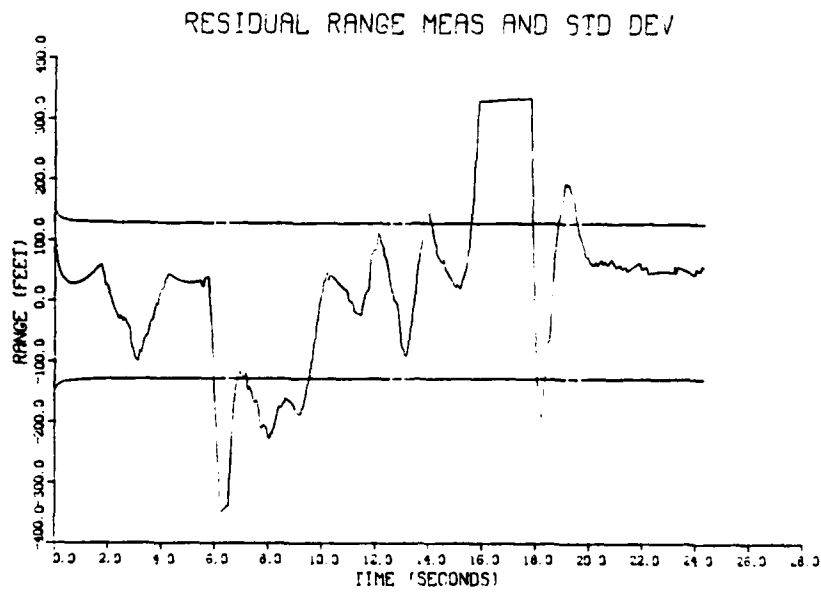


Fig. A.8(a),(b) Extended Kalman filter state estimate and standard deviation after two iterations.



(a)



(b)

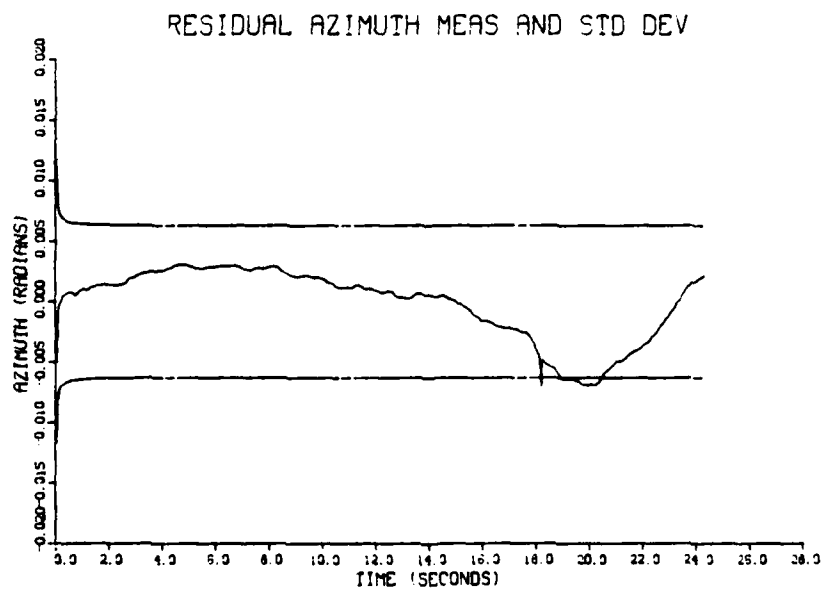
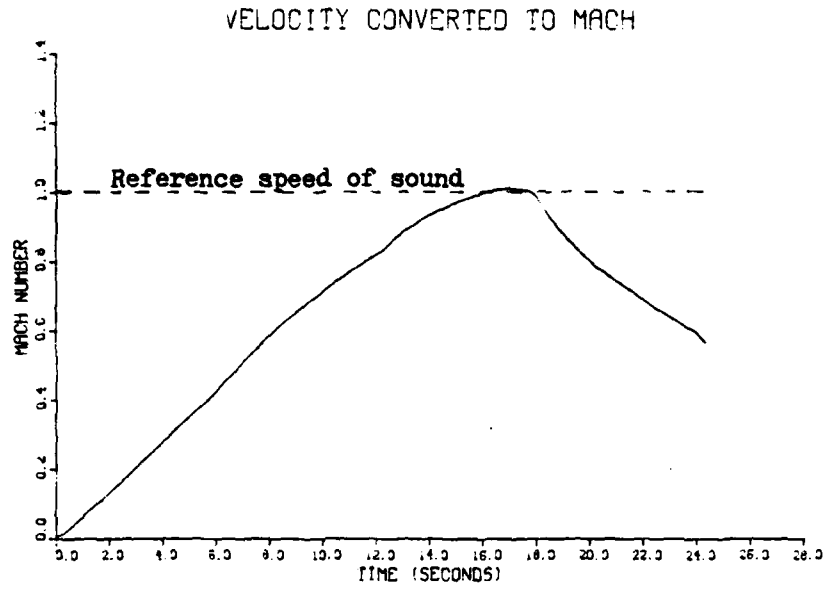


Fig. A.9(a),(b) Range and Azimuth residuals and standard deviations after two iterations.

(a)



(b)

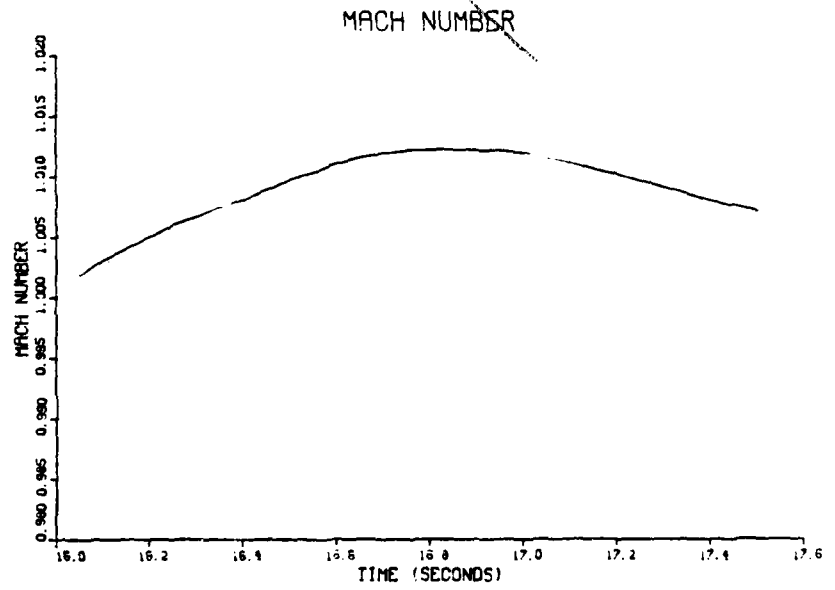


Fig. A.10(a),(b) Velocity converted to Mach number after two iterations of the Extended Kalman filter.

## Appendix B. Optimal Smoother Computer Program

This appendix includes a listing of the computer program used to incorporate the Meditch (5) backward-recursive optimal linear smoother algorithm described in detail in Chapter II. The data required for this program includes the current sample time,  $t_i$ , state estimate vector before update, covariance matrix before update (stored in upper triangular form), state estimate vector after update, and covariance matrix after update (stored in upper triangular form) from  $t_0$  to  $t_f$ .

For this analysis the state estimates and covariance before and after each measurement update are stored as a result of one run of the extended Kalman filter implemented in SOFE. A short data reformatting program was used to put the data at the final time first and the remaining data records in backward-recursive form to the initial time. This enables the smoother program to read forward through the data but actually compute quantities "backward" in time. The Meditch algorithm requires  $\hat{\underline{x}}(t_i^+)$  and  $\hat{\underline{x}}(t_{i+1}^-)$  for one calculation at each sample time. The data was put in the following order to allow for a step-by-step "read" of the required quantities for each time of calculation. Each data record contains the following information in the order shown:

1. time,  $t_i$
2. state vector at time  $t_i$  after update,  $\hat{\underline{x}}(t_i^+)$

3. covariance matrix at time  $t_i$  after update,  $\underline{P}(t_i^+)$
4. state vector at time  $t_i$  before update,  $\hat{\underline{x}}(t_i^-)$
5. covariance matrix at time  $t_i$  before update,  $\underline{P}(t_i^-)$

The order of the system used in the rocket car analysis allowed for storage of formatted records. A higher order system will probably require more efficient data storage and improved formatting of smoother printed output.

PROGRAM SMOOTH(INPUT,OUTPUT,TAPE5=INPUT,TAPE6=OUTPUT,TAPE7,  
TAPE8,TAPE9)

THIS IS THE EXECUTIVE ROUTINE OF A FIXED INTERVAL  
SMOOTHER ALGORITHM. THE DEVELOPMENT OF THE ALGORITHM  
IS THE RESULT OF WORK DONE BY J. S. MEDITCH AND  
PUBLISHED IN INFORM AND CONTROL, 1967.

THIS ALGORITHM USES THE OUTPUT OF A FORWARD RUNNING  
KALMAN FILTER (IN THIS CASE AN EXTENDED FILTER). IT  
PROPAGATES A SMOOTHED ESTIMATE OF THE STATE VECTOR AND  
COVARIANCE MATRIX BACKWARD FROM AN INITIAL CONDITION  
AT THE FINAL TIME OF THE FORWARD FILTER. THIS RESULTS  
IN AN IMPROVED STATE ESTIMATE AND LOWER COVARIANCE.

DATA FROM THE FORWARD FILTER IS STORED ON MAGNETIC TAPE  
IN THE FOLLOWING FORMAT FOR EACH RECORD:

1. TIME
2. XFMINUS - VECTOR OF STATE ESTIMATES BEFORE  
MEASUREMENT UPDATE
3. PFM - UPPER TRIANGULAR COVARIANCE MATRIX  
BEFORE MEASUREMENT UPDATE (STORED IN THIS  
MANNER FOR COMPACTNESS)
4. XFPLUS - VECTOR OF STATE ESTIMATES AFTER  
MEASUREMENT UPDATE
5. PFP - UPPER TRIANGULAR COVARIANCE MATRIX  
AFTER MEASUREMENT UPDATE

DEFINITION OF VARIABLES IN MEDITCH ALGORITHM

XFMINUS - VECTOR OF (NS) STATES BEFORE UPDATE  
XFPLUS - VECTOR OF (NS) STATES AFTER UPDATE  
XFTE - SMOOTHED ESTIMATE OF STATE VECTOR  
PFMINUS - COVARIANCE MATRIX BEFORE UPDATE  
PFPLUS - COVARIANCE MATRIX AFTER UPDATE (NSXNS)  
PFTF - SMOOTHED COVARIANCE  
AMAT - SMOOTHING ESTIMATOR GAIN MATRIX (NS X NS)  
PHI - STATE TRANSITION MATRIX FOR ADJOINT SYSTEMS  
PHI = EXP (F \* T) (TRANPOSED)

STARTING CONDITION FOR SMOOTHER

XFTE(TF)=XFPLUS(TF)  
PFTF(TF)=PFPLUS(TF)  
PROPAGATION OF STATE ESTIMATE  
XFTE(TI)=XFPLUS(TI)+AMAT(TI)(XFTE(TI+1)-XFMINUS(TI+1))  
AMAT(TI)=PFPLUS(TI)+PHI(TI+1,TI)+PFMINUS(TI+1)\*\*-1  
PFTF(TI)=PFPLUS(TI)+AMAT(TI)(PFTF(TI+1)-PFMINUS(TI+1))\*  
AMAT(TI)TRANPOSED

IN ADDITION TO THE ROUTINES HERE, THE DAVID L. KLEINMAN  
LIBRARY OF LINEAR SYSTEMS PROGRAMS IS USED TO PROVIDE  
VECTOR AND MATRIX OPERATIONS.

COMMON /MAIN1/ NDIM,NDIM1,COM1(10,10)  
COMMON /MAIN2/ COM2(10,10)  
COMMON /INOU/ KIN,KOUT,KPLOT,KDATA,KUSER  
COMMON /DIM/ NS,NTR,NSEC,NSAMP,NSTEP  
COMMON /PHI/ PHI(10,10)

```

COMMON /XFP/ XFPLUS(10)
COMMON /XFM/ XFMINUS(10)
COMMON /FPV/ PFP(55)
COMMON /PFV/ PFM(55)
COMMON /PFP/ PFPLUS(10,10)
COMMON /PFM/ PFMINUS(10,10)
COMMON /A/ AMAT(10,10)
COMMON /XFTF/ XFTF(10)
COMMON /PFTF/ PFTF(10,10)
COMMON /HEADING/ TITLE(20),ADATE,ATIME
COMMON /TIME/ T,TO,TF
LOGICAL PLOTEM,DATACHK,USEROUT
NAMELIST /IN/,NS,NTR,NSAMP,TO,TF,DATACHK,PLOTEM,USEROUT
DATA NDIM,NDIM1/10,11/
DATA KIN,KOUT,KPLOT,KDATA,KUSER/5,6,7,8,9/

C INITIALIZE AND READ IN VARIABLES FROM INPUT FILE
C
NS=0
NTR=0
NSAMP=0
NSEC=0
TO=0.
TF=0.
T=0.
USEROUT=.FALSE.
DATACHK=.FALSE.
PLOTEM=.FALSE.
NSTEP=0

C READ TITLE AND PRINT TO OUTPUT
C
CALL DATE(ADATE)
CALL TIME(ATIME)
READ(KIN,1000) TITLE
WRITE(KOUT,1001)TITLE,ADATE,ATIME

C READ(KIN,IN)
WRITE(KOUT,IN)

C NSTEP=INT(NSAMP*(TF-TO))+1

C INITIALIZE COMMON BLOCKS AND FIND FINAL TIME CONDITION
C CALL ONCE(DATACHK)
C LOOP FOR SMOOTHER CALCULATIONS
C
CALL GETMINS
CALL GETPLUS
CALL MAKEA
CALL SMOOTHX
CALL SMOOTHP
CALL OUT(PLOTEM,USEROUT)
IF(T.EQ.TO) GOTO 20
GOTO 10

C

```

60

65

70

75

80

85

90

95

100

105

110

```
1000 FORMAT(20A4)
1001 FORMAT("1SMOOTHER1",10X,20A4,10X,2A10)
20 STOP "SMOOTHER1 FINISHED"
END
```

115

```

SUBROUTINE ONCE
1 SUBROUTINE ONCE(DATACHK)
C CALLED ONLY ONCE PER RUN TO INITIALIZE ALL
C MATRICES AND FIND THE FINAL TIME CONDITION.
C CAN BE USED TO READ IN A TIME-INVARIANT MATRIX.
C
COMMON /MAIN1/ NDIM,NDIM1,COM1(10,10)
COMMON /MAIN2/ COM2(10,10)
COMMON /INOU/ KIN,KOUT,KPLOT,KDATA,KUSER
COMMON /DIM/ NS,NTR,NSEC,NSAMP,NSTEP
COMMON /PHI/ PHI(10,10)
COMMON /XFP/ XFPPLUS(10)
COMMON /XFM/ XFMINUS(10)
COMMON /PFMV/ PFM(55)
COMMON /PFV/ PFP(55)
COMMON /PFM/ PFMINUS(10,10)
COMMON /PFP/ PFPPLUS(10,10)
COMMON /A/ AMAT(10,10)
COMMON /XFTF/ XFTF(10)
COMMON /PFTF/ PFTF(10,10)
COMMON /TIME/ T,TO,TF
LOGICAL DATACHK
C
C ZERO ALL REQUIRED MATRICES AND VECTORS
C
CALL ZROIZE(NS,NS,PHI)
CALL ZROIZE(1,NS,XFPPLUS)
CALL ZROIZE(1,NS,XFMINUS)
CALL ZROIZE(1,NTR,PFM)
CALL ZROIZE(1,NTR,PFP)
CALL ZROIZE(NS,NS,PFPPLUS)
CALL ZROIZE(NS,NS,PFMINUS)
CALL ZROIZE(NS,NS,AMAT)
CALL ZROIZE(1,NS,XFTF)
CALL ZROIZE(NS,NS,PFTF)
CALL ZROIZE(NDIM,NDIM,COM1)
CALL ZROIZE(NDIM,NDIM,COM2)
C
C READ IN TIME-INVARIANT PHI MATRIX
C IN THIS CASE, PHI WAS SIMPLY SET IN THE SUBROUTINE
C
DO 10 I=1,NS
PHI(I,1)=1.0
CONTINUE
10 PHI(3,1)=0.05
PHI(4,2)=0.05
PHI(5,5)=-.9512
PHI(5,1)=-.001229
PHI(5,3)=-.04877
C
C SEARCH DATA FILE FOR FINAL TIME AND SET INITIAL
C CONDITION FOR BACKWARD PROPAGATION
C
READ(KDATA,90) T,(XFTF(J),J=1,NS),(PFP(J),J=1,NTR)
FORMAT(F6.2,7E15.7,4(/7E15.7))
90 CALL MAKEP(NS,PFP,PFTF)
C

```



```
60      C
      C
      C      PRINT FINAL TIME CONDITIONS
      C      WRITE(KOUT,1000) T
      C      WRITE(KOUT,1001)
      C      DO 50 I=1,NS
      C      WRITE(KOUT,1002) I,XFTF(I)
      C      CONTINUE
      C      WRITE(KOUT,1003)
      C      DO 60 I=1,NS
      C      WRITE(KOUT,1004) (PFTF(I,J),J=1,NS)
      C      CONTINUE
      C
      C      1000 FORMAT("1SMOOTHER INITIAL CONDITION AT TF=",F6.2,".")
      C      1001 FORMAT("OSTATE VECTOR AT FINAL TIME:")
      C      1002 FORMAT("OELEMENT(",I2,")=",E13.5)
      C      1003 FORMAT("//,"COVARIANCE MATRIX AT FINAL TIME:")
      C      1004 FORMAT(1H01OE13.5)
      C
      C      IF (DATACHK) STOP "FORMAT CHECK OF DATA COMPLETE"
      C      RETURN
      C      END
```

```
1      SUBROUTINE GETMINS
      C
      C READS DATA FILE AND FINDS XFMINUS VECTOR AND
      C PFM VECTOR. FILLS PFMINUS MATRIX.
      C
5      COMMON /XFM/ XFMINUS(10)
      COMMON /PFMV/ PFM(55)
      COMMON /PFM/ PFMINUS(10,10)
      COMMON /INDU/ KIN,KOUT,KPLOT,KDATA,KUSER
      COMMON /DIM/ NS,NTR,NSEC,NSAMP,NSTEP
      COMMON /TIME/T,TO,TF
      C
      C READ (KDATA,91) (XFMINUS(I),I=1,NS),(PFM(I),I=1,NTR)
      C 91
      C FORMAT(7E15.7,4(/7E15.7))
      C
      C FILL PFMINUS MATRIX
      C
      C CALL MAKEP(NS,PFM,PFMINUS)
      C
      C RETURN
      C END
20
```

```
1 SUBROUTINE GETPLUS  
C READS DATA FILE AND FINDS XFPLUS AND PFPLUS  
C FOR PREVIOUS SAMPLE TIME. FILLS IN PFPLUS MATRIX.  
5 COMMON /INDU/ KIN,KOUT,KPLOT,KDATA,KUSER  
COMMON /DIM/ NS,NTR,NSEC,NSAMP,NSTEP  
COMMON /XFP/ XFPLUS(10)  
COMMON /PFV/ PFPV(55)  
COMMON /PFP/ PFPPLUS(10,10)  
COMMON /TIME/ T,T0,TF  
10 READ (KDATA,92) T, (XFPLUS(I),I=1,NS),(PFP(I),I=1,NTR)  
FORMAT(F6.2,7E15.7,4(/7E15.7))  
92  
15 C FILL IN PFPLUS MATRIX  
C CALL MAKEP(NS,PFP,PFPLUS)  
20 C RETURN  
END
```

SUBROUTINE MAKEA

```

1      C
2      C COMPUTES SMOOTHER GAIN MATRIX, A
3      C REQUIRES A MATRIX INVERSE ROUTINE
4      C AND A MATRIX MULTIPLICATION ROUTINE.
5      C
6      COMMON /MAIN1/ NDIM,NDIM1,COM1(10,10)
7      COMMON /INOU/ KIN,KOUT,KPLOT,KDATA,KUSER
8      COMMON /DIM/ NS,NTR,NSEC,NSAMP,NSTEP
9      COMMON /PHI/ PHI(10,10)
10     COMMON /PFP/ PFPPLUS(10,10)
11     COMMON /PFM/ PFMINUS(10,10)
12     COMMON /A/ AMAT(10,10)
13
14     C DIMENSION PFINV(10,10), A1(10,10), A2(10,10)
15     C
16     C EQUATE DUMMY MATRIX WITH PFMINUS
17     C
18     C CALL EQUATE(A1,PFMINUS,NS,NS)
19     C
20     C INVERT PFMINUS. PRINT ERROR MESSAGE IF PFMINUS
21     C IS OF DEFICIENT COMPUTATIONAL RANK TO INVERT
22     C
23     C MT=1
24     C CALL GMINV(NS,NS,A1,PFINV,MR,MT)
25     C
26     C MULTIPLY PHI MATRIX BY PFINV
27     C
28     C CALL MAT1(PHI,PFINV,NS,NS,NS,A2)
29     C
30     C COMPUTE AMAT MATRIX (AMAT=PFPPLUS*A2)
31     C
32     C CALL MAT1(PFPPLUS,A2,NS,NS,NS,AMAT)
33     C
34     C RETURN
35     C END

```

```

1      SUBROUTINE MAKEP(N,PIN,POUT)
      C
      C   FILLS IN FULL MATRIX FROM A VECTOR MATRIX
      C   STORED IN UPPER TRIANGULAR FORM.
      C   PIN IS STORED IN THE FOLLOWING ORDER:
      C
      C   PIN(1)=P(1,1)
      C   PIN(2)=P(1,2)
      C   PIN(3)=P(2,2)
      C
      C   ETC.
      C
      C   DIMENSION PIN(55), POUT(10,10)
      C
      C   ICOL=1
      C   N1=1
      C   DO 10 I=1,ICOL
      C     POUT(I,ICOL)=PIN(N1)
      C     N1=N1+1
      C   CONTINUE
      C   IF (ICOL.EQ.N) GOTO 30
      C     ICOL=ICOL+1
      C     GOTO 20
      C
      C   N1=1
      C   N2=2
      C   DO 40 J=N2,N
      C     POUT(J,N1)=POUT(N1,J)
      C   CONTINUE
      C   IF (N2.EQ.N) GOTO 50
      C     N1=N1+1
      C     N2=N1+1
      C     GOTO 60
      C
      C   50 RETURN
      C   END

```

```

1 SUBROUTINE SMOOTHX
C COMPUTES THE "SMOOTHED" ESTIMATE OF STATE VECTOR
C AS IT PROPAGATES BACKWARD IN TIME.
5 C REQUIRES VECTOR ADDITION AND VECTOR MULTIPLICATION
C ROUTINES TO BE USED.
C
C COMMON /DIM/ NS,NTR,NSEC,NSAMP,NSTEP
C COMMON /XFP/ XFPLUS(10)
C COMMON /XFM/ XFMINUS(10)
C COMMON /A/ AMAT(10,10)
C COMMON /XFTF/ XFTF(10)
C
10 C DIMENSION A(10), B(10), C(10)
C
15 C EQUATE A DUMMY VECTOR A TO XFTF
C AND FIND THE DIFFERENCE BETWEEN XFTF AND
C XFMINUS
C
20 C DO 10 I=1,NS
C A(I)=XFTF(I)
C CONTINUE
C CALL VADD(NS,-1.0,A,XFMINUS)
C
25 C COMPUTE AMAT TIMES VECTOR DIFFERENCE
C
C CALL VMAT1(AMAT,A,NS,NS,B)
C
30 C COMPUTE NEW XFTF VECTOR(SMOOTHED ESTIMATE)
C
C DO 20 I=1,NS
C C(I)=XFPLUS(I)
C CONTINUE
C CALL VADD(NS,1.0,C,B)
C
35 C SET NEW ESTIMATE
C
C DO 30 I=1,NS
C XFTF(I)=C(I)
C CONTINUE
40 C RETURN
C END

```

```
1 SUBROUTINE SMOOTHP
C COMPUTES THE "SMOOTHED" COVARIANCE MATRIX AS
C IT PROPAGATES BACKWARD IN TIME.
5 C REQUIRES MATRIX ADDITION AND MULTIPLICATION
C ROUTINES TO BE USED.
C
COMMON /MAIN1/ NDIM,NDIM1,COM1(10,10)
COMMON /DIM/ NS,NTR,NSEC,NSAMP,NSTEP
COMMON /PFP/ PFPPLUS(10,10)
COMMON /PFM/ PFMINUS(10,10)
COMMON /A/ AMAT(10,10)
COMMON /PFTF/ PFTF(10,10)
15 C DIMENSION PDIFF(10,10), APAT(10,10)
C COMPUTE DIFFERENCE BETWEEN PFTF AND PFMINUS
C
C CALL MADD1(NS,NS,PFTF,PFMINUS,PDIFF,-1.0)
20 C COMPUTE MATRIX PRODUCT AMAT*PDIFF*AMAT(T)
C
C CALL MAT3(NS,NS,AMAT,PDIFF,APAT)
C COMPUTE NEW VALUE FOR PFTF
25 C
C CALL MADD1(NS,NS,PFPLUS,APAT,PFTF,1.0)
C
30 RETURN
END
```

```

1      SUBROUTINE OUT(PLOTEM,USEROUT)
C
C      WRITES OUTPUT FILE, PLOT FILE AND USER FILE
C      AS DESIRED AND INSTRUCTED BY USER ASSIGNED
C      VALUES FOR PLOTEM,USEROUT.
C
      COMMON /INOU/ KIN,KOUT,KPLOT,KDATA,KUSER
      COMMON /DIM/ NS,NTR,NSEC,NSAMP,NSTEP
      COMMON /XFP/ XFPLUS(10)
      COMMON /PFP/ PFPLUS(10,10)
      COMMON /XFTF/ XFTF(10)
      COMMON /PFTF/ PFTF(10,10)
      COMMON /HEADING/ TITLE(20), ADATE, ATIME
      COMMON /TIME/ T,T0,TF
      LOGICAL PLOTEM,USEROUT
      DIMENSION SIGMA(10)
C
C      PRINT OUTPUT TO PRINTER FILE
C
      WRITE(KOUT,1005) T
      WRITE(KOUT,1001) (XFPLUS(I),I=1,NS)
      WRITE(KOUT,1002) (PFPLUS(I,I),I=1,NS)
      WRITE(KOUT,1003) (XFTF(I),I=1,NS)
      WRITE(KOUT,1004) (PFTF(I,I),I=1,NS)
C
C      WRITE TO PLOTTER FILE
C
      IF (PLOTEM) GO TO 10
      GO TO 20
10     WRITE(KPLOT) T,(XFPLUS(I),I=1,NS),(XFTF(I),I=1,NS),
      &      (PFPLUS(I,I),I=1,NS),(PFTF(I,I),I=1,NS)
C
C      WRITE DESIRED VARIABLES TO USER FILE
C
20     IF (USEROUT) GOTO 30
      GOTO 40
30     WRITE(KUSER) T, (XFTF(I),I=1,NS), (PFTF(I,I),I=1,NS)
C
1000  FORMAT("1H1SMOOTHER1",10X,20A4,10X,2A10)
1001  FORMAT("/OFORWARD FILTER STATE ESTIMATE:",/1H0,10E15.7)
1002  FORMAT(/,"DIAGONAL ELEMENTS OF FILTER COVARIANCE MATRIX:",
      /1H0,10E15.7)
1003  FORMAT(/,"OSMOOTHER ESTIMATE OF STATE:",/1H0,10E15.7)
1004  FORMAT(/,"DIAGONAL TERMS OF SMOOTHER COVARIANCE MATRIX:",
      /1H0,10E15.7)
1005  FORMAT(/,"20X,"SMOOTHER OUTPUT AT TIME=",F6.2)
40     RETURN
      END

```

CARD NR.	SEVERITY	DETAILS	DIAGNOSIS OF PROBLEM
40	I	58 CD 40	FIELD WIDTH IS GREATER THAN 137 CHARACTERS. IT MAY EXCEED THE I/O DEVICE CAPACITY.
40	I	61 CD 40	TOTAL RECORD LENGTH IS GREATER THAN 137 CHARACTERS. IT MAY EXCEED THE I/O DEVICE CAPACITY.
41	I	20 CD 42	FIELD WIDTH IS GREATER THAN 137 CHARACTERS. IT MAY EXCEED THE I/O DEVICE CAPACITY.



CARD NR.	SEVERITY	DETAILS	DIAGNOSIS OF PROBLEM
41	I	23 CD 42	TOTAL RECORD LENGTH IS GREATER THAN 137 CHARACTERS. IT MAY EXCEED THE I/O DEVICE CAPACITY.
43	I	58 CD 43	FIELD WIDTH IS GREATER THAN 137 CHARACTERS. IT MAY EXCEED THE I/O DEVICE CAPACITY.
44	I	59 CD 43	TOTAL RECORD LENGTH IS GREATER THAN 137 CHARACTERS. IT MAY EXCEED THE I/O DEVICE CAPACITY.
44	I	20 CD 45	FIELD WIDTH IS GREATER THAN 137 CHARACTERS. IT MAY EXCEED THE I/O DEVICE CAPACITY.
44	I	23 CD 45	TOTAL RECORD LENGTH IS GREATER THAN 137 CHARACTERS. IT MAY EXCEED THE I/O DEVICE CAPACITY.

```
1 SUBROUTINE ZROIZE(M,N,A)
C ZEROS AN M X N MATRIX, A
C
5 DIMENSION A(10,10)
C
C DO 10 I=1,M
C DO 20 J=1,N
C A(I,J)=0.
C CONTINUE
C 10 CONTINUE
C
C RETURN
C END
```

## Bibliography

1. Fraser, D.C. A New Technique for the Optimal Smoothing of Data, Ph.D. Dissertation, Massachusetts Institute of Technology, Cambridge, June 1967.
2. Fraser, D.C. and J.E. Potter. "The Optimum Linear Smoother as a Combination of Two Optimum Linear Filters." IEEE Transactions on Automatic Control VII, 4: 387-390. (1969).
3. Hamilton, D.E. Evaluation of the Land Speed of Sound Record Attempt by the Budweiser Rocket Car, unpublished historical report, Edwards AFB, CA, July 1982.
4. Maybeck, P.S. Stochastic Models, Estimation, and Control, Volume I and II, Wright-Patterson AFB, OH, 1982.
5. Meditch, J.S. "On Optimal Linear Smoothing Theory," Information and Control, XX, 598-615. (1967).
6. Musick, S.H. "SOFE: A Generalized Digital Simulation for Optimal Filter Evaluation, User's Manual," Technical Report, AFWAL-TR80-1108, Wright-Patterson AFB, OH, October 1980.
7. Musick, S.H. et. al. "SOFEPL: A Plotting Postprocessor for SOFE User's Manual," Technical Report, AFWAL-TR-80-1109, Wright-Patterson AFB, OH, November 1981.
8. Neter, J. et. al. Applied Statistics, Boston, 1978.

VITA

Captain David A. Reinholz was born on 7 January 1952 in Midland, Texas. He graduated from high school in Delavan, Wisconsin, in 1970 and attended the United States Air Force Academy from which he received a Bachelor of Science in Aeronautical Engineering in June 1974. He completed pilot training and received his wings in August 1975. He served as a C-130 pilot in the 41st Tactical Airlift Squadron, Pope AFB, North Carolina from January 1976 to April 1979. From May 1979 to April 1982 he served as an instructor pilot and Undergraduate Pilot Training Class Commander in the 47th Flying Training Wing, Laughlin AFB, Texas. He entered the School of Engineering, Air Force Institute of Technology, in June 1982.

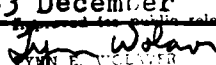
Permanent address: 10047 Windburn Trail  
Converse, Texas 78109

UNCLASSIFIED

SECURITY CLASSIFICATION OF THIS PAGE

AD-A136 919

REPORT DOCUMENTATION PAGE

1a. REPORT SECURITY CLASSIFICATION <b>UNCLASSIFIED</b>		1b. RESTRICTIVE MARKINGS	
2a. SECURITY CLASSIFICATION AUTHORITY		3. DISTRIBUTION/AVAILABILITY OF REPORT Approved for public release; distribution unlimited	
2b. DECLASSIFICATION/DOWNGRADING SCHEDULE			
4. PERFORMING ORGANIZATION REPORT NUMBER(S) <b>AFIT/GAE/AA/83D-2019</b>		5. MONITORING ORGANIZATION REPORT NUMBER(S)	
6a. NAME OF PERFORMING ORGANIZATION School of Engineering	6b. OFFICE SYMBOL (If applicable) AFIT/ENY	7a. NAME OF MONITORING ORGANIZATION	
6c. ADDRESS (City, State and ZIP Code) Air Force Institute of Technology Wright-Patterson AFB, Ohio 45433		7b. ADDRESS (City, State and ZIP Code)	
8a. NAME OF FUNDING/SPONSORING ORGANIZATION	8b. OFFICE SYMBOL (If applicable)	9. PROCUREMENT INSTRUMENT IDENTIFICATION NUMBER	
8c. ADDRESS (City, State and ZIP Code)		10. SOURCE OF FUNDING NOS.	
11. TITLE (Include Security Classification) See Box 19		PROGRAM ELEMENT NO.	PROJECT NO.
		TASK NO.	WORK UNIT NO.
12. PERSONAL AUTHOR(S) David A. Reinholz, B.S., Capt, USAF			
13a. TYPE OF REPORT MS Thesis	13b. TIME COVERED FROM _____ TO _____	14. DATE OF REPORT (Yr. Mo., Day) 1983 December	15. PAGE COUNT 184
16. SUPPLEMENTARY NOTATION <div style="text-align: right;">             LYNN E. MCEWEN            Dean for Research and Professional Development            Air Force Institute of Technology (AFIT)            Wright-Patterson AFB, OH 45433         </div>			
17. COSATI CODES		18. SUBJECT TERMS (Continue on reverse if necessary and identify by block number)	
FIELD	GROUP	Kalman Filter, Extended Kalman Filter, Data Smoothing, Optimal Smoothing, Estimation	
09	04		
19. ABSTRACT (Continue on reverse if necessary and identify by block number)			
<p>Title: STOCHASTIC ESTIMATION APPLIED TO THE LAND SPEED OF SOUND RECORD ATTEMPT BY A ROCKET CAR</p> <p>Thesis Chairman: James K. Hodge, Captain, USAF</p>			
20. DISTRIBUTION/AVAILABILITY OF ABSTRACT UNCLASSIFIED/UNLIMITED <input checked="" type="checkbox"/> SAME AS RPT. <input type="checkbox"/> DTIC USERS <input type="checkbox"/>		21. ABSTRACT SECURITY CLASSIFICATION UNCLASSIFIED	
22a. NAME OF RESPONSIBLE INDIVIDUAL James K. Hodge, Captain, USAF		22b. TELEPHONE NUMBER (Include Area Code) 513-255-3517	22c. OFFICE SYMBOL AFIT/ENY

UNCLASSIFIED

SECURITY CLASSIFICATION OF THIS PAGE

Optimal linear smoothing theory is applied to the data from the land speed of sound record attempt of a three-wheeled rocket car on 17 December 1979. A forward-backward estimation method is used which employs a seven state forward-running extended Kalman filter and a Meditch-form backward recursive 'fixed interval' smoothing algorithm. Data for this analysis is supplied by a longitudinal accelerometer mounted on the vehicle and tracking radar measurements of range, azimuth, and elevation. States of interest include two components of vehicle position and velocity, accelerometer time-correlated error, and radar range and bias errors.

Two iterations of the forward-backward smoothing algorithm provide excellent convergence of state estimates and error variance. Based on this analysis a peak speed estimate of 1082.028 ft/sec or 1.008 Mach is obtained at 16.85 seconds from the start of the high speed run. After two iterations of the smoother the standard deviation of the peak speed estimate is reduced to 1.055 ft/sec. We conclude with a confidence level of nearly one, based on the assumptions and modeling techniques employed in this analysis, that the rocket car did, in fact, exceed the reference speed of sound on 17 December 1979.

UNCLASSIFIED

SECURITY CLASSIFICATION OF THIS PAGE

END

DATE

FILMED

2-84

DTIC